Contribution to the development of wide-band signalprocessing techniques for new sonar technologies

Jitendra Singh Sewada

THÈSE

Pour obtenir le grade de

DOCTEUR DE L'UNIVERSITÉ GRENOBLE ALPES

Spécialité : SIGNAL IMAGE PAROLE TELECOMS

Arrêté ministériel : 25 mai 2016

Présentée par

Jitendra Singh SEWADA

Thèse dirigée par **Cornel IOANA**, Maitre de conférences, Université Grenoble Alpes
et codirigée par **Jérôme MARS**, Professeur, Université Grenoble Alpes

préparée au sein du **Laboratoire Grenoble Images Parole Signal Automatique**
dans **l'École Doctorale Electronique, Electrotechnique, Automatique, Traitement du Signal (EEATS)**

Contribution à l'élaboration d'un signal à large bande techniques de traitement pour les nouvelles technologies de sonar

Contribution to the development of wide-band signal processing techniques for new sonar technologies

Thèse soutenue publiquement le **21 février 2020**,
devant le jury composé de :

Monsieur Cornel IOANA
MAITRE DE CONFERENCES HDR, GRENOBLE INP, Directeur de thèse
Monsieur Alexandru SERBANESCU
Professeur, Military Technical Academy, Bucharest, Rapporteur
Monsieur Ali MANSOUR
Professeur des Universités, ENSTA Bretagne, Rapporteur
Monsieur Jérôme MARS
Professeur des Universités, Université Grenoble Alpes, Co-directeur de thèse
Madame Nadège THIRION-MOREAU
Professeur des Universités, Université de Toulon, Présidente

T H E S I S

CONTRIBUTION TO THE DEVELOPMENT OF WIDE-BAND SIGNAL PROCESSING TECHNIQUES FOR NEW SONAR TECHNOLOGIES

Presented and defended by

Jitendra Singh SEWADA

for obtaining the

DOCTORATE DEGREE

of *University of Grenoble Alpes*

Doctoral School: *Electronique, Electrotechnique, Automatique, Traitement du Signal* ***(EEATS)***

Specialization: ***SIGNAL, IMAGE, PAROLE, TÉLÉCOMS***

Thesis directed by Cornel IOANA and Jérôme MARS

Prepared in the Grenoble Image Parole Signal Automatique laboratory (GIPSA-lab) and

ITER Systems

Defended in Grenoble, on 21st February 2020, in front of the jury:

Reviewers:	Alexandru SERBANESCU	- Professor, Military Technical Academy, Bucharest, Romania
	Ali MANSOUR	- Professor, ENSTA Bretagne, France
Examiner:	Nadège THIRION-MOREAU	- Professor, University of Toulon, France
Invited:	Matt GEEN	- Technical Director, ITER Systems
	David MAILLOTTE	- Managing Director, ITER Systems

Dedicated to Kiran.

TABLE OF CONTENTS

GLOSSARY & ACRONYMS VIII

CHAPTER 1 INTRODUCTION 1

1.1. CONTEXT 1
1.2. UNDERWATER EXPLORATION 1
1.3. PROBLEM STATEMENT 2
1.4. THESIS OUTLINE 3

CHAPTER 2 STATE OF ART 5

2.1. OBJECTIVE: BATHYMETRY 5
2.2. GENERAL INTRODUCTION TO SEAFLOOR MAPPING SYSTEMS 5
2.3. EXISTING TECHNIQUES 8
2.3.1 Interferometers 8
2.3.2 Multibeam Beamformer 10
2.3.3 Comparison Between Interferometers and Beamformers 11
2.4. BATHYSWATH 12
2.4.1 Transmitter Design 12
2.4.2 Receiver Design 14
2.5. MOTIVATION OF THIS WORK 15
2.5.1 Range – Resolution Trade-off 15
2.5.2 Angular Measurement Uncertainty 16
2.6. CHAPTER SUMMERY 16

CHAPTER 3 BASICS OF SIGNAL PROCESSING METHODOLOGY AND EXPRIMENT 17

3.1. INTERFEROMETRY METHOD 17
3.2. MATCHED FILTER 18
3.3. EXPERIMENT SETUPS 21
3.3.1 Water Tank Setup 21
3.3.2 Pontoon Setup 22
3.3.3 Boat Setup 23

CHAPTER 4 BATHYMETRY QUALITY ESTIMATION 25

4.1. EXTERNAL MEASUREMENT UNCERTAINTY 26
4.2. RANGE MEASUREMENT 27
4.2.1 Time of Arrival Uncertainty 27
4.2.2 SV measurement Uncertainty 27
4.3. ANGULAR MEASUREMENT UNCERTAINTIES 28
4.3.1 Transducer Manufacturer Accuracy 28
4.3.2 Phase Ambiguity 28

4.4. Phase Measurement Uncertainty 34
4.4.1 Additive Noise 36
4.5. Decorrelation in the Received Signals 39
4.5.1 Spatial Decorrelation 40
4.5.2 Angular Decorrelation 43
4.6. Overall Signal to Noise Ratio 46
4.7. Summary of the Chapter 50

CHAPTER 5 IMPROVEMENTS WITH WIDEBAND SIGNALS 51

5.1. Improvement in single sensor measurements 51
5.1.1 Range – Resolution Trade-off 51
5.1.2 Summary of the Section 60
5.2. Angle Measurement Improvements 62
5.2.1 Robustness to Additive Noise 62
5.2.2 Robustness to Spatial Decorrelation 63
5.2.3 Robustness to Angular Decorrelation 65
5.2.4 Overall SNR Improvements 67
5.2.5 Considerations on Practical Implementation of Wideband Processing 69
5.3. Pulse Shape design 69
5.3.1 Smoothed Transmit Envelope 70
5.4. Filter Design 73
5.5. Conclusion of the Chapter 74

CHAPTER 6 CONCLUSION & PERSPECTIVE 77

6.1. Work Summery 77
6.2. Perspective 79

APPENDIX 81

PUBLICATIONS 92

External 92
Internal 92

BIBLIOGRAPHY 94

TABLE OF FIGURES

Figure 1 Sidescan image of a sunken jetty taken during a survey 6
Figure 2 Swath bathymetry sonar setup illustration 7
Figure 3. Point-cloud view of a Digital Terrain Model (DTM) created using Bathyswath 8
Figure 4 Basic Setup of an Interferometer (Top View) 9
Figure 5. Cross-profile view of spread of depth across the range 10
Figure 6 Multibeam Beamformer Setup 10
Figure 7. Interferometric vs Beamformer multibeam sonars [4] 11
Figure 8. Swath width Comparison of Beamformer and Bathyswath-2 Interferometer [4] 11
Figure 9 Bathyswath System Setup 12
Figure 10 Bathyswath functional block diagram and the R&D works done in this thesis 14
Figure 11 Receiver architecture used by Bathyswath; this work is focused on the components in red 15
Figure 12. Basic setup of interferometry data acquisition 17
Figure 13 Matched filter examples with narrowband and wideband signals 20
Figure 14 Matched Filter implementation using FFT 21
Figure 15 Experiment setup–1: Water tank Setup 22
Figure 16 Experiment setup-2: Pontoon setup, depth under transducer is 1.5m 22
Figure 17 Experimental Setup-3: Boat setup used for the experiments 23
Figure 18 Bathymetry Degradation Sources 25
Figure 19 Depth uncertainty measured for different profiles of a shallow water survey (Data courtesy: ITER Systems) 26
Figure 20 Angle measurements from the phase difference measured at 1λ apart receivers 29
Figure 21 Angle measurements from the phase difference measured at λ/2 apart receivers 30

Figure 22 Angle measurements from the phase difference measured at 8.5λ apart receivers 31
Figure 23 Angle measurements over Range calculated with Vernier pair 31
Figure 24 Depth vs horizontal range (Cross Profile), showing false bottom at different angles (picture taken during a test survey in Annecy lake with Boat setup)..... 32
Figure 25. Phase Difference between resulting Vernier pair of 0.5λ, 1λ and Physical receiver pair separated by 2λ and 8.5λ as a function of angle of incidence. Vernier pair 0.5λ is unambiguous..... 33
Figure 26 Angle estimation before (red) and after Vernier method is applied 34
Figure 27 Standard Deviation in depth measurements taken with different transmitted pulse length (Experiment Setup: Pontoon)..... 36
Figure 28 Sonar equation illustration for an active sonar 37
Figure 29 SNR accounting additive noise only, estimated for CW (8.5μs), CW (42.75μs) 38
Figure 30 Phase Difference standard deviation for the measurements done using CW (8.5μs) and CW (42.75μS) as the transmitted pulse. 39
Figure 31 Sliding footprint problem with interferometers 41
Figure 32 Computed equivalent SNR for sliding footprint effect (left) and resulting phase difference measurement error (right)..... 42
Figure 33 Angular decorrelation due to beam footprint of resolution cell 43
Figure 34 Computed SNR_Angle vs Horizonal Range 45
Figure 35 Phase difference standard deviation given for Baseline decorrelation..... 46
Figure 36 Measurement geometry in Nadir region 46
Figure 37 Overview off different SNR sources and the total SNR..... 47
Figure 38 Phase difference standard deviation with different noise sources (e.g. Sliding footprint, Angle Decorrelation, Additive Noise etc.) 48
Figure 39 Resulting total SNR for different length CW pulses and LFM pulse..... 49
Figure 40 Phase difference measurement errors given using the total SNR calculation. 49

Figure 41 Standard deviation in depth measurement given over the across track range; mathematical model (red) compared with real data (blue) 50
Figure 42 Spectrogram of CW signal with rectangular envelope 52
Figure 43 Backscattered echoes with transmitted CW pulse with pulse width of (a) 2 cycles (b) 10 cycles & (C) 20 cycles..... 53
Figure 44 Received signal intensity after Matched filter, for 2-cycles (Red), 10 cycle (Green) and 20 cycles (Blue) 54
Figure 45 Cross profile view of depth while using CW pulse with transmitted pulse length a) & b) 8.5µs and c) & d) 42µs..... 55
Figure 46 Spectrogram of a Linear Frequency Modulated Pulse (LFM) with rectangular envelope..... 57
Figure 47 Water tank experiment: Backscattered echoes with LFM transmit pulse a) Pulse duration = 0.5ms, b) Pulse Duration = 0.65ms 58
Figure 48 Cross profile view of depth while using LFM transmit pulse 58
Figure 49 Spectrogram of a Linear Frequency Modulated Pulse (LFM) with rectangular envelope..... 59
Figure 50 Water tank experiment: Backscattered echoes with EFM as transmit pulse; pulse length: 0.62ms 60
Figure 51 Matched filter outputs with different transmit pulses 61
Figure 52 SNR accounting additive noise only, estimated for LFM (80µs), CW (8.5µs) and CW (42.75µs)..... 62
Figure 53 Phase Difference standard deviation only considering the sliding footprint effect, estimated for different length CW pulses and LFM pulses. 63
Figure 54 SNR only accounting the sliding footprint effect, estimated for CW pulses with different pulse length and LFM transmitted signals..... 64
Figure 55 Phase Difference standard deviation only considering the sliding footprint effect, estimated for different length CW pulses and LFM pulses. 65
Figure 56 SNR only considering the Baseline decorrelation given over the horizontal range..... 66
Figure 57 Phase Difference standard deviation only considering the sliding footprint effect, LFM transmit pulse compared with a short and a long CW pulse..... 66

Figure 58 Autocorrelation function of CW pulse and LFM with equivalent bandwidth (left), with different length (right) 67
Figure 59 Total SNR model for CW and LFM transmitted pulses..... 68
Figure 60 Phase difference standard deviation for total SNR vs Across track range... 69
Figure 61 Tranmit pulse as input and output to piezoelectric..... 70
Figure 62 Signal envelopes given for different smoothing level (0% = original square envelope)..... 71
Figure 63 Auto-correlation function of transmitted signals with envelopes mentioned in Figure 63, (0% = original square envelope & 100% is for full cosine envelope) 72
Figure 64 Auto-correlation function of transmitted signals with envelopes mentioned in, Figure 62 but with increased transmit pulse length to compensate the energy loss(0% = original square envelope & 100% is for full cosine envelope)..... 72
Figure 65 CW (blue), LFM with square envelope (black), LFM with cosine envelope or 100% smoothed envelope (red)..... 73
Figure 66 Auto-correlation of transmitted LFM pulse(blue) and widowed transmit pulses with Hamming window (green), Hann (magenta), Gaussian (black) and Taylor (red)..... 74
Figure 67 Depth uncertainty estimation with different level of transmit envelope smoothness initial signal 0% (red), 20% (green) and 50%(blue) of the original pulse length..... 75
Figure 68 Sound wave propagation due to changing sound velocity..... 81
Figure 69. Cross profile (Nadir Depth = 51m) 88
Figure 70. 2-D waterfall view of seabed while boat passes over seabed 88
Figure 71. Measurement geometry in nadir region..... 89
Figure 72 Footprint patch in nadir region and far range (left), footprint length given over horizontal range..... 90

Glossary & Acronyms

WORDS & ACRONYMS	DEFINITION
AoA	Angle of Arrival
AUV	Autonomous underwater vehicle; un-tethered underwater robot
Bathyswath	Interferometric sonar system from ITER Systems
boresight	Interferometric axis
cross-Profile	Spread of depth over horizontal range
CW	Continuous Wave: using a single frequency
DTM	Digital Terrain Modal
EFM	Exponential Frequency Modulated
FFT	Fast Fourier Transform
FM	Frequency Modulated
interferometric axis	The normal to the sonar transducer in the vertical; where the angle of arrival relative to the transducer is 0°
LFM	Linear Frequency Modulated
MBES	Multi Beam Echo-Sounder
MF	Matched Filter
nadir	The region directly beneath the sonar transducers; more precisely, the point on the seabed where a normal to the seabed passes through the transducers
PDBS	Phase Differencing Sonar System (Interferometer)
ping	Transmit-return cycle of an acoustic sonar system
PWM	Pulse width Modulation
ROV	Remotely operated vehicle: tethered underwater robot
sidescan	A sonar imaging technique that plots strength of acoustic echo against range as greyscale pixels, building up a strip image as the vessel moves forwards over the seabed
SNR	Signal to Noise
$SNR_{Additive}$	SNR due to additive noise only
SNR_{Angle}	SNR due to Angular decorrelation only
SNR_{Shift}	SNR due to sliding footprint decorrelation only
Swath	A horizontal broad strip area insonified by sonar on sea bottom
ToA	Time of Arrival

This page is left blank intentionally

CHAPTER 1 INTRODUCTION

1.1. Context

In recent years we have obtained high-resolution images of the Moon and Mars but the view underwater is still blurred. There is a need for high-resolution and accurate seabed maps and 3D images for secure navigation, environmental studies, archaeological surveys, economic exploitation, and industrial inspections. There has been significant development in the underwater surveying equipment since the World War 1. Most new generation vessels are equipped with some kind of sonar technology for different applications e.g. underwater navigation, target detection, bathymetry, underwater communication, acoustic source detection and collision avoidance. There has been a significant development in underwater survey equipment, including Interferometers.

Our studies are mainly focused on bathymetric sonars, especially interferometers, also know phase differencing sonars. The accuracy of measurements is an important aspect for bathymetric surveying, as is the cost and speed of survey. International standards are available for categorizing the quality of surveys, and so ensure safe navigation. We will be referring to the publication “Standards for hydrographic Surveys” (S-44) by the International Hydrographic Organisation (IHO) [1].

This research is the joint project of ITER Systems and GISPA-lab. ITER Systems is a small company located next to Lake Annecy in France, which specialises in the design of bathymetry sonar surveying equipment. Bathyswath is the main product range of the company. Bathyswath is wide swath sonar system designed for surveying underwater surfaces. It provides high-density bathymetry and sidescan data. It is particularly adapted for shallow water areas, because it uses “Interferometry” technology, also known as Phase differencing Bathymetry System (PDBS).

1.2. Underwater Exploration

About 71% of the earth’s surface is covered with water, and most of that water is in oceans. Freshwater resources, such as lakes, rivers and reservoirs are essential for the survival of animals and plants. Oceans and waterways have become a vital part of maritime industries, such as transportation of goods and people. So, it is important to have knowledge of waterways for the safety of the ships and boats. Another need for underwater exploration is for scientific researches e.g. archaeology, marine biology etc.

The common terms used with the mapping of seafloors are bathymetry, charting, hydrography and seabed classification. Purposes of bathymetry mapping include:

- Navigation maps and charts
- Maintenance of docking ports
- Environmental studies
- Offshore engineering
- Biological oceanography
- Maritime archaeology
- Hydroelectric plants and cooling water reservoir maintenance

A large percentage of the ocean floor is only surveyed at a very coarse resolution, and better hydrographic information will result in many new uses that we have not yet thought of.

1.3. Problem Statement

As mentioned earlier, many types of acoustic measurement equipment are available to investigate the sea bottoms. Our main interest is in the study of **interferometry techniques of measurement**. We believe that the interferometry technique has lots of potential, although it has a smaller market-share than other bathymetric technologies. The wide swath given by an interferometer makes it a desirable tool in shallow water environments, where time and cost of survey plays an important role. It also gives a wide swath when an underwater vehicle is operating close to the seabed, for example to get good sidescan data and to take photographs. “Sidescan” is a sonar imaging technique that plots strength of acoustic echo against range as greyscale pixels, building up a strip image as the vessel moves forwards over the seabed. The best image contrast is given when the sonar beam makes a shallow angle with the bottom, so sidescan sonars are used with towfish or mounted on underwater vehicles e.g. AUVs & ROVs. Interferometers can be used in these scenarios to give high resolution sidescan images with depth information for each insonified point on the ocean floor.

With the increase in the coastal activities, there is an increasing need for high-resolution bathymetry and sidescan imagery.

Using narrowband (single-frequency) acoustic signals requires a trade-off between range and resolution. Ambient noise and a high absorption coefficient degrade the transmitted and backscattered echoes and limit the achievable swath range of a swath bathymetry sonar. Thus, high-energy transmitted pulses are desirable to achieve a sufficiently wide swath width, which most often is achieved by increasing the width of the transmitted pulses. A longer transmitted pulse contains higher energy; hence the

intensity of far range backscattered echoes is also higher and distinguishable in ambient noise. However, a longer pulse also makes a bigger footprint (insonified area) on the sea bottom, and degrades resolution: the ability to measure the two closely placed targets (scatters on sea floor).

The other problem lies with the ability to measure the depths accurately in a noisy environment. Depth measurement with interferometric technique is done by measuring the incident angle, which is calculated from phase difference measurements at receive array. So, any error in phase measurements results in inaccurate bathymetry. That makes it highly sensitive to all phase related noise sources

In this research work we aim to investigate the major quality degradation issues from the signal processing point of view, and we propose some ways to improve the current techniques.

1.4. Thesis Outline

This thesis is divided into 6 chapters. This first chapter gives a basic introduction to the purpose of this research work.

The Chapter 2 aims to give the reader a quick introduction to the state of the art in bathymetry measuring sonar systems. It presents the fundamentals of seabed mapping systems. We introduce two widely used swath measuring sonar systems and the basic differences between them. We explore the design of the Bathyswath system, a new-generation sonar system provided by ITER Systems. It ends with providing the motivation of this thesis.

Chapter 3, entitled “Basics of signal processing methodology and experiment”, introduces the signal processing methodology used for this work. We introduce here the interferometric method of bathymetry calculation used with Bathyswath, which is appropriate for the shallow water environment We introduce the matched filtering technique, which was used throughout the research work. The current version of Bathyswath does not use the matched filter technique. We provide three different setups for experiments to explore and validate our findings.

In Chapter 4 we give an uncertainty model from the signal processing point of view. Here we focus on different noise sources in the overall bathymetry degradation, considering why and how these different noise sources can affect the bathymetry measurement accuracy and to what extent. All the studies here are done for Continuous Wave (CW) pulses, which are currently used in the Bathyswath-2 system. At some extent we also cover the current state of the art methods used in Bathyswath to overcome some of the problems introduced in this chapter.

In Chapter 5 we propose the use of wideband signals to overcome the problems introduced in previous chapters. We start with solving the range-resolution trade off by doing an assessment of different signals, e.g. narrowband and wideband signals. Then in the second section of the chapter, we propose wideband signals to overcome the previously introduced bathymetry degradation sources. We explore each noise source separately and compare the improvements in individual noise components given by wideband pulses. We end the chapter by assessing the overall improvement from using wideband signals, while introducing the limitations and issues with this approach. In the end of Chapter 5 we propose some of the techniques that can be used to overcome the problems related to the nadir region and in improving performance of the interferometry technique.

We conclude in Chapter 6 and give a perspective for the future developments in the interferometry method of bathymetry measurement

CHAPTER 2 STATE OF ART

2.1. Objective: Bathymetry

The study of underwater depth in any water body (sea, river, lake etc) is known as bathymetry. Many types of surveying equipment are available to measure underwater depth. The most well-known acoustic systems are single beam sounder, multibeam echosounder, sidescan sonar and synthetic aperture sonar. Generally, bathymetry is done by estimating a two-way propagation time and incidence angle of backscattered echoes to calculate the water depth at a reference point. All these measurements are stitched together to create a continuous DTM (Digital Terrain Model), which can be used to represent the seafloor as a 3D point cloud [2].

Light-based systems, such as airborne lidar scanners and laser scanners are also used for bathymetry measurements and underwater structure inspection. But acoustical measurement techniques remain the first choice for hydrography, due to underwater acoustical wave propagation properties and the fact that electromagnetic waves, including light, do not propagate well in water, particularly seawater. Only multibeam sounders (beamformers and Interferometers) are studied here in detail. The presented developments focus on the improvement of interferometric technique of bathymetry measurement. Some of the problems and solutions also stand true for the beamformers.

The aim of this chapter is to provide the reader the essential information on sonar systems and their principles in order to better understand the need for this research work. The following key points are described in this chapter:

- Sonar Systems
- Interferometric Technique
- Comparison Between Interferometers and Beamformers
- The Bathyswath System

2.2. General introduction to seafloor mapping systems

One of the first uses of underwater acoustics to detect vessels was by Leonardo Da Vinci in 1490. He inserted a metal tube in the water to detect a vessel's noise at distance. The first bathymetric maps ever published were in 1853 by Fontaine Maury, in Explanations and sailing Directions to Accompany the wind and Current Charts. The first echosounder was patented by Herbert Grove Dorsey in 1928 and he called it Fathometer

because it measures fathoms, a unit of length for measuring the depth of water[2]. Before World War II, the structure of seafloor was mostly unknown. Now, high precision GNSS (global navigation satellite systems) positioning has made it much easier to create accurate maps for topographic survey as well as hydrographic surveys.

Initially, singlebeam echosounders were used to measure the depth directly below a boat. Singlebeam echosounders are simple to use. They are installed under a boat, looking directly at the bottom of the sea, and measuring depth by detecting the first echo reflected from the seabed. Singlebeam echosounders are still widely used, due to their simplicity of use and low cost.

Later, sidescan sonar systems were developed to look at a wider area. A sidescan sonar usually consists of single hydrophone and projector; usually, the same physical transducer element is used for both receive and transmit functions [3]. They create a fan-shaped acoustic beam on both port and starboard sides, covering a large area of the sea floor with each ping (transmit-return cycle). A greyscale image can be extracted from the received amplitude of the backscattered echoes. This can be analysed using the sonar equation; see to Chapter 3.

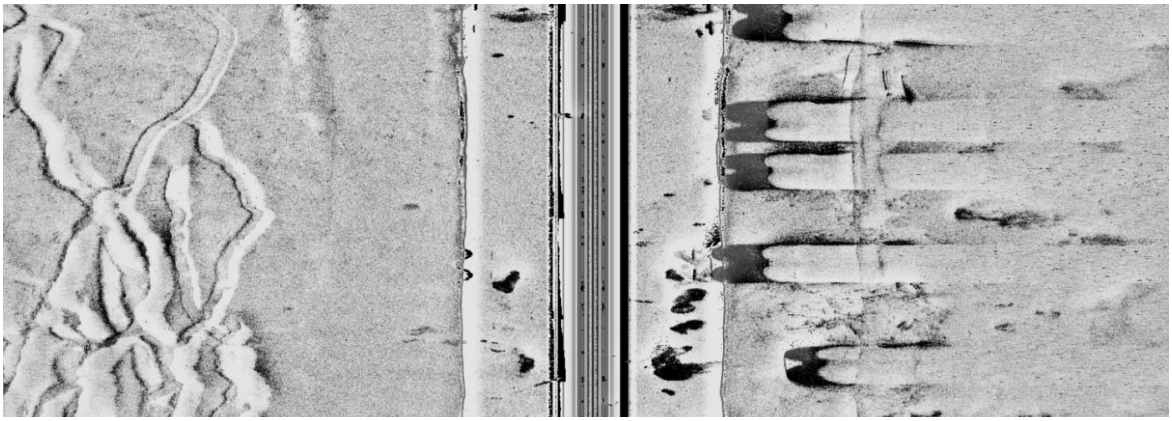

Figure 1 Sidescan image of a sunken jetty taken during a survey

(Source: ITER Systems)

Multibeam echosounders (MBES) can measure bathymetric profiles of a wide area in a single ping. This can be done either by either forming multiple beams across track at reception or by measuring the angle of arrival from received backscattered echoes. With the evolution of recent technology, the multibeam echosounders are capable of high ping rates, which increases the productivity and reduces the cost of surveys.

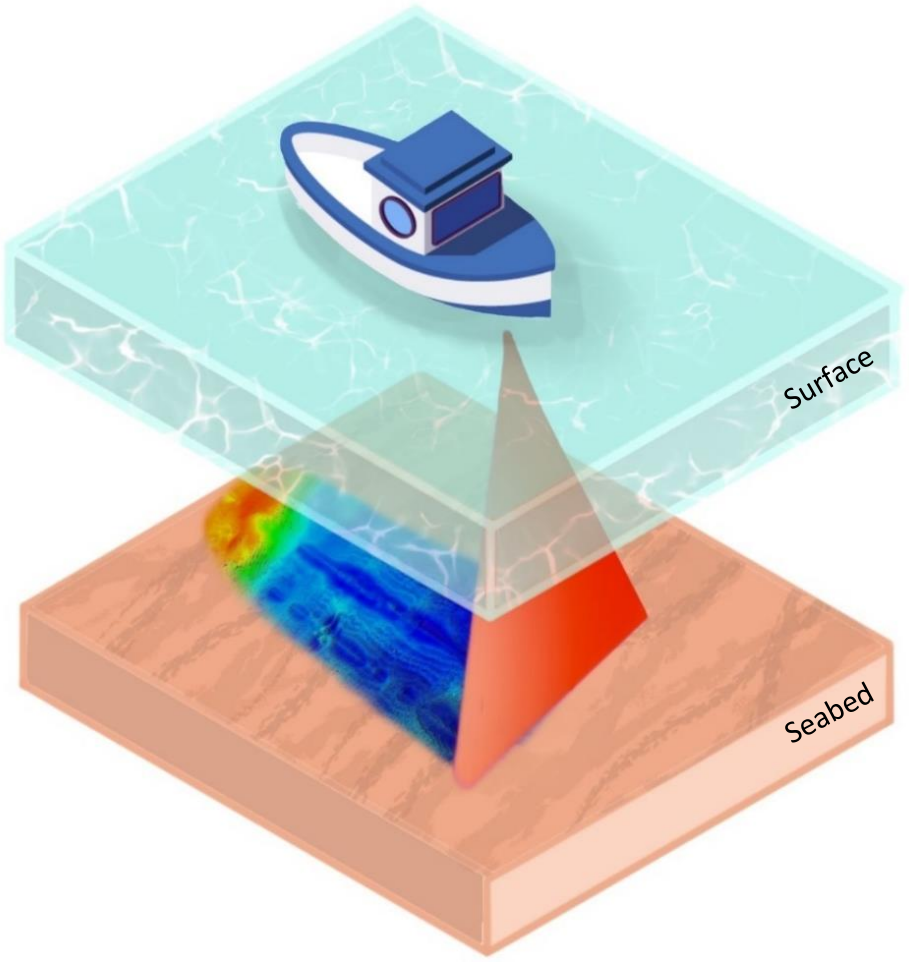

Figure 2 Swath bathymetry sonar setup illustration

There are two well-known ways to do bathymetry measurements across the swath on the seabed: 1) The beamforming technique, also known as Multibeam Echo-Sounder (MBES), and 2) Phase Differencing Bathymetric Sonar PDBS), also known as interferometric sonar. There are other ways, but they aren't used much anymore for swath bathymetry, e.g. scanned angle beam, and frequency-angle methods, as used in Blueview. Both beamforming and interferometry method have their merits and drawbacks, but both are widely used for high resolution bathymetry surveys. See section 2.3 for a detailed comparison. Figure 2 represents a basic setup of a multibeam bathymetry sonar, installed on the bow-mount of a boat.

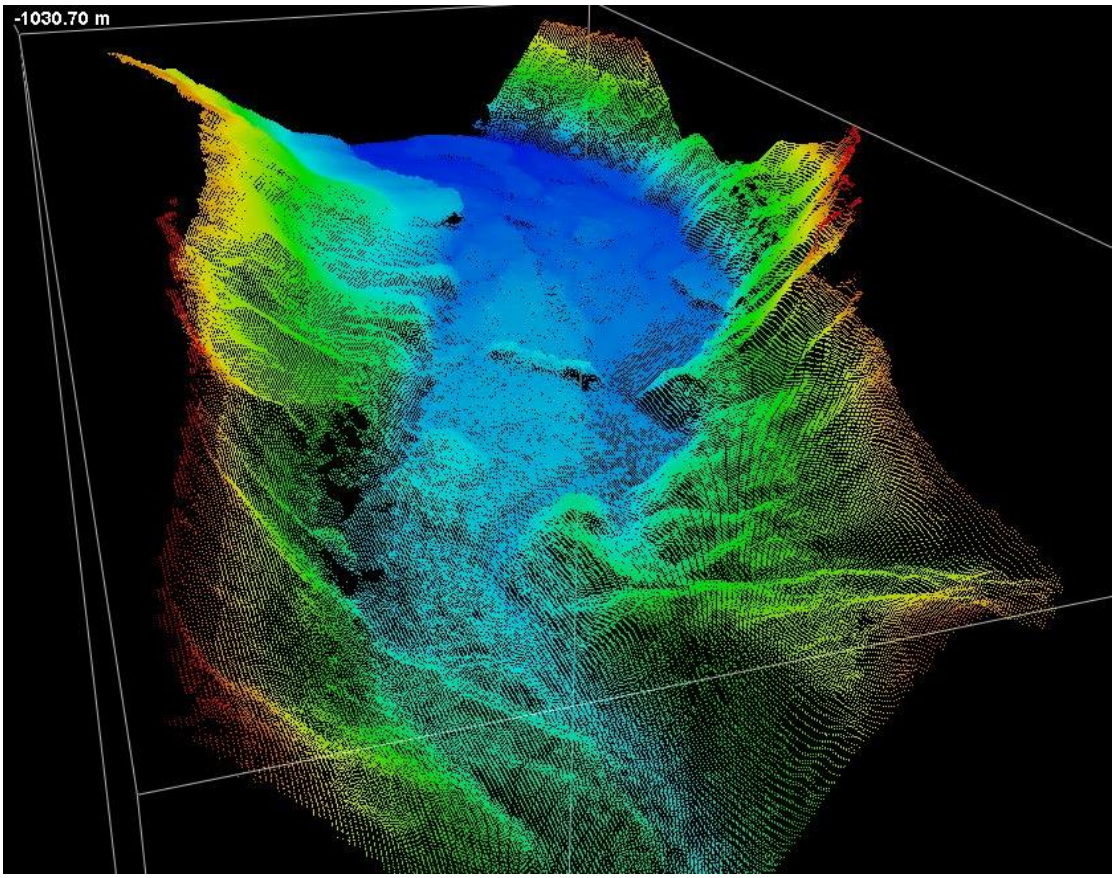

Figure 3. Point-cloud view of a Digital Terrain Model (DTM) created using Bathyswath (Source: ITER Systems)

2.3. Existing Techniques

Interferometers and multibeam beamformers are two of the most known techniques used for wide swath bathymetry surveys [12], but still considered as two different tools in surveyor's toolkit. Interferometers are mostly preferable in shallow water (<50m), where the wide swath range of sonar increases the surveying speed and reduces the surveying cost for a large survey area. Beamformers tend to have a greater depth range for transducers of the same size.

2.3.1 Interferometers

The word "interferometry" in sonar technology comes from the initial use of interference patterns in sidescan sonar images to find the Angle of Arrival (AoA), known as the Lloyd's mirror effect [9]. This effect was limited to relatively flat seabeds, because the interference pattern is caused by combination of the direct path and sea surface reflection. The repetitive fringes can be interpreted as useful depth information [9]. But the results were highly inaccurate and rarely useful, due to the reliability on flat seabed and calm sea surface, which is a rare condition in the real environment.

Later, an improved version of the sonar interferometer was developed, known as “Telesounding”, where a reflector was placed near the surface to get more reliable and controlled interference fringes [10]. But the reflector plate was very inconvenient to use, and inaccurate due to the complexity of estimating the angle of arrival from a set of fringes.

Recent interferometers use a different approach to adding two or more signals to get an interference pattern. Phase difference between received echoes at two or more receivers is used to calculate the Angle of Arrival (AoA). P. Denbigh used the term “Bathymetric Sidescan sonar”, acronym BASS, to describe the phase differencing technique [10].

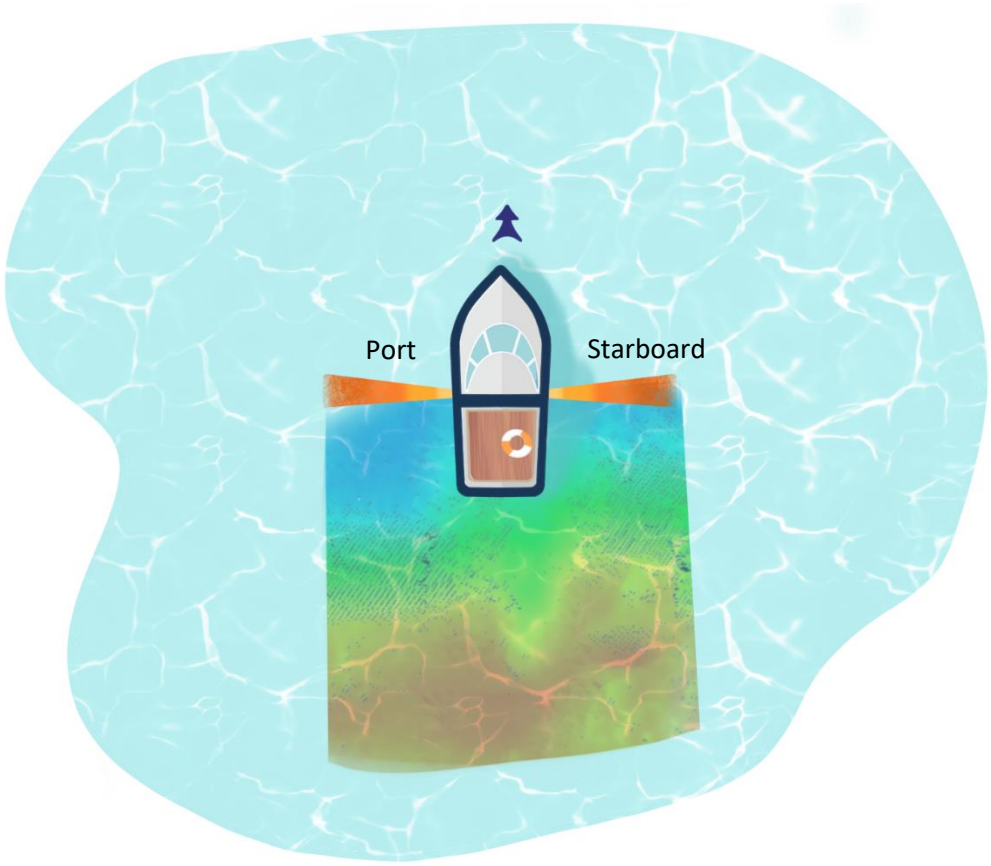

Figure 4 Basic Setup of an Interferometer (Top View)

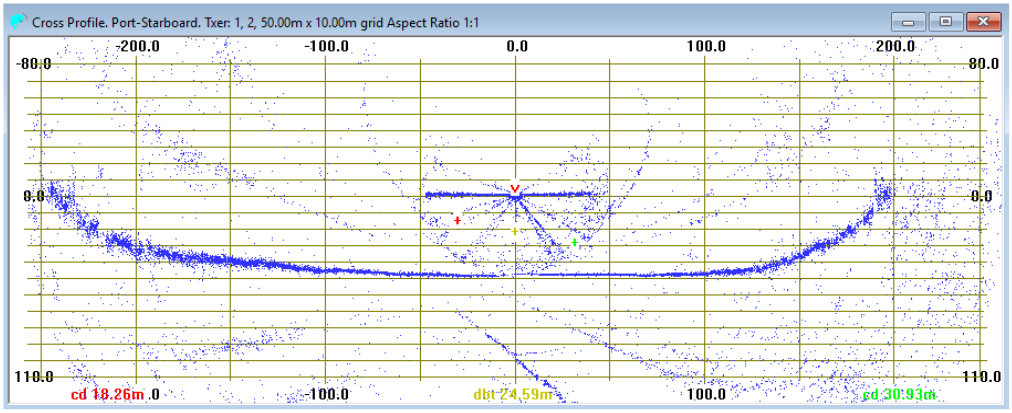

Figure 5. Cross-profile view of spread of depth across the range

Figure 5 presents the cross-profile view of a single ping taken during a survey in Annecy lake. Blue points are the unfiltered received signals at the sonar electronics. These points include the estimated position of seabed and the intrinsic noise of hardware.

Once the slant range and incidence angle are estimated correctly, these values can use used to calculate the seafloor depth points using a cylindrical coordinate system. These depth points can be merged with GNSS and INS data to get a DTM map of seafloor (Figure 3).

2.3.2 Multibeam Beamformer

A beamformer creates a number of beams and detects the range to the seabed for each beam. A transmit array insonifies a part of seabed, then a receive array measures the range to seabed in the direction of each beams formed using beamforming techniques [4] [17].

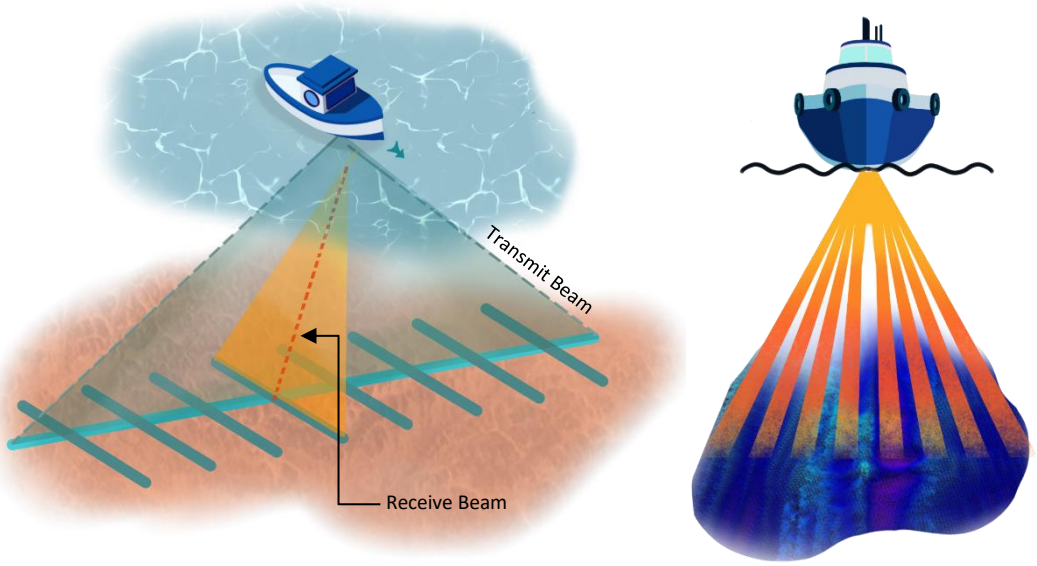

Figure 6 Multibeam Beamformer Setup

2.3.3 Comparison Between Interferometers and Beamformers

The major difference between both systems is the technique used to measure range and angle of backscattered echoes. Both systems measure range and angle of samples collected over the across-track going outwards from transducer.

An interferometer measures the angle of the received backscattered wavefront in a time of arrival sequence of samples. The slant range is calculated from the travel time and the sound velocity in water. Angle and slant range is used to produce coordinates in depth and horizontal range. An interferometer can measure angle and range for all the received signals, so resolution can be much higher than with conventional beamformers.

A beamformer measures the range to the bottom on each of a set of formed beams.

To summarise, beamformers measure range for each of set of beams at a known angle, and interferometers measure angle for each set of ranges.

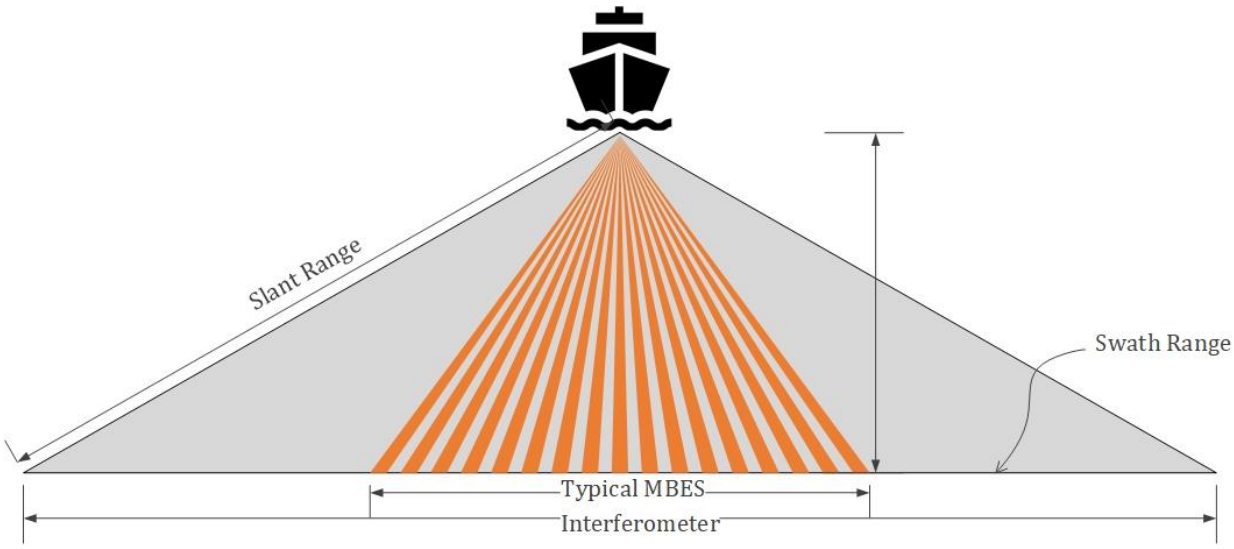

Figure 7. Interferometric vs Beamformer multibeam *sonars [4]*

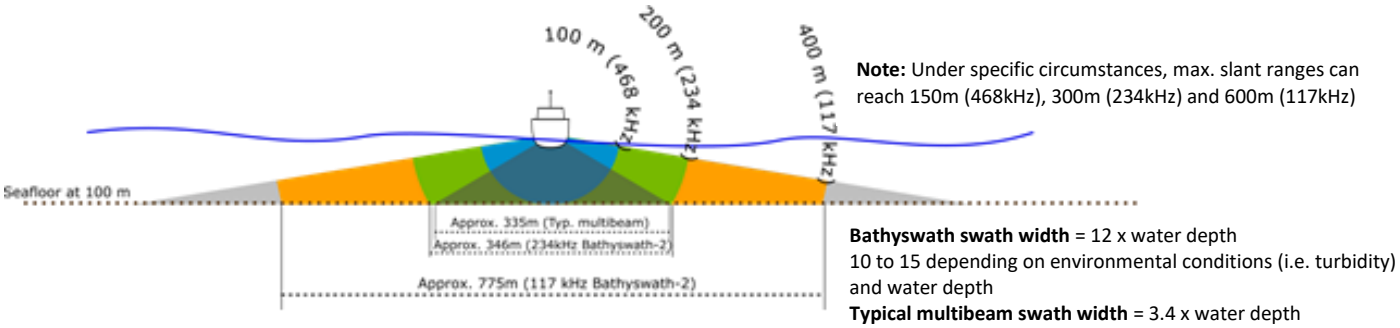

Figure 8. Swath width Comparison of Beamformer and Bathyswath-2 Interferometer [4]

A typical beamformer has swath width 3.4 times to water depth, where an interferometer can achieve swath width 15 to 20 times to water depth. A multibeam sonar system has low angular resolution due to the fixed number of beams, but it is preferable while seeing a complex structure. An interferometer can only measure one angle for each step-in range, creating “range ambiguity”.

Some authors propose to use both multibeam and interferometer on a single vehicle, where multibeam will serve as the gap filler for the interferometer. Such setup will benefit from the wide swath range as well as sufficient data at nadir region of the interferometer. The nadir gap is one of the drawbacks of using interferometry method of bathymetry. A fusion algorithm can be used to extract the highest quality data from the overlapped data [5].

2.4. Bathyswath

The Bathyswath system is a direct decedent of the first commercially available interferometer, which was designed at Bath University, UK. It is manufactured by ITER Systems, France. Most of the material used in this research is provided by ITER Systems, including the sonar transducer and electronics.

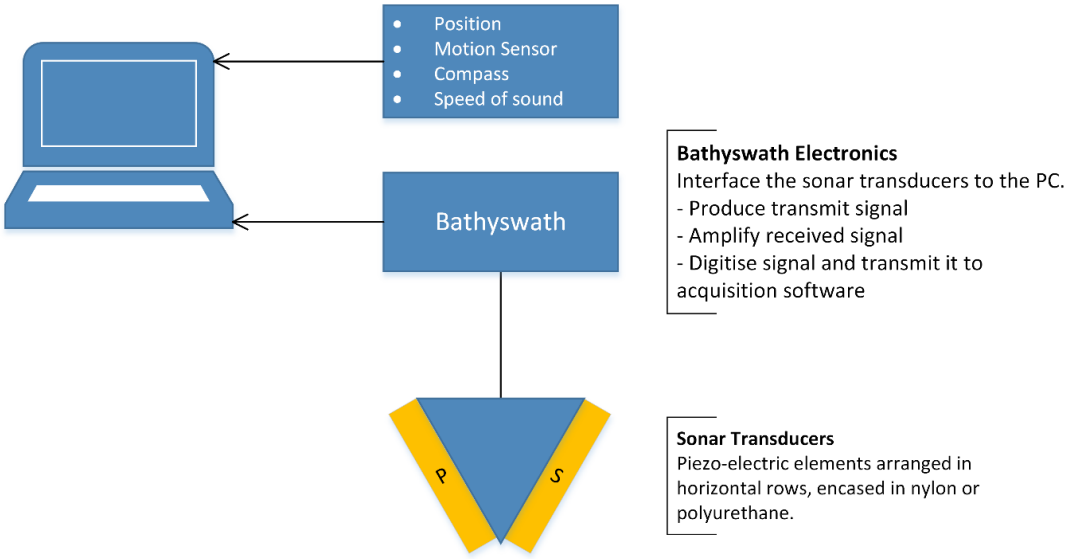

Figure 9 Bathyswath System Setup

2.4.1 Transmitter Design

Transmitter design plays a big role in the advancement of this research. The transmitter must be able to provide a train of pulses, optionally selected from a set of waveforms e.g. CW, LFM, EFM, etc. A classical class-D amplifier design is used to generate those pulses.

Figure 10 represent the summarised version of a sonar transmitter design. Here we take the reference of Bathyswath internal design documents.

- FPGA
    - Interface between Power Amplifier and Software controller
    - Waveform generation (gate signals for class-D amplifier)
    - Real-time waveform parameter controller
- Power Amplifier
    - Boost convertor to generate high energy for transmission
    - Class-D Amplifier for PWM modulated transmit pulses
    - Matching transformers for optimum energy transfer between electronics boards and transducer

For this research, we will be mostly working on the waveform generation part, which can be altered in the firmware without having any hardware changes (Highlighted components in Figure 10)

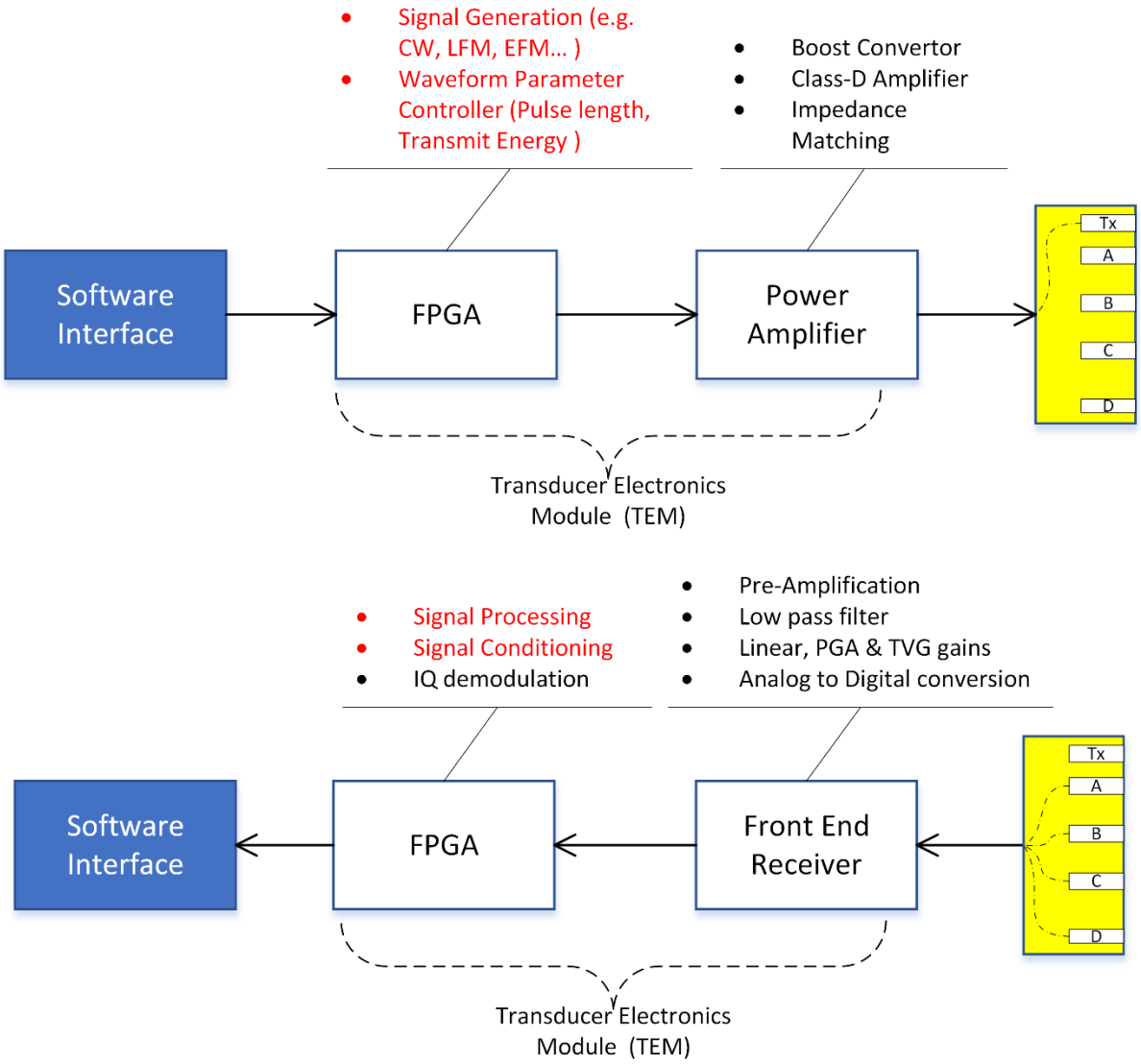

Figure 10 Bathyswath functional block diagram and the R&D works done in this thesis

2.4.2 Receiver Design

A Bathyswath sonar transducer consists of four receiver channels. An acquisition board, also known as Transducer Electronics Module (TEM), does all the necessary computing for the acquisition. A TEM consists of an onboard FPGA, which generates the transmit pulse sequence for the power amplifier (Figure 11) and receives the raw backscattered data, filters and amplifies it as per requirements, digitises it, adds timestamps and then forward it to a personal computer (PC). The current production Bathyswath system detects all the echoes over the noise floor as backscattered data points and the then the interferometry method is applied in software (Bathyswath Swath Processor, provided by ITER systems). For simplicity in this work, the Bathyswath acquisition software is only used to store the raw data in IQ format, and then all the

algorithms were implemented in MATLAB. This thesis work is focused on the components highlighted with red in Figure 11.

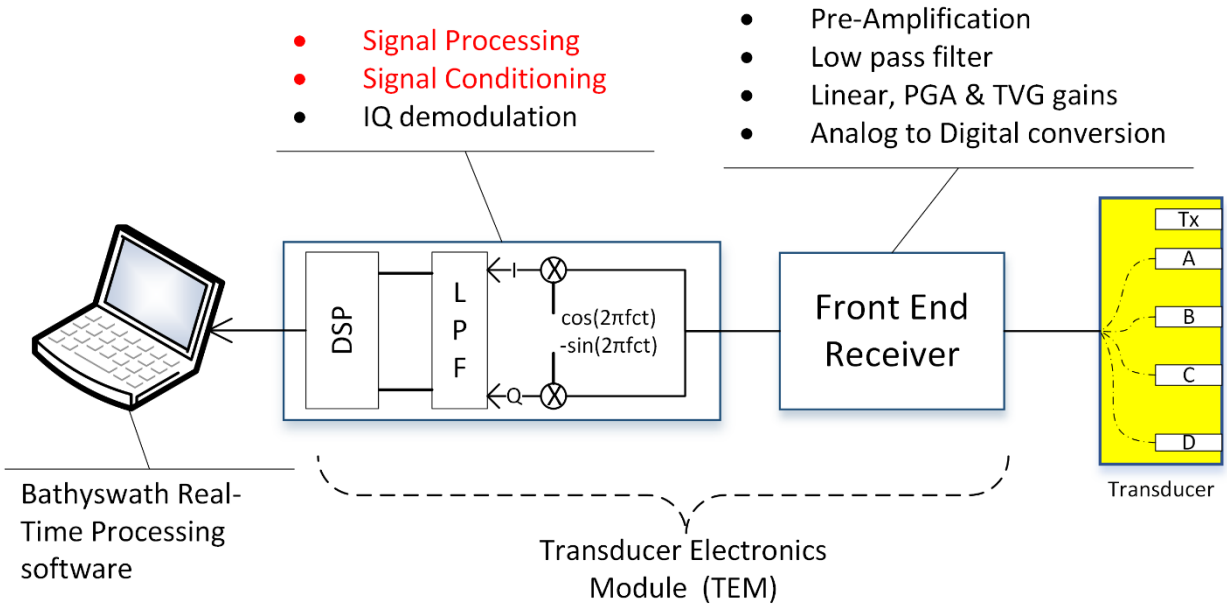

Figure 11 Receiver architecture used by Bathyswath; this work is focused on the components in red

2.5. Motivation of this Work

2.5.1 Range – Resolution Trade-off

Bathymetry maps are more precise when the number of depth measurements per seabed surface unit is high. For a sonar or radar system, the ability of a sensor to detect two neighbouring objects (targets)independently from each other is called resolution. For bathymetry sonars it is also known as across track resolution, and it can be given by the minimum distance between two detected points on seabed. The ability to distinguish targets that are at the same angle but at different ranges is called range resolution. For an imaging sonar, range resolution is an important quality criterion. Survey data standards such as IHO S44 define a minimum detection resolution, which can be interpreted as sounding density. IHO S44 Special Order requires the detection of a cube one metre by one metre. Hydrographic organisations interpret this is requiring 9 soundings per square metre [1].. This must be after filtering, so the processing gain that can be obtained by spatial filtering is limited by this requirement. Hence a higher spatial resolution is desired to achieve these industry requirements.

The along-track resolution of an interferometer comes from the beam width, pulse repetition frequency and vessel speed.

Range resolution mostly depends on the width of the transmitted pulse and the receiver parameters and efficiency; these depend on the sonar frequency used. Higher frequencies have better resolution due to a smaller wavelength and smaller sampling interval. A smaller wavelength results in a smaller transmitted envelope, although generally wavelength is much smaller than the limits, such as the required sampling period. However, a higher frequency system has a shorter range due to higher absorption loss in the water. A longer range can be achieved by using longer pulses but then we must trade off with the range resolution of the system.

Section 5.1.1 of Chapter 5 gives a detailed explanation of range-resolution trade off problem in sonar systems, with an assessment of different types of signals.

2.5.2 Angular Measurement Uncertainty

One of the contributions of this thesis work is to model the different noise sources affecting bathymetry measurements. Most of the noise model estimations stand true for both bathymetry techniques, beamforming (MBES) and interferometry. But our focus will be on the noise factors for interferometry only. There has been lots of work done for MBES error modelling but few for interferometers. We demonstrate that how the overall performance can be improved with wideband signals and processing techniques and their limitation.

2.6. Chapter Summery

In this chapter, we have described the state of art techniques used for interferometers, and explored underwater acoustic wave propagation. This helps us to understand better the functionality of a system, and we introduced the major problems faced by an interferometer to get a high resolution and an accurate bathymetry measurement. In the next chapter, we will start with the range-resolution trade off in classic CW systems and explore the different noise sources which degrade the bathymetry quality. A wideband approach to overcome these problems and the limitation with pulse compression technique are explored in the following chapters.

CHAPTER 3 BASICS OF SIGNAL PROCESSING METHODOLOGY AND EXPRIMENT

3.1. Interferometry Method

The previous chapter presented the two main methods for seafloor mapping. In this work, we focus on interferometry.

Figure 12 shows a basic setup for an interferometer. A set-up with two receivers is enough to demonstrate the basic interferometry method. However, more receiver pairs are used with Bathyswath, to improve the measurement accuracy (discussed later in next chapter). Let's consider that receiver-***A*** and receiver-***B*** are separated by a distance ***d*** and backscattered echoes are coming in from a direction of **θ** from transducer axis.

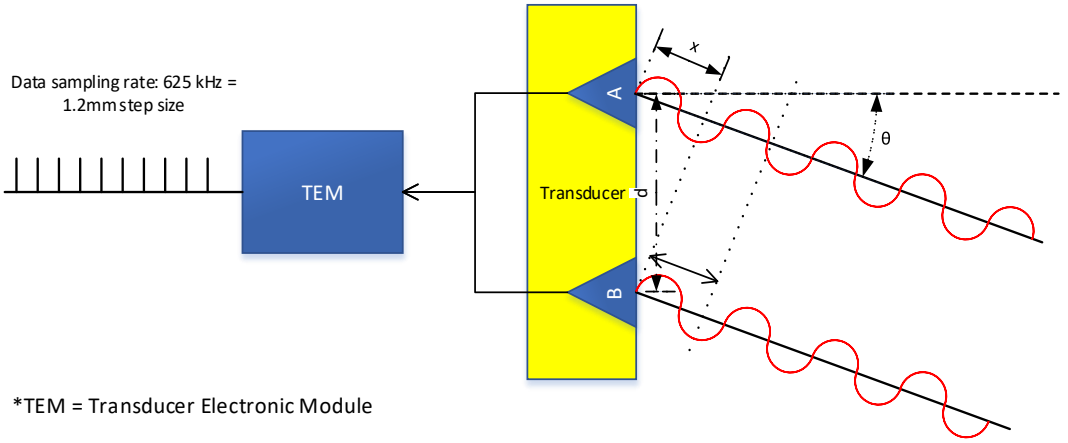

Figure 12. Basic setup of interferometry data acquisition

The angle of arrival can be written as:

$$\theta = arcsin\left(\frac{x}{d}\right) \qquad 3.1$$

Phase is the distance along the wavelength so phase difference can be written as:

$$\Delta\varphi = \frac{2\pi}{\lambda}\, x \qquad 3.2$$

From 3.1 & 3.2, the angle of arrival can be written as:

$$\theta = arcsin\left(\frac{\Delta\varphi}{2\pi}\frac{\lambda}{d}\right) \qquad 3.3$$

The transducer can be designed with the spacing relative to the sonar wavelength. I.e., a relative separation between receiver of $d' = \frac{d}{\lambda}$

This gives us the basic interferometric equation:

$$\theta = arcsin\left(\frac{\Delta\varphi}{2\pi\, d'}\right) \quad 3.4$$

If S_a and S_b are received backscattered signals at receiver A and receiver B respectively, which are separated by *d* distance, then the interferometry term can be written as $S_a S_b^*$, where * denotes the conjugate of complex signal.

Hence, the phase difference of interferometry term can be given by:

$$\Delta\varphi = arg\{S_a S_b^*\} \quad 3.5$$

$$\Delta\varphi = k\, d\, sin(\theta) \quad 3.6$$

where k = 2π/λ is known as the wavenumber and $d = d'\lambda$ is the spacing between receive pairs. The wavelength (λ), is computed from the sonar frequency (set in the electronics) and the sound velocity (SV) at the transducer, which needs to be measured at the time of bathymetry measurements (explained in 4.2.2).

Obviously, an accurate estimation of the phase difference between the received signals is required for a good estimation of an angle of arrival. A central solution for accurate phase estimation is the matched filter, which is described in the next section.

3.2. Matched Filter

Matched Filter (MF) is widely used with radar and sonar systems for signal detection from noisy received signals. It improves the signal to noise ratio of the desired received signal. The output of a matched filter is obtained by correlating a known signal (emitted signal or estimated emitted signal) with the unknown or noisy signal (backscattered echoes from seabed).

The Matched Filter is a linear time invariant (LTI) system, so the output of filter is convolution of input signal and impulse response.

$$y(t) = s(t) * h(t) \quad 3.7$$

$$y(t) = \int_0^t x(\tau).h(t-\tau)d\tau \quad 3.8$$

For a discrete system, it can be expressed as:

$$y[n] = \sum_k x[k]h[n-k] \quad 3.9$$

In detection theory, when the output of a Matched Filter exceeds a defined threshold, that counts as the received echo from the target. And using the propagation delay and the SV (Sound Velocity) we can estimate the slant range of the target (seabed

in our case). A Matched Filter correlates the received signals with a stored replica or estimated replica of the reference signal (transmitted signal in our case).

In the underwater propagation environment, where the propagation loss is high, the backscattered echoes are very weak, so a linear filter that can maximize the signal to noise ratio is highly desirable. This is done by matching the received signal with a reverse conjugate copy of the transmitted signal. The impulse response of the filter can be given by:

$$h(t) = \overline{s(-t)} \qquad 3.10$$

n(t) is an additive noise term, and δ_T is the delay operator.

Average input signal power over a pulse duration T is given by

$$S_i = {}^{E}/_{T} \qquad 3.11$$

The matched filter input SNR is given by:

$$SNR_i = {}^{S_i}/_{N_i} \qquad 3.12$$

If the matched filter receiver bandwidth is denoted by B, then the noise power within the filter bandwidth is given by:

$$N_i = 2B.{}^{N_0}/_{2} \qquad 3.13$$

Using the above equations:

$$SNR_i = \frac{E}{N_0 BT} \qquad 3.14$$

The output signal to noise ratio can be given as:

$$SNR_0 = \frac{|y_s|^2}{N_0} \qquad 3.15$$

y_s is the desired signal and the noise power spectral density can be written as N_0.

The increase in output SNR over the input SNR can be given by:

$$\frac{SNR_O}{SNR_i} = 2BT \qquad 3.16$$

The term BT is referred as the “Time-Bandwidth Product” of a matched filter. The output SNR is increased by factor BT over the input SNR, so it can be called filter gain or processing gain for sonar equation. For narrowband (CW) pulses the BT tends to unity, but it can be increased by using wideband modulated pulses.

Figure 13 presents the backscattered signal from a water tank experiment (discussed in next section 3.3.1).On left we have the received backscattered signals with CW and FM transmitted pulse and on right the matched filter output of these received signals. Experiment setup and measurement parameters used in this figure are discussed in next section and chapter 5.

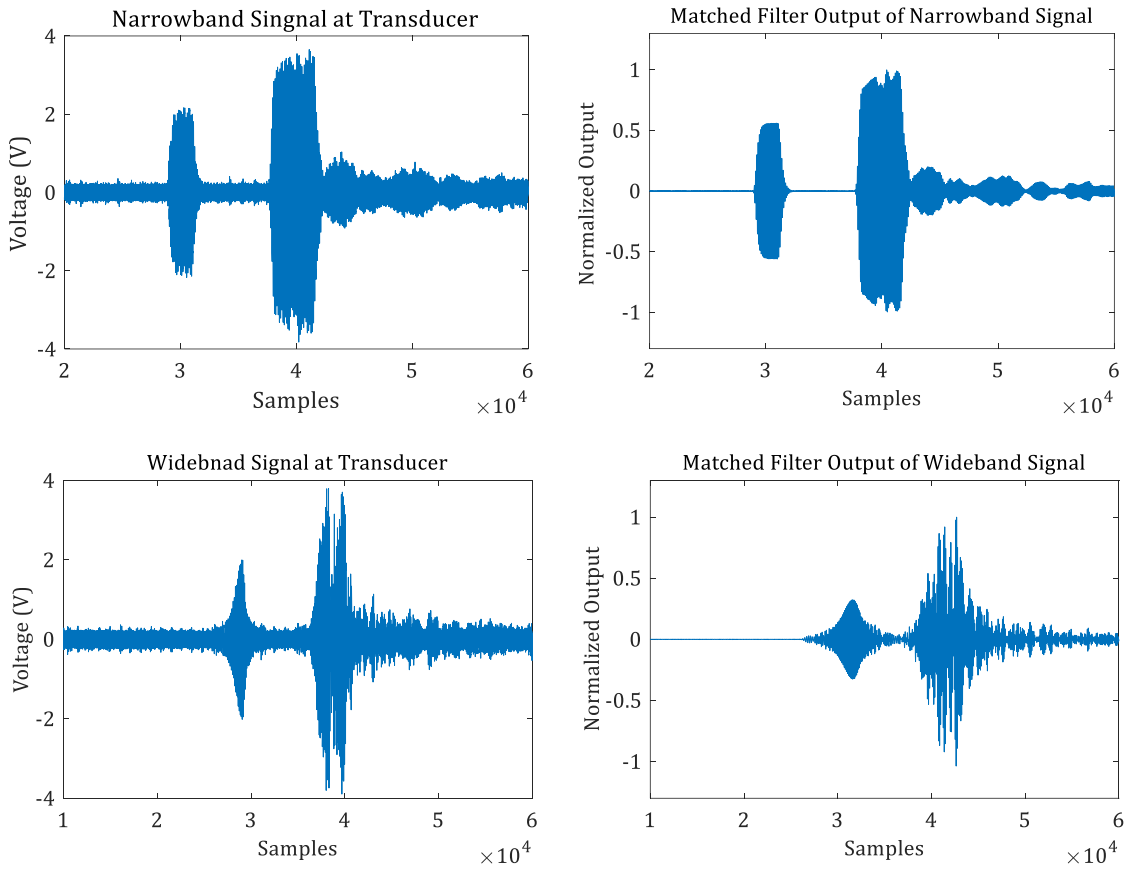

Figure 13 Matched filter examples with narrowband and wideband signals

To conclude, a matched filter is a linear filter used to maximise the output signal to noise ratio in active systems where we have prior knowledge of received backscattered signal shape, considered as a delayed transmitted signal. If the receiver’s transfer function is perfectly matched to that of the backscattered echo, then the processing gain is equal to the time-bandwidth product (BT), otherwise processing gain becomes smaller than BT.

For the design point of view, a matched filter can be implemented using the properties of Fourier Transform. Taking Fourier Transform of equation 5.1:

$$FFT\{s(t) * h(t)\} = S(f).H(f) \qquad 3.17$$

where "*" operator symbolically represents convolution and "." represents multiplication. The matched filter output can be recovered by taking the inverse FFT of the output of the multiplier:

$$y(t) = FFT^{-1}\{S.H\} \qquad 3.18$$

Figure 14 presents implementation of a Matched filter using FFT. This design can be implemented in an FPGA using "off the shelf" intellectual property (IP) blocks.

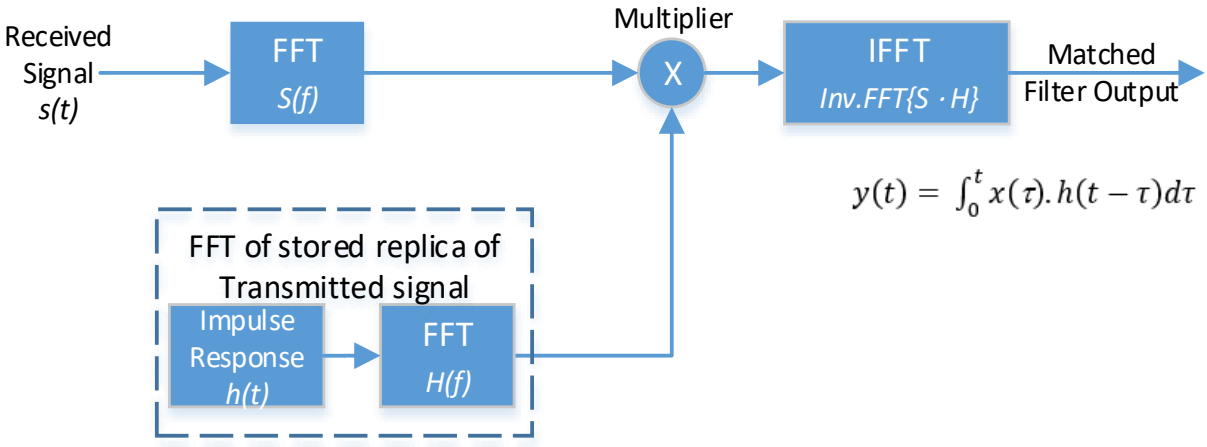

Figure 14 Matched Filter implementation using FFT

Matched filter designs can be improved for our applications, and this is discussed later in this research work. A pulse compression technique is later elaborated in the range resolution section, which is based on the use of a matched filter with wideband signals to improve the spatial resolution of sonar.

3.3. Experiment Setups

Before continuing further with refining the design, we validate the hypotheses above by experiment. Since this research work was supported by the ITER Systems, we had full access to sonar equipment for experiments. It allowed us to collect data in different setups to understand better the interferometer's functionality and try out new ideas to improve it.

3.3.1 Water Tank Setup

The first experiment setup is set indoors in a small water tank of 2 cubic metre size. A Bathyswath V1 transducer is used for these experiments. This has four receive staves and one transmit stave, with a resonant frequency of 468 kHz. It is fixed to one wall of tank with 30° of tilt angle, looking outwards and downwards. This is the most

common mounting configuration for an interferometer. In the picture below, the whole system is rotated by 90°relative to a boat scanning the seafloor.

A ladder shaped target was placed in front of transducer face at 60cm distance. The target is made of adjustable cylindrical rungs with 28mm diameter. These rungs can be moved to increase and decrease the separation between them. Minimum possible separation between rungs is 1cm. Unused rungs are covered with sound absorbing foam to reduce the interference.

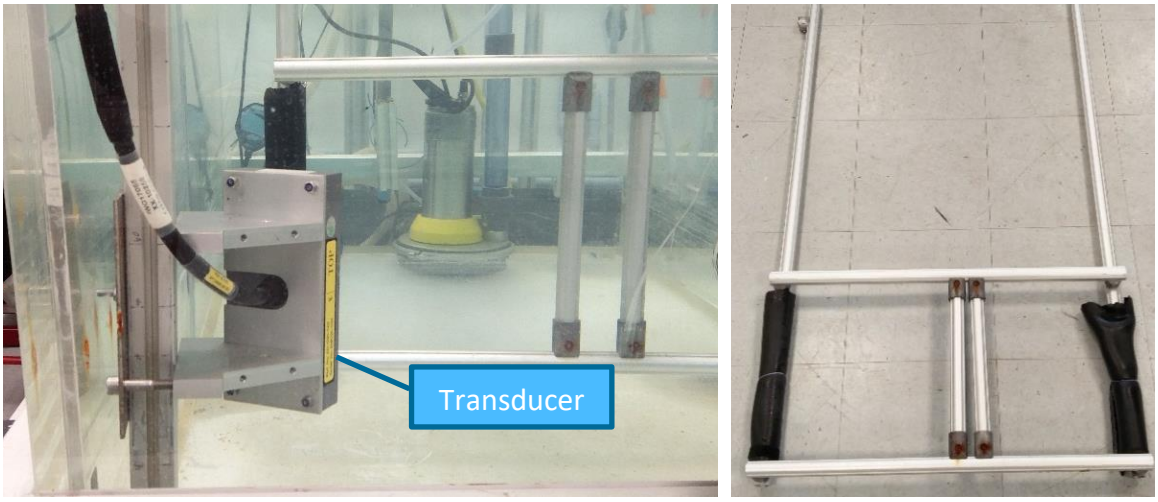

Figure 15 Experiment setup–1: Water tank Setup

3.3.2 Pontoon Setup

To get closer to the real environment we installed a fixed setup on a pontoon in Lake Annecy. Here, the water depth under the transducer is quite shallow, around 1.3 metres at the time of the experiment, and it is fairly flat for few metres. We installed a single transducer of 234kHz resonant frequency looking outwards into the lake. A sound velocity profile was taken at the time of the experiments.

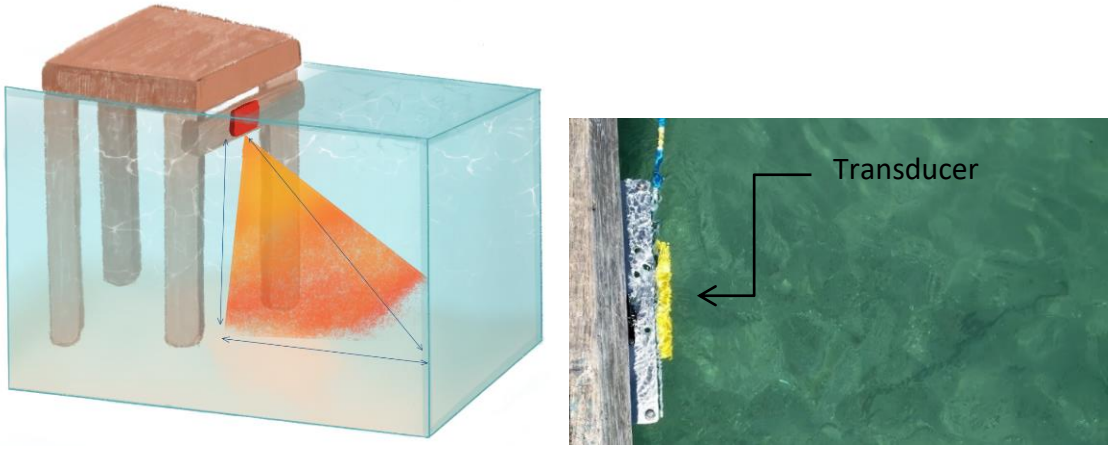

Figure 16 Experiment setup-2: Pontoon setup, depth under transducer is 1.5m

3.3.3 Boat Setup

Figure 17 shows a complete surveying setup installed on a small boat, deployed in Annecy Lake. The system used here is Bathyswath-2 SU, which is integrated with necessary ancillary devices: GNSS, INS, SVS, etc.

Figure 17 Experimental Setup-3: Boat setup used for the experiments

All these experimental setups have been used to validate step by step the methods developed in this thesis and to assess the performances of the bathymetry estimation. The theoretical criteria are discussed in the next chapter.

This page is left blank intentionally

CHAPTER 4 BATHYMETRY QUALITY ESTIMATION

In this section we will elaborate the different problems and issues related to bathymetry measurements using interferometry techniques, which direct the way we concentrated our researches. Some of the problems are also true for other bathymetry measurement techniques but we focus here on the interferometric technique. Bathymetry degradation causes can be divided into the following categories, and are discussed further in the sections and the sub-sections of this chapter

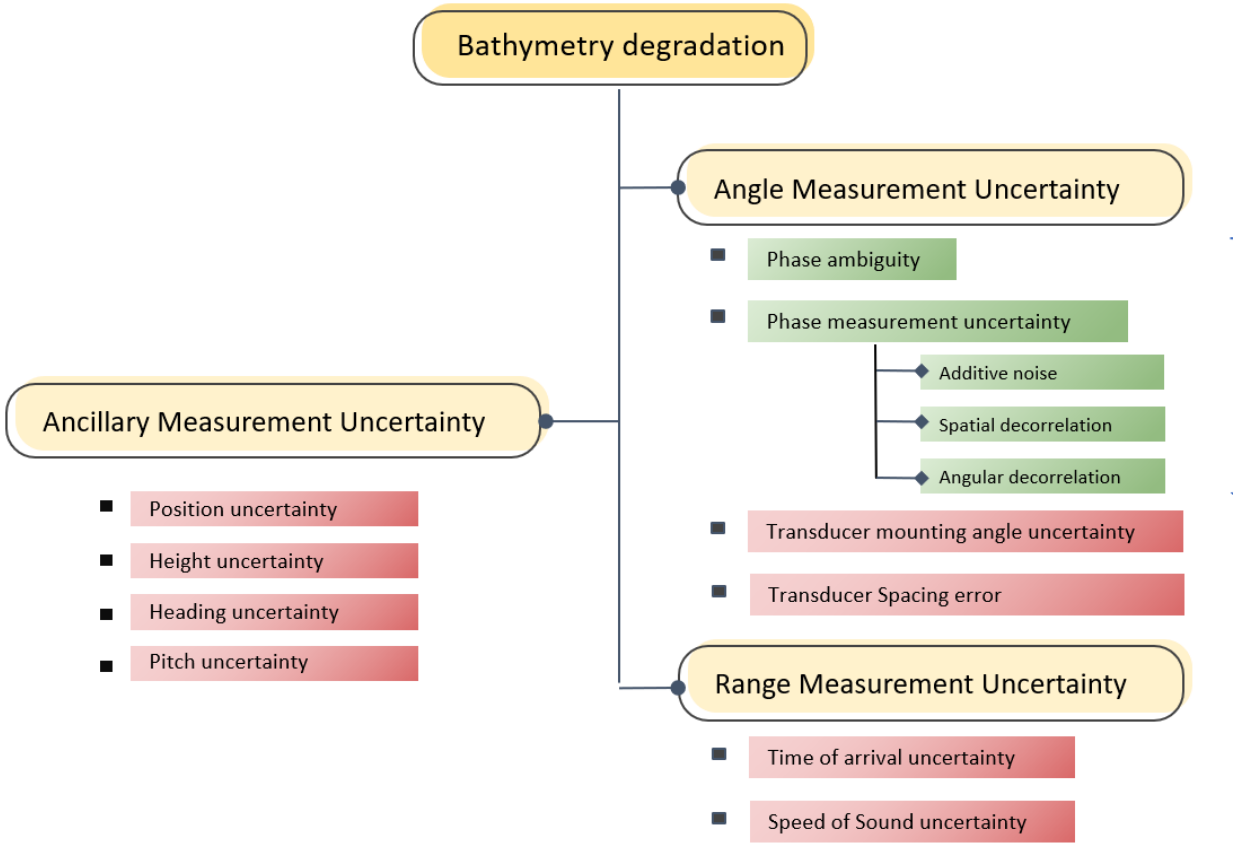

Figure 18 Bathymetry Degradation Sources

Figure 19 presents the uncertainty in bathymetry data collected with the Bathyswath interferometer (Experiment setup: Boat, see 3.3.3). Different coloured lines present the uncertainty taken from the different sets of samples. The depth under the transducer is around 1.5 metres, giving us an across track distance of 15 metres on each side of vehicle. These uncertainties can be related to the chart above and can be estimated separately.

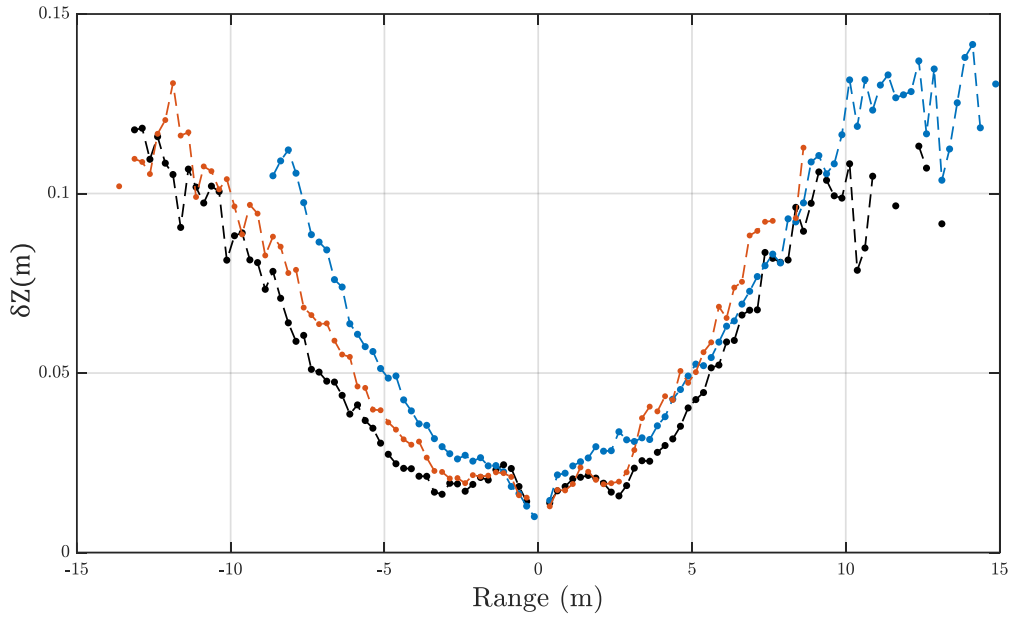

Figure 19 Depth uncertainty measured for different profiles of a shallow water survey (Data courtesy: ITER Systems)

We won't be discussing much about the ancillary measurement uncertainties, and will concentrate on bathymetry degradation causes from the signal processing point of view. Our main goal here is to study different bathymetry degradation causes and how they can be improved by signal processing techniques.

4.1. External Measurement Uncertainty

To complete a survey, a sonar system is usually equipped with ancillary devices, such as:

- GNSS (Global Navigation Satellite System) for position measurement
- IMU (Inertial Measurement Unit) for roll and pitch measurements
- SVP (Sound Velocity Profiler) for sound velocity measurement in the water column
- Compass for heading measurement; a dual antenna GNSS setup is also used to measure the heading of the surveying vessel

Final bathymetry accuracy can be degraded if any of these measurements are uncertain. We won't be discussing the effect of ancillary devices measurement uncertainties, because all the external bathymetry degradation causes are independent of the signals used or the processing techniques used.

4.2. Range Measurement

Rage measurement can be affected by the measurement uncertainty in Time of Arrival (ToA) and uncertainty in ray tracing the propagation path, which depends on the measurement accuracy of sound velocity in water column.

4.2.1 Time of Arrival Uncertainty

The measurement accuracy can be affected by the system's ability to measure the time of arrival at reception.

The ToA error due to shift in footprint can be given by:

$$\delta t = \frac{2\,\delta x}{c} sin\,\theta \qquad 4.1$$

Where, δx is the shift in footprint sue to time of arrival uncertainty

$\boldsymbol{\Theta}$ is the angle of arrival at transducer and $\boldsymbol{c}$ is the speed of sound.

Technological advancement in recent years gives us accurate digital measurement equipment and components, providing accurate temporal measurement.

However, fixed shifts in time are more common. For example, a) filters can introduce a fixed time delay b) timing is usually from the start of the transmit pulse, so we need to subtract half that to get to the distance of the centre of the pulse's footprint on the bottom, c) wideband processing can add more time delays. We consider that all these timing errors are taken in the account and thus, we won't be considering uncertainties due to ToA measurement errors

4.2.2 SV measurement Uncertainty

From the measurement point of view, there are two parts to SV correction: calculating the angle of arrival, and computing the refraction and range changes from the SVP. The correct wavelength (λ) used in the interferometry equation (section 3.1) is computed from the sonar frequency used by hardware and the SV (Sound Velocity) at the transducer.

A sound velocity profile is necessary to model accurately the sound propagation from transducer to sea-bottom and vice-versa (see Annex A for more details). The accuracy of those measurements directly affects the depth measurements so it is important to use a highly accurate sound velocity profiler and the measurements should be taken often during a survey. Sound velocity changes with water depth due to changes in temperature and salinity. Both of those change with time and location. Not only do SV profiles cause angle errors through refraction, but also through change in range due to

changing SV along the path of the sound “ray”; the ray-tracing process must take account of both effects. The measurements done in this research work are in shallow water and a single sound velocity was measured at the level of transducer.

4.3. Angular Measurement Uncertainties

The angular accuracy of a sonar system can be related to many factors. The ability of interferometers to measure angle accurately depends on the following factors:

- Transducer manufacture accuracy
- Hardware calibration accuracy
- Phase measurement accuracy

4.3.1 Transducer Manufacturer Accuracy

Angle measurement accuracy of a sonar can be directly related to the transducer manufacture accuracy. As an example, the accuracy of transducer manufacture provided by the supplier is $\delta d_{txer-err} = 0.2 * 10^{-3}$metres [16].

The final measurement of elevation angle is done using the widest receive pair spacing. For a spacing of N wavelengths (N*λ), there are N phase – angle cycles for and angle jump of 90° (See Figure 22). Each phase – angle cycle gives an angular sector of 90/N. An error in spacing probably due to manufacturing accuracy limitation gives a proportional error across this angular sector.

Taking Figure 22 as an example, where the widest spacing is 8.5λ, the error due to manufactured spacing can be given by:

$$\delta\theta_{txer-err} = \frac{\delta d_{txer-err}}{d\,.\lambda}.\left(\frac{90^{\circ}}{d}\right) \qquad 4.2$$

where d is the widest receiver spacing (8.5λ) in this case.

For a system operating from 100kHz to 500kHz, the error due to transducer manufacturing corresponds to 0.01° to 0.08°. These frequency dependent spacing errors are smaller than the other errors not related to frequency. They are also constant for any given system, so are systematic errors that can be calibrated out.

4.3.2 Phase Ambiguity

Interferometric technique or phase differencing techniques can be performed using two receive sensors. The interferometric equation (2.3.1) has two major problems while calculating the angle from measured phase difference from a pair of receivers. The receive pair separation, also known as baseline, plays an important role in the measurement accuracy here.

- **Ambiguous Measurements:** If the receive array pair separation is greater than one wavelength of the received backscattered echoes, then the measured phase difference wraps around at least once, so a given phase angle corresponds to more than once elevation angle. Figure 20 [1] represents angle calculated with the interferometry equation using phase differences at two receivers that are separated by one wavelength (1λ). Here the phase difference ramp wraps around at least one time, hence each phase difference corresponds to two angle values.

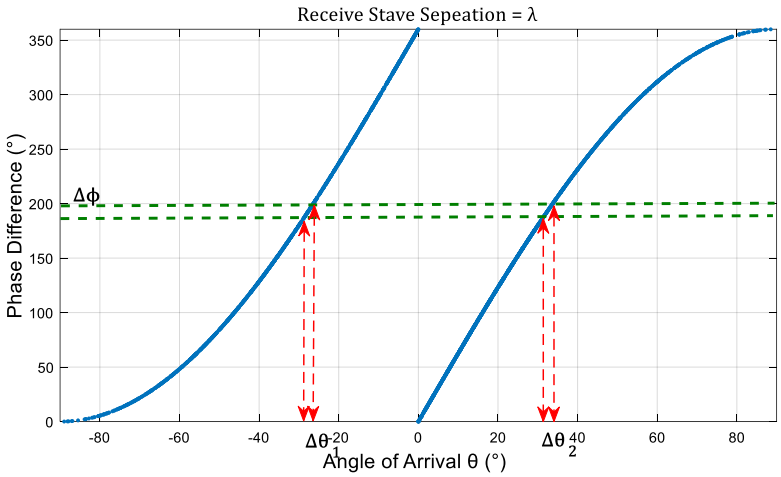

Figure 20 Angle measurements from the phase difference measured at 1λ apart receivers

  - We could get an unambiguous angle measurement (one phase difference measured corresponding to one angle), by reducing the separation between receive staves or using separate staves with smaller separation. Figure 21 shows angle measurement results using half wavelength ($\lambda/2$). And now same phase difference instant ($\Delta\phi$) returns unambiguous angle value ($\Delta\theta$). However, each stave must have a finite height of around one wavelength, in order to get a good response efficiency and a good vertical beam shape, so a half-wavelength separation between them is not possible.

[1] Real experimental data is used here for figures, but the results stands correct for any measured values or simulated values.

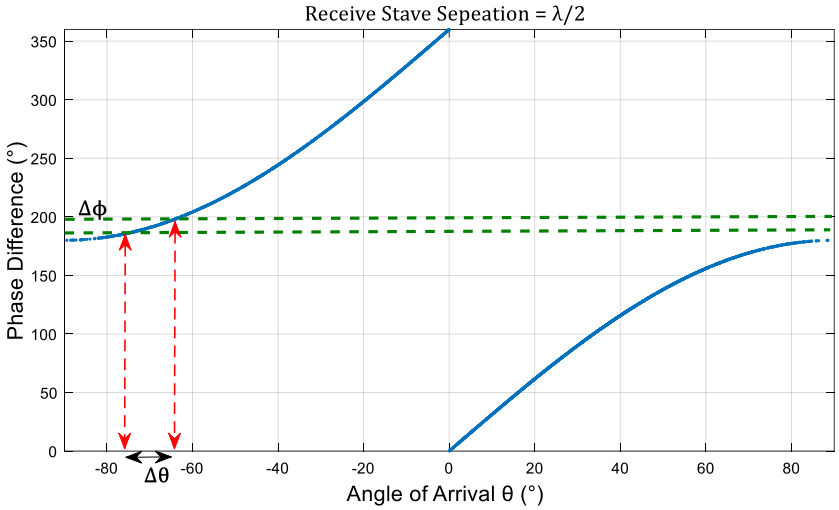

Figure 21 Angle measurements from the phase difference measured at λ/2 apart receivers

- **Measurement accuracy:** By using half wavelength (λ/2) separated receiver pair we do get unambiguous angle calculation but the Phase to Angle curve is very shallow. That means that a phase difference measurement returns a highly uncertain angle value. Measurement errors get worse when going away from the zero-phase-instant (ZPI), normal to interferometry axis. Figure 21 shows that the angle measurement variance ($\Delta\theta$) is much wider compared to Figure 20 for the same phase difference variance ($\Delta\phi$).
    - Now consider a receive pair with separation of 8.5λ, the maximum physical separation for our transducer staves. We notice that the phase to angle curve is quite steep, almost vertical, so the angle is highly ambiguous. In this case there are seventeen possible angles of incidence for a given phase difference value. But if we can resolve which one is the correct one, then due to the sharp relation between phase and angle we can get a highly accurate angle of arrival measurement.

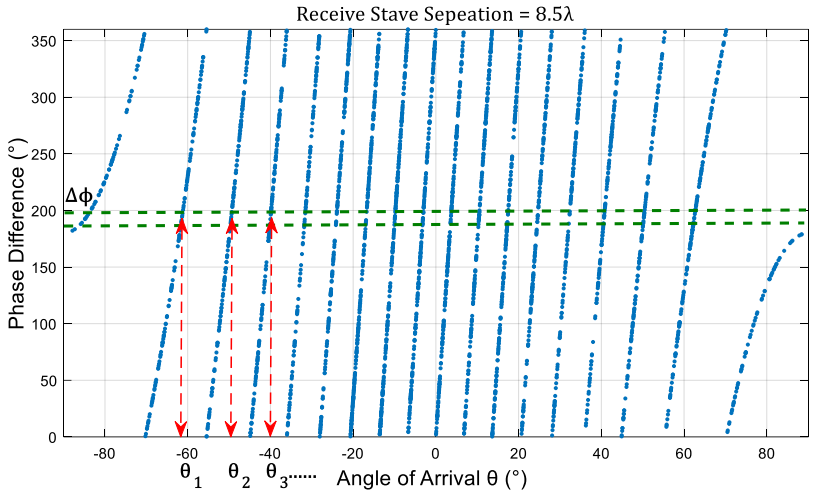

Figure 22 Angle measurements from the phase difference measured at 8.5λ apart receivers

- Figure 23 explains clearly the error associated with closely placed receive arrays for sounding data collected with pontoon experiment (3.3.2). There is no ambiguity while calculating the angle from the phase difference values but the angle gets very noisy. Referring to Figure 24[2], which shows the "false bottoms" at different angle steps, coming from picking up the wrong phase ramp.

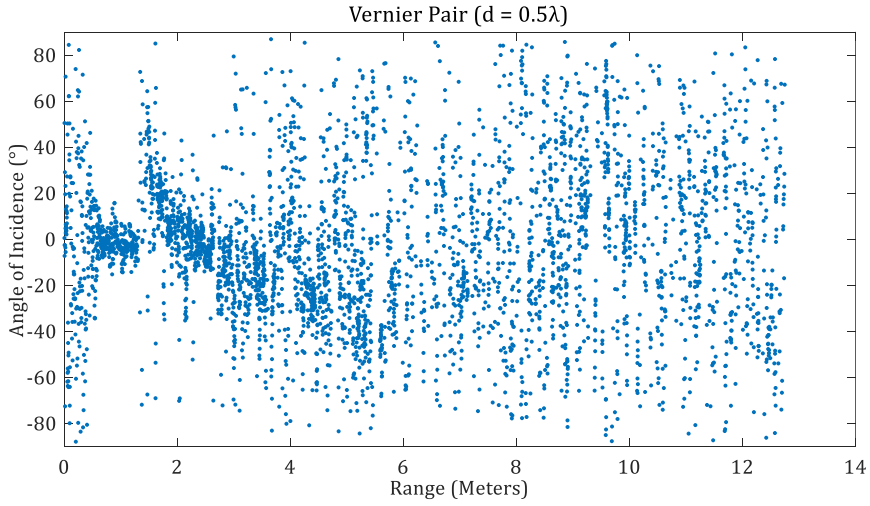

Figure 23 Angle measurements over Range calculated with Vernier pair

[2] The screen capture was taken from Bathyswath Swath Processor software, during a test survey in Annecy lake with the boat setup, as discussed in 3.3.3

In next section we will introduce the Vernier method [19] to solve the phase ambiguity induced measurement errors.

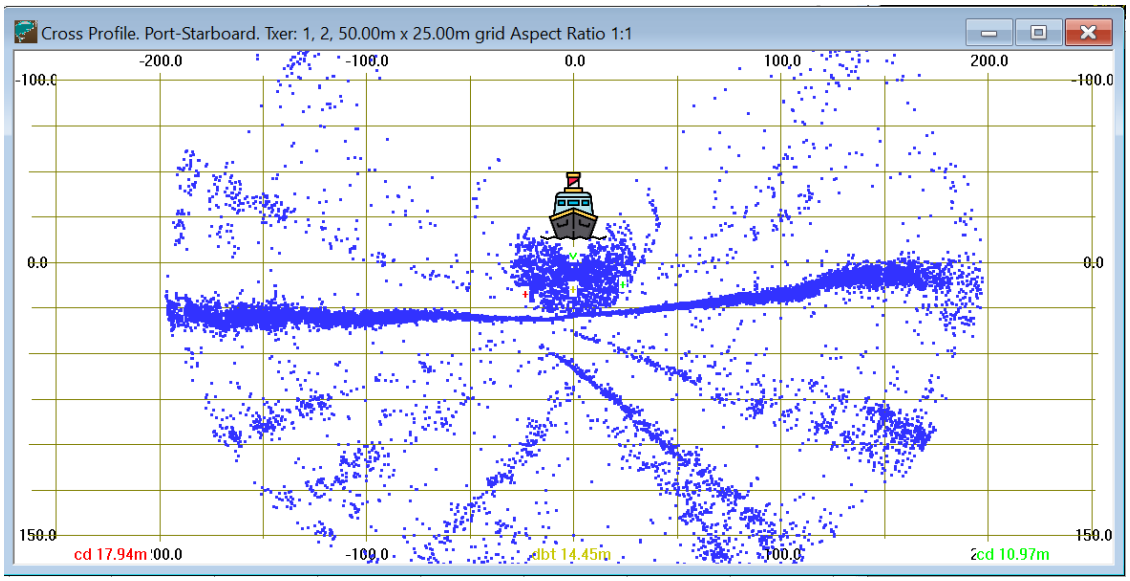

Figure 24 Depth vs horizontal range (Cross Profile), showing false bottom at different angles (picture taken during a test survey in Annecy lake with Boat setup)

4.3.2.1 Vernier Method

As discussed in the previous section the 2π ambiguity is one of the drawbacks of interferometry technique. So, to calculate correctly the angle values we need to find precisely the phase jumps around ±π. One way to solve the ambiguity for a widely spaced receiver pair is by keeping track of the phase jumps and considering the phase jumps are slower than then ambiguous phase ramps. The technique is more complex because we need to have a correct starting point and it is less accurate. Another drawback is that the phase tracking method doesn't work if the signal is lost, for example shadow of a target, then the system loses track and there is a jump in the angle. A more accurate and robust alternative is Vernier method, and we discuss it in this chapter.

The Vernier method is widely used with the interferometry sonar systems to resolve ambiguous phase to angle values. This method was first mentioned in 1982 by Cloet et al. from the University of Bath in context of bathymetric sonar equipment [13]. They used a tow-fish system operating at 303kHz frequency. It used two widely spaced receive pairs, with separation 13λ and 14λ.

The idea is simple and doesn't require extra equipment or changes in hardware. It creates an artificial receiver pair with a small separation by subtracting the phase difference measurements of two pairs [27], [28]. For instance, a 3.5λ and 3.0λ apart physical receiver pair can be used to create a receive pair of 0.5λ pair by subtracting the phase difference from the two pairs. The angle calculated using this artificial pair gives

unambiguous results, although they are quite noisy due to shallow phase to angle ramp (refer to Figure 21). It gives the position of phase jumps, which can be used to select the correct phase to angle ramp for a wider receiver pair.

Figure 25 explains that with increasing receive array separation the number of possible angles of incidence for a given phase values increases. The 0.5λ and 1λ receive pairs are artificially created by subtracting other pairs. Bathyswath-2 transducers have four pair of receive arrays with a maximum physical separation (between top and bottom array) of 8.5λ and a minimum of 2.0λ.

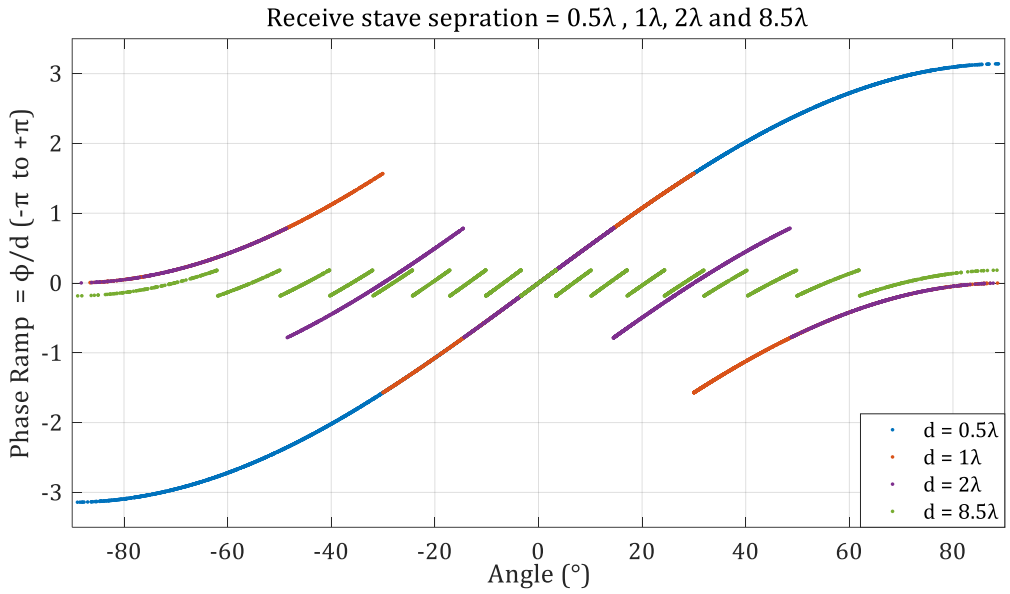

Figure 25. Phase Difference between resulting Vernier pair of 0.5λ, 1λ and Physical receiver pair separated by 2λ and 8.5λ as a function of angle of incidence. Vernier pair 0.5λ is unambiguous.

A successive computation method is used to estimate more accurately the angle from the measured phase values. In this method we start form the least ambiguous pair e.g. a Vernier pair of 0.5 λ separation, and move upwards to the most ambiguous pair (8.5 λ). At each iteration, a more accurate angle is calculated, and the previously measured angle (Vernier pair to start with) lets us choose the correct angle values from the set of ambiguous choices. The process is repeated, until we get the results from the pair with widest separation.

Figure 26 presents the angle values measured from received signals at a pair with 3.5λ separation, before (in red) and after the successive Vernier computation (blue point). Here we demonstrate the successful estimation of phase jumps while having the higher accuracy of measurement from widely separated receive pairs.

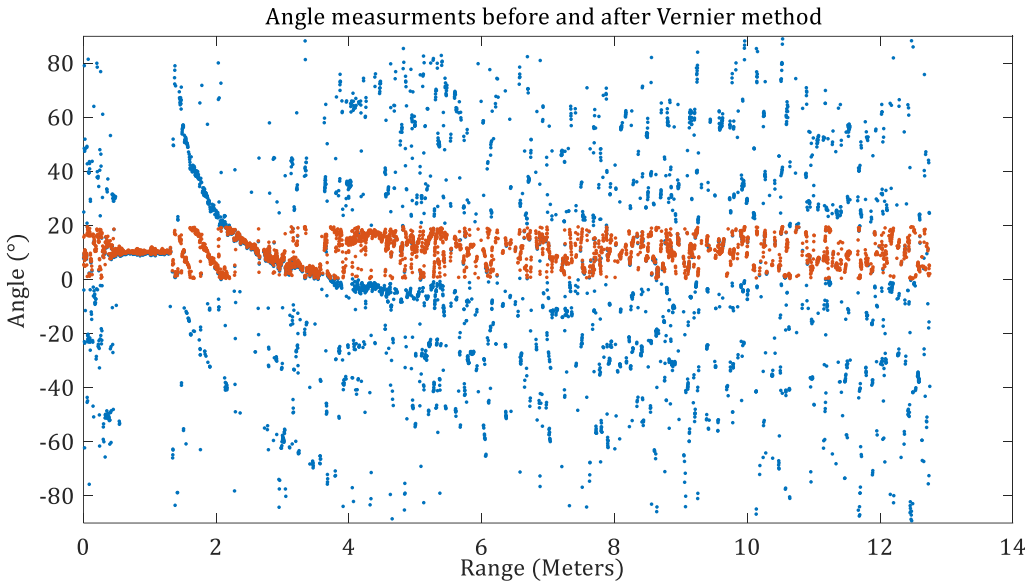

Figure 26 Angle estimation before (red) and after Vernier method is applied

So, we can conclude that by using widely separated receivers (wider baseline) we can decrease the angular measurement errors due to sharp phase to angle curve, but at cost of ambiguous phase difference measurements.

4.4. Phase Measurement Uncertainty

There are several different sources of errors in the phase measuring sonars (Interferometers). The data quality estimation can be computed using estimation of these measurement errors. Phase measurement error estimation is the most complicated one in our case. The Interferometry technique is theoretically quite simple, but the practical realization gets quite complex. The bathymetry accuracy largely depends on the phase measurements, which are quite sensitive. A noisy phase measurement leads to a fluctuating angle of arrival (AoA) measurement and hence inaccurate bathymetry.

Even a highly calibrated system can have noisy measurements due to ambient noise, multipath interference from sea-surface, etc.

A bathymetry measurement error is combination of ToA (time of arrival) measurement error and AoA (angle of arrival) estimation errors.

$$\frac{\delta H}{H} = \frac{\delta t}{t} + tan(\theta + \alpha) \,.\, \delta\theta \qquad 4.3$$

We consider that the time of arrival measurements are sufficiently accurate, and errors from them can be neglected. So, for an angle error δθ, the depth estimation error can be given as:

$$\frac{\delta H}{H} \approx tan(\theta + \alpha)\delta\theta \quad 4.4$$

The phase measurement error is obtained by taking the derivatives of equation (3.6)

$$\Delta\varphi = 2\pi \frac{d}{\lambda} sin(\theta) \quad 4.5$$

Thus, the angle measurement error for our system with d' = d λ, can be written as:

$$\delta\theta = \frac{\delta\Delta\varphi}{2\pi\, d'} \frac{1}{cos(\theta)} \quad 4.6$$

Thus, the relative depth error:

$$\frac{\delta H}{H} = \frac{\delta\Delta\varphi}{2\pi\, d'} \frac{tan(\theta+\alpha)}{cos(\theta)} \quad 4.7$$

where, θ is angle of arrival from the interferometric axis and α is elevation angle of transducer.

From this, it appears that bathymetry measurement can be directly related to phase measurement error and its proportional relation. In this chapter we will discuss the different noise sources in the estimation of the phase ramps, which leads to uncertain depth measurements.

We can write the phase difference measurement error estimation using the approximation given by Lurton [24] & [22].

$$\delta\Delta\varphi = \frac{2}{\sqrt{\frac{12}{\pi^2} + SNR(1 + 0.05\, \frac{SNR}{SNR+1} ln(SNR))}} \quad 4.8$$

Equation 4.8 provides an important relation between the SNR and the phase difference measurement error, which will be used throughout this thesis to calculate the phase difference variance for different noise sources.

From equation 4.7 and 4.8, we can relate the final depth measurement uncertainty (δH) to the SNR of the received signals, discounting other noise sources.

Figure 27 presents depth uncertainties estimated from the pontoon test with different pulse lengths and with and without considering the processing gain of the system. These uncertainties are estimated by calculating the standard deviation considering a flat seabed and averaged for 10 realisations. Later same method will be used to verify the final error model.

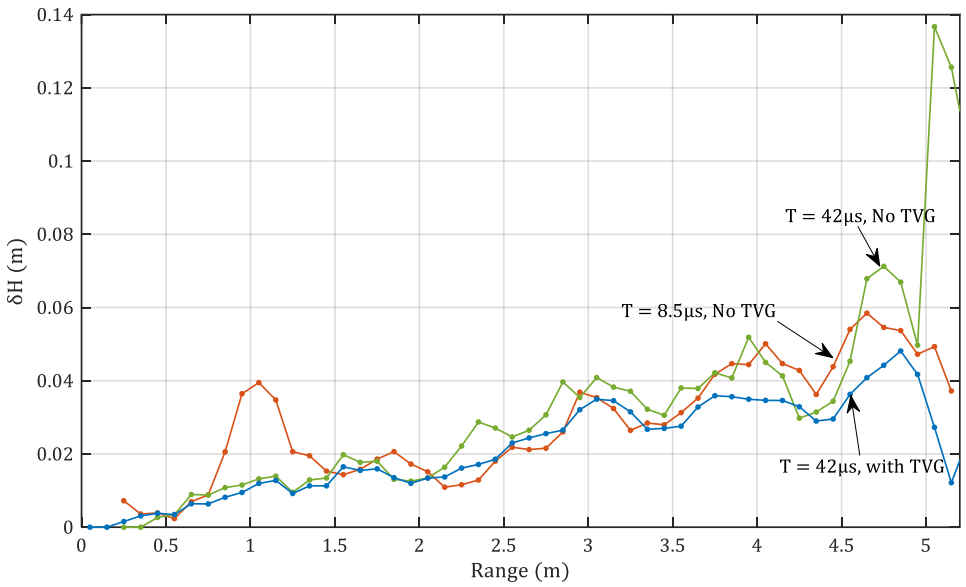

Figure 27 Standard Deviation in depth measurements taken with different transmitted pulse length (Experiment Setup: Pontoon)

4.4.1 Additive Noise

Additive noise plays a big role in limiting the accuracy of interferometric sonars. A wide range is one of the key factors in interferometers and a high additive noise can limit the slant range and reduce the accuracy of angle measurement. Here, we give a quick introduction to the active sonar equation and an estimation to calculate of additive noise effect on bathymetry measurements.

4.4.1.1 Sonar Equation

The sonar equation is a way to understand the different components of a received signals in presence of a noisy environment [17]. The sonar equation relates the received signal at hydrophone to the transmitted signal power for one- or two-way propagation, taking account into the source level, sound spreading, sound absorption, transmission loss, ambient noise, directivity of hydrophone, back scatter strength etc [3].

The sonar equation of the active sonar equation is:

$$SNR = Signal - Noise + Gain$$

$$SNR = SL - 2TL + TS - NL + DI + PG \qquad 4.9$$

Sonar equation Components:

SL	Source Level
NL	Noise Level

Sonar System	DI	Directivity Index
	PG	Processing Gain
Propagation Channel	TL	Transmission Loss
	RL	Reverberation Level
	NL	Noise Level
Target	TS	Target Strength
	SL	Target Source Level

*All values are in dB

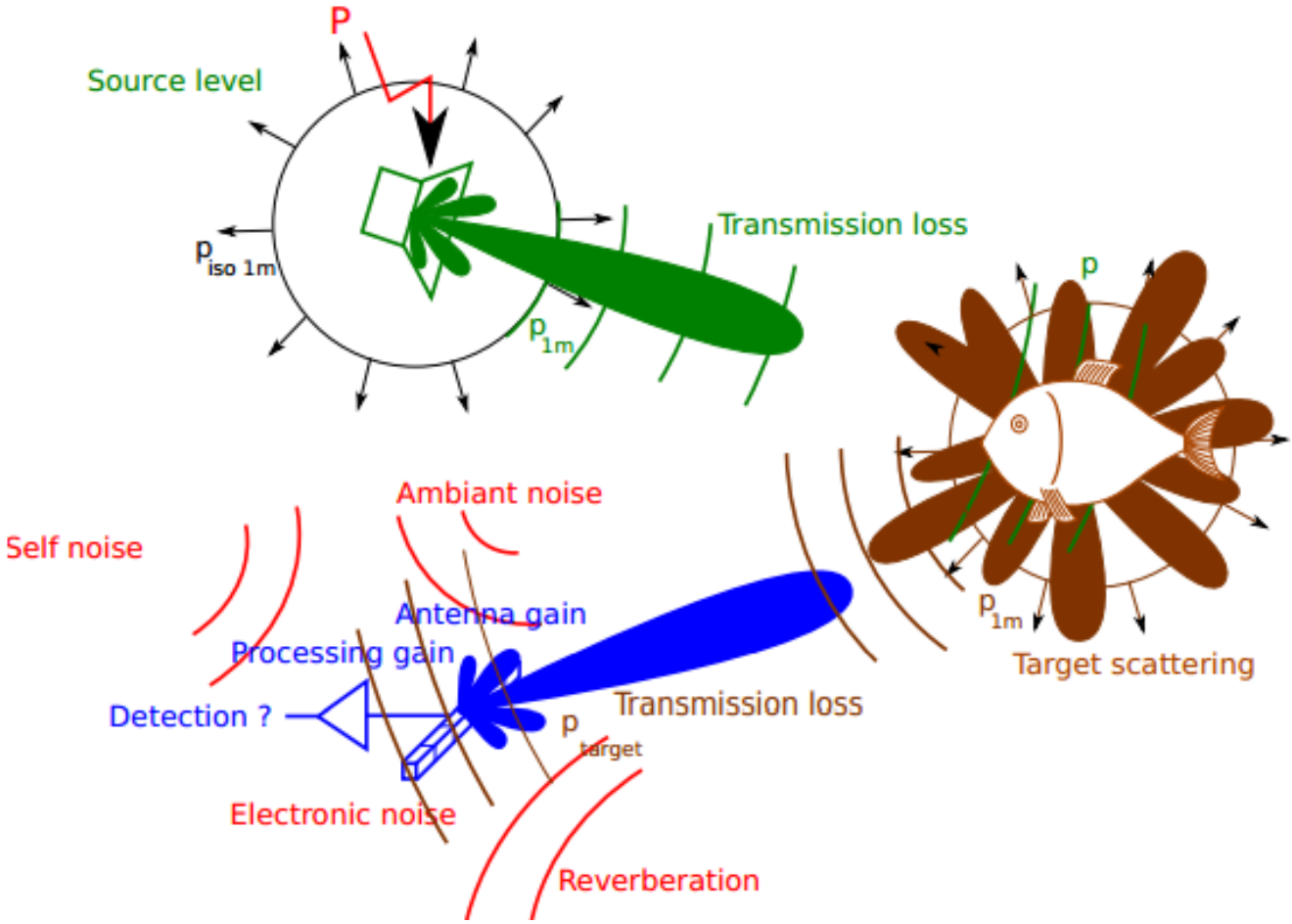

Figure 28 Sonar equation illustration for an active sonar

The individual term of equation 4.5 can be written further as following:

Source Level	$SL(\theta_e) = S_v + 20\,log_{10}(V_{rms})$

Transmission Loss	$TL \approx 20\,log_{10}\,R + \alpha R$
Target Strength	$\mathrm{TS} = \mathrm{BS} + 10\log A$
Noise Level	$\mathrm{NL} = \mathrm{NL}_0 + 10\log_{10}(\mathrm{B})$
Directivity Index	$DI_e = 20\,log_{10}\left(\frac{P_{1m}(\theta,\psi)}{P_{iso1m}}\right)$
Processing Gain[3]	$\mathrm{PG} = 10\ \log_{10}\mathrm{BT}$

Refer to Annex B for the detailed description of each term.

Figure 29 presents the resulting SNR values given by the equation 4.5. The results are given for the two different pulse lengths e.g. 8.5µs and 42µs. It can be noted that a longer pulse has higher SNR especially in the area away from the nadir region[4]. The dotted lines are the taken with the field data, neglecting other noise sources.

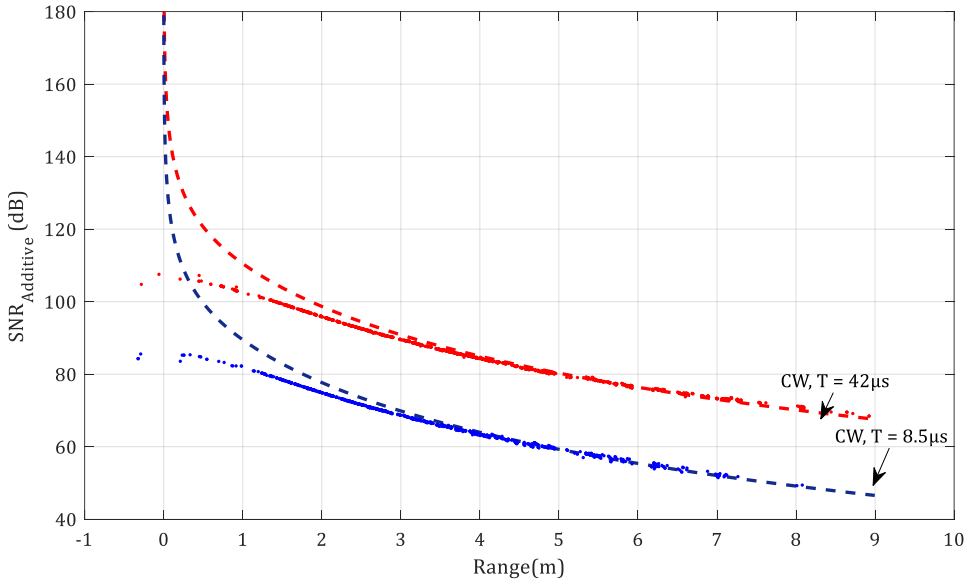

Figure 29 SNR accounting additive noise only, estimated for CW (8.5µs), CW (42.75µs)

Where Figure 30 presents the resulting phase difference standard deviation given over the across track range. With a smaller pulse length, the uncertainties are more dominating at the far range of the swath.

[3] Processing gain for a matched filter is given by the time-bandwidth product (BT), otherwise it depends on the receiver design.

[4] Nadir region phenomena is introduced in the Annex C

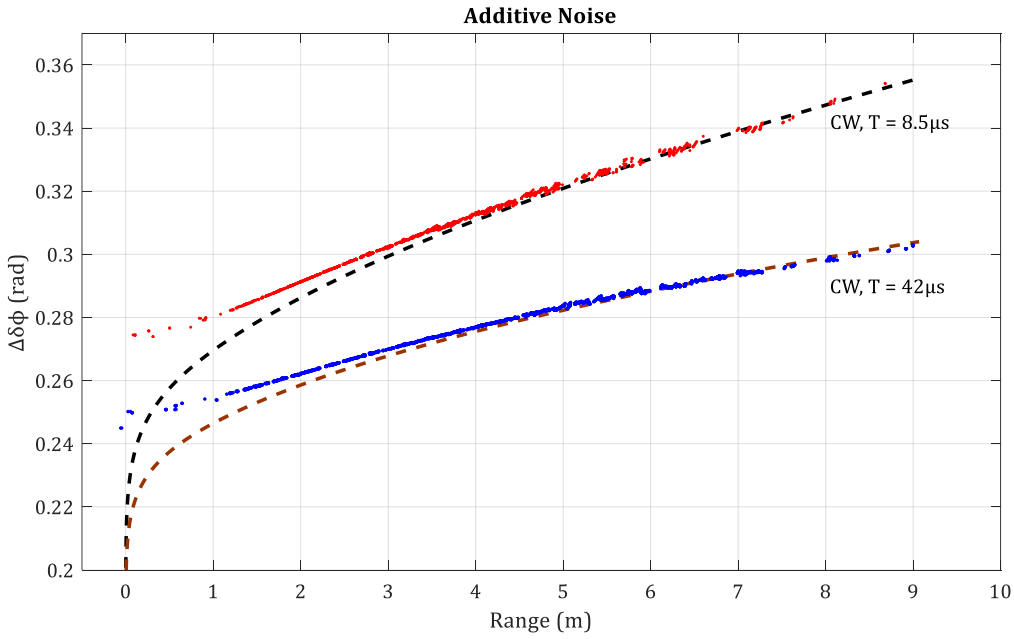

Figure 30 Phase Difference standard deviation for the measurements done using CW (8.5μs) and CW (42.75μS) as the transmitted pulse.

4.5. Decorrelation in the Received Signals

The coherence coefficient gives the degree of similarity between two signals, in our case the received signals used in the interferometry term ($S_a S_b^*$). A coherence level between the received signal at different receive elements at a given time instant can be used to estimate the phase measurement accuracy. The interferometry technique is based on the phase difference measured between two receive sensors[5] at a given instant. These two sensors must receive roughly the same signal originating from the same sea bottom area to achieve the maximum measurement accuracy. The degree of relationship between these two signals can be measured statistically by taking a complex correlation of the received signals. This tells us how much both receive staves (sensors) are related.

Highly coherent signals have the least phase measurement errors, hence more accurate overall bathymetry measurements. The correlation between signals is highly dependent on several parameters, e.g. hardware design, transducer design, different noise sources as well as the relative deformation of the received signals.

[5] Interferometry can be done using two sensors only but in case of more sensors, induvial correlation coefficient can be found for each receive pair.

The cross-correlation coefficient is given by the ratio between the expected values of interferometry term $(S_a S_b^*)$ and the square root of the product of the expected signal values:

$$\eta = \frac{|\langle S_a S_b^* \rangle|}{\sqrt{\langle S_a S_a^* \rangle \langle S_b S_b^* \rangle}} \qquad 4.10$$

In following sections, we are going to discuss the effect of different noise contributing factors which decorrelate the received signals from each other, which contributes to bathymetry measurement errors.

4.5.1 Spatial Decorrelation

At a given time, the footprints seen by the different receive arrays are slightly different; this phenomenon is known as *spatial Decorrelation* or the *sliding footprint effect*, which contributes to the degradation of phase measurements due to low signal coherence [22].

Ideally, the received signal on two receiver's arrays should only differ to each other by the propagation delay. Hence, the phase difference would be the only function of propagation path difference. All the calculations done for interferometry techniques are done considering the signal received at a given instant of measurement, backscattered from the same footprint on the seabed. So, if the received signal at both receivers have response from some uncommon scatters, that contributes to measurement errors.

Considering a very short transmitted pulse, the footprint can be considered as a single scatterer; otherwise the footprint size depends on the transmitted pulse duration (T) in case of CW pulse or equivalent duration after the pulse compression at receiver end (1/B); and the grazing angle on the seabed.

The effective footprint used for bathymetry calculation is the common footprint seen by the both receivers, and it contributes to a higher correlation coefficient. The uncommon part of the footprint leads to the decorrelation of interferometry term, called spatial decorrelation, giving higher uncertainties in final bathymetry measurements.

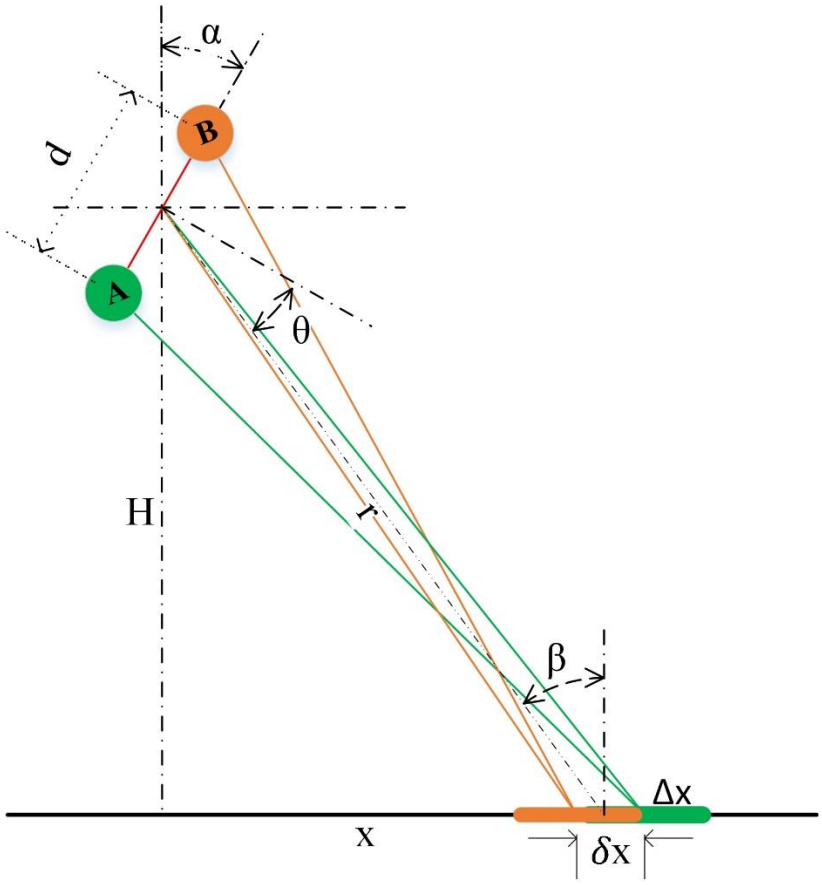

Figure 31 Sliding footprint problem with interferometers

The footprint length is expressed in signal length and the angle using the well-known relation[25]. This can easily be calculated for a pulse duration of T.

$$\Delta x = |x_t - x_{t-T}| \qquad 4.11$$

This projection of signal width on seabed with respect to an incident angle can be approximated to

$$\Delta x \approx \frac{cT}{2\,cos(\theta+\alpha)} \qquad 4.12$$

where θ is angle of arrival, α is tilt angle of transducer and T is the effective pulse length of the transmitted signal.

The shift in footprint seen between two receivers is called footprint shift (δx). It can be expressed as the variation in the position of centre coordinate of footprint seen by both receivers separately, and can be approximated from the following expression given in [22] &[25].

$$\boldsymbol{\delta x} \approx \frac{\boldsymbol{d}}{\boldsymbol{2}} \frac{\boldsymbol{sin(\theta)}}{\boldsymbol{cos(\theta+\alpha)}} \qquad 4.13$$

If we consider that the uncommon scatterers' (shifted footprint) contribution in the received signal at receiver A and B is not correlated and the common footprint echoes at both receivers are perfectly correlated, and ignoring other noise sources here, and considering that the insonified intensity is uniform over the whole footprint length, then the equivalent signal to noise ratio for shifting footprint is given by:

$$\boldsymbol{SNR_{shift}} \approx \frac{\boldsymbol{\Delta x - \delta x}}{\boldsymbol{\delta x}} \qquad 4.14$$

By putting the values of d_x and δ from 5.5 & 5.6:

$$\boldsymbol{SNR_{shift}} \approx \frac{\boldsymbol{cT}}{\boldsymbol{d\,cos(\theta + \alpha)}} - \mathbf{1} \qquad 4.15$$

So, the SNR from a shifting footprint depends on the pulse length, angle of arrival and the tilt angle of transducer. A short pulse length is noisier than a long pulse length. The wideband signal envelope length "T" is the length of the pulse compressed signal (T = 1/B). The widest receive pair has the highest sliding footprint effect. In our case, 8.5λ.

Figure 32 presents the SNR and phase difference standard deviation considering a noise free scenario with only the spatial decorrelation, where the mathematical model (black dashed line) is matched with real data (red points). The sliding ladder effect is minimum for signals coming from the direction of transducer axis (normal to transducer face in Figure 31).

The effect of sliding footprint can be reduced by changing the tilt angle (Elevation Angle) of sonar transducer but that is also limited by other parameters such as reduction of range due to multipath… We did these experiments with a tilt angle of 30°; which gives us the optimal results. The SNR is quite low in the nadir region. The sliding footprint effect is minimum in the area towards the interferometric axis, hence there is a sharp peak in the SNR_{SL} in that region.

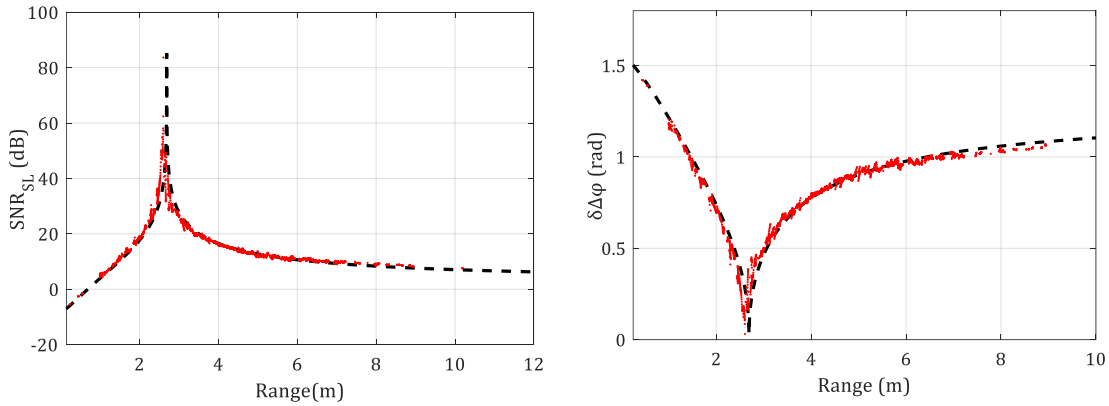

Figure 32 Computed equivalent SNR for sliding footprint effect (left) and resulting phase difference measurement error (right)

4.5.2 Angular Decorrelation

Most of the sonar measurement estimations are done considering the target as a single point scatterer, so the size of a target on the seabed has no influence on the phase measurements. But in reality, the actual signal footprint is largely depending on the wavelength and size of transmitted signal. So, the backscattered echo is the combination of these individual point scatters, which adds up to a noisy phase measurement. This effect is called angular decorrelation or baseline decorrelation, described and discussed by Jin & Tang in a journal paper [26]. In radar literature it is known as “glint”. They mentioned that the uncertainties in phase difference measurements due to baseline decorrelation is one of the dominant sources of error.

In interferometric SAR community, baseline decorrelation has been known for a while now, because SAR usually have a large baseline hence large error. In the underwater acoustic field this effect cannot be neglected, but it is not fully grasped in context of signal processing techniques.

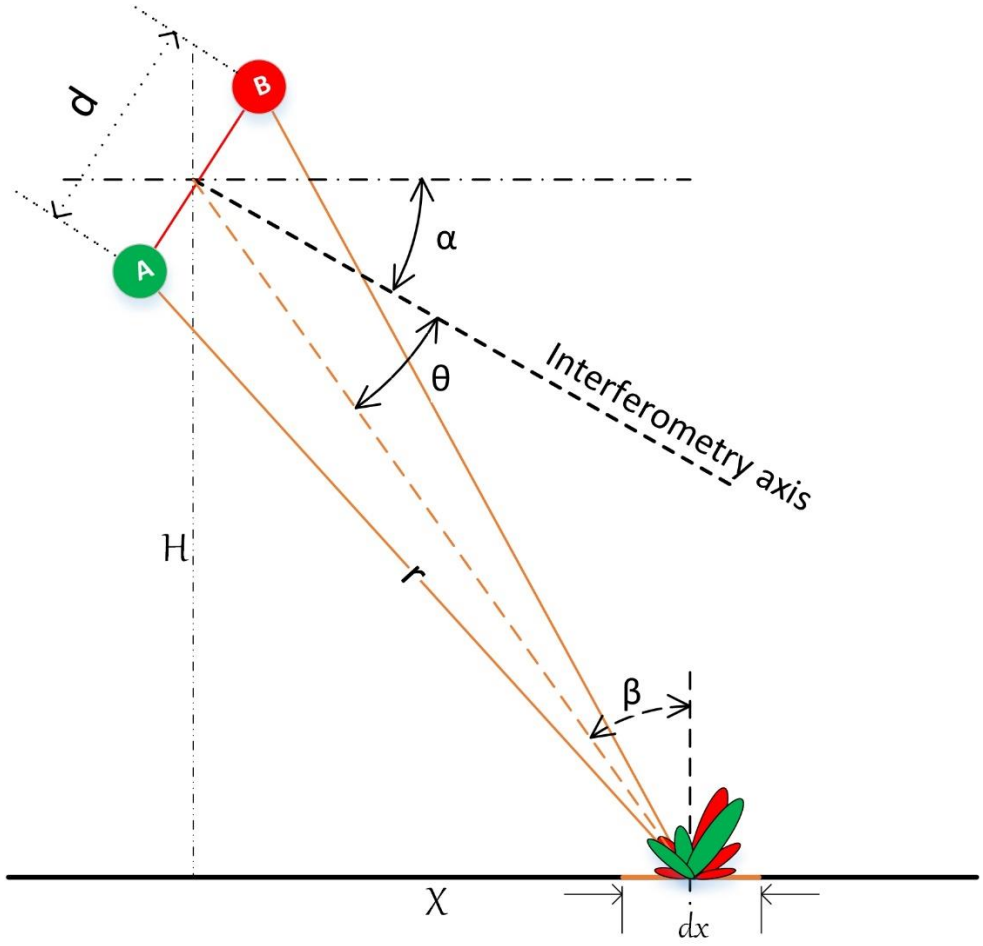

Figure 33 Angular decorrelation due to beam footprint of resolution cell

The interface pattern seen by two closely placed receivers is not exactly the same, assuming that the scattering surface consists of many distributed scatterers within the target footprint, which results in the reduction in coherence ratio between these two receive outputs.

Let's recall the interferometric coherence coefficient given by:

$$\eta = \frac{|\langle S_a S_b^* \rangle|}{\sqrt{\langle S_a S_a^* \rangle \langle S_b S_b^* \rangle}} \qquad 4.16$$

Considering baseline decorrelation only for a system of CW transmitted square envelope

$$\eta = sinc\left[\frac{kD}{\pi H}\frac{cT}{4} sin(\theta + \alpha)\, tan(\theta + \alpha)\, cos(\theta)\right] \qquad 4.17$$

$$\eta = sinc\left[\frac{kD}{\pi H}\frac{cT}{4} cos(\beta)\, cot(\beta)\, cos(\theta)\right] \qquad 4.18$$

α is depression angle of transducer mount and θ is angle of arrival from interferometry axis.

The equation (4.14) is still valid for frequency modulated signals when the pulse compressed energy envelope is considered as the transmitted energy envelope. The width of the envelope is given by the output bandwidth of matched filter $\left(T = {}^{1}/_{B}\right)$, which is considered as the equivalent pulse duration in case of wideband signals.

Let's consider that the noise at the two receivers is N_a & N_b, considering all the noise sources. The received signals can be written as:

$$S_a = S_c . N_a$$

$$S_b = Sc . N_b \qquad 4.19$$

$where\ N_a$ and N_b are independent, with the same mean and same standard deviation. Treating baseline decorrelation as the only equivalent noise source, the signal to noise ratio in the term of coherence coefficient of interferometry term ($S_a S_b^*$) [Jin and Tang 1996, Lurton 2001] can be given by:

$$SNR_{Angle} = \frac{\eta}{1-\eta} \qquad 4.20$$

Results represented by Jin & Tang [26] & Lurton [22] are also validated for our interferometer setup with 30° of elevation angle. The SNR considering the baseline decorrelation effect is usually high enough and has very low impact on the phase measurements for angles beyond the interferometric axis (normal to transducer face), except at long range. But it is comparatively low for angles between vertical and the interferometric axis. Figure 34 validates the above statement, and Figure 35 corresponds

to the equivalent phase difference standard deviation ($\delta\Delta\varphi$). Red points present the data collected in shallow water (z = 1.5m) and dotted lines are the mathematical model given by equation 4.22.

Figure 34 presents the results of equation 4.20 SNR considering a noiseless environment except the decorrelation due to the individual scatterers in the footprint. From the SNR curve, we can see that the SNR stays high for most of the swath range, except for the nadir region[6].

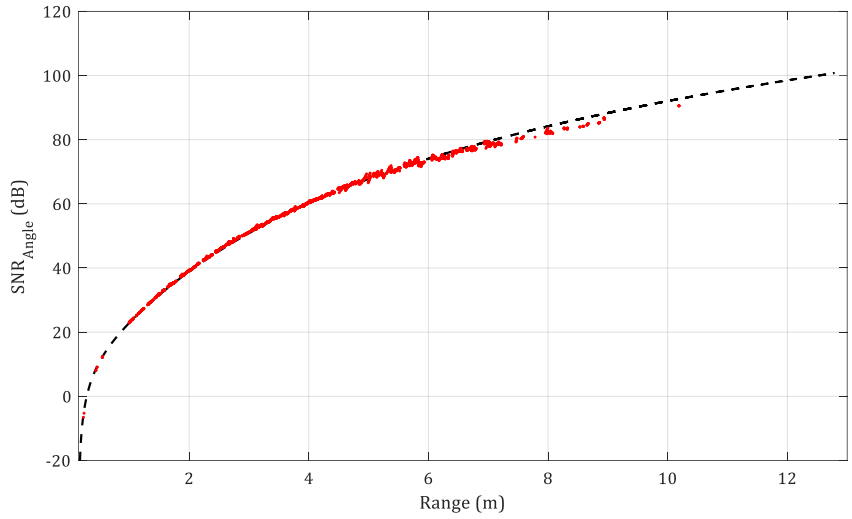

Figure 34 Computed SNR_Angle vs Horizonal Range

Figure 35 presents the standard deviation in phase difference measurements for our interferometric setup (d = 8.5λ), the standard deviation (δΔϕ) drops to almost zero for a wider swath. The angular decorrelation usually have big impact in multibeam echosounders, but it should also be considered for a tilted interferometer, where its effect dominates in the nadir region. Interferometers already suffer from the low data density in the nadir region, which can be related mainly to the geometrical setup of an interferometer (Figure 36), and low SNR due to baseline decorrelation is a further problem for the interferometry method. In this section we discuss the baseline decorrelation behaviour with different pulse lengths and frequency modulated signals. Results in Figure 34 & Figure 35 are taken when the transmit pulse is CW and the energy envelope width (T) is 42.75µs.

[6] Region directly below the transducer, also known as nadir gap and it creates a huge measurement gap in a dual transducer configuration.

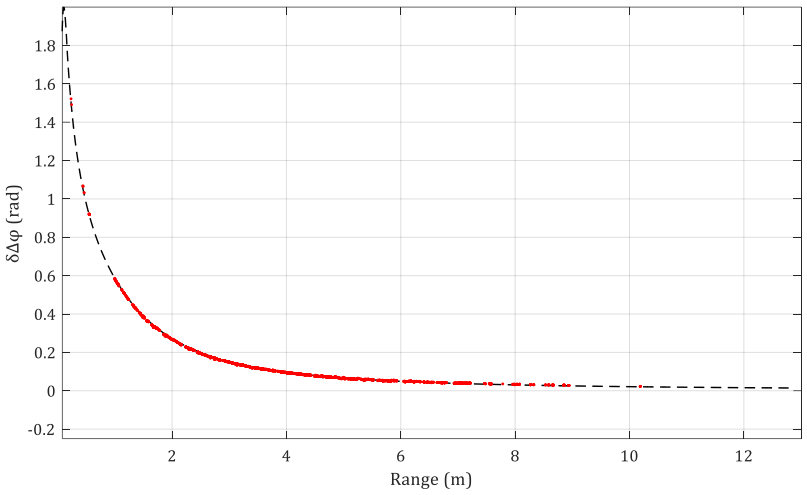

Figure 35 Phase difference standard deviation given for Baseline decorrelation

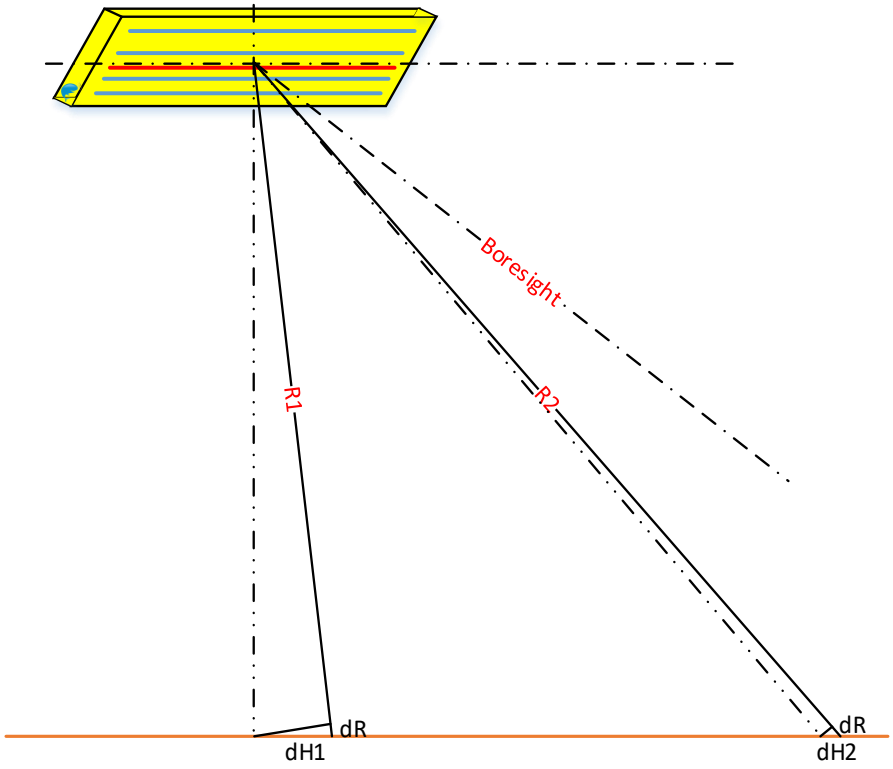

Figure 36 Measurement geometry in Nadir region

4.6. Overall Signal to Noise Ratio

The resulting signal to noise ratio should be considered to assess the benefits of different techniques used. As mentioned earlier, we will only be considering the degradation sources from the signal processing point of view, ignoring external factors impacting the measurement quality.

Lurton proposes to add up the individual noise sources e.g. additive noise and intrinsic noise (baseline decorrelation and spatial decorrelation)[24]. This gives a resulting SNR, assuming that all noise sources are statistically independent. The resulting noise can be written as

$$N_{tot} = N_{add} + N_{SL} + N_{angle} \qquad 4.21$$

The resulting signal to noise ratio (SNR) from all three degrading sources mentioned in this chapter is:

$$\frac{1}{SNR_{total}} = \frac{1}{SNR_{add}} + \frac{1}{SNR_{ang}} + \frac{1}{SNR_{shift}} \qquad 4.22$$

Figure 37 shows all the noise source contributions and the resulting SNR calculated using equation 4.22.

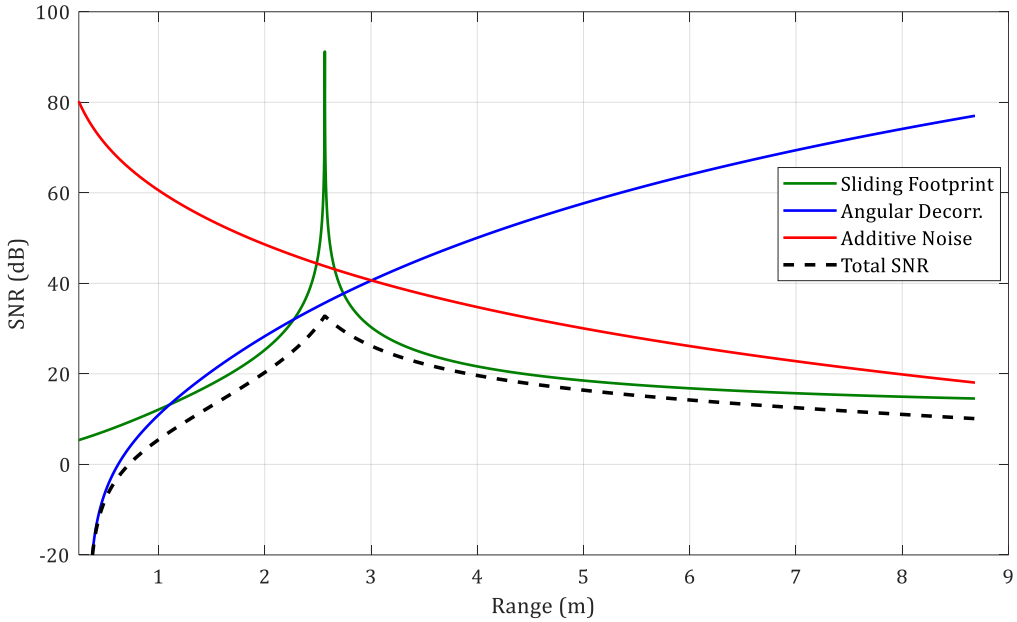

Figure 37 Overview off different SNR sources and the total SNR

Pujol, 2007 [33] mentions a way to add up the bathymetry error quadratically.

$$\delta Z_{tot}^2 = \delta Z_{Add}^2 + \delta Z_{SL}^2 + \delta Z_{angle}^2 \qquad 4.23$$

A slightly improved version of equation 4.22 is can be written as ([19] & [31])

$$\frac{1}{SNR_{tot}} = \frac{I}{SNR_{add}} + \frac{1}{SNR_{SL}} + \frac{1}{SNR_{angle}} + \frac{1}{(SNR_{add}.SNR_{SL}SNR_{angle})} \qquad 4.24$$

Equation (4.22) is not significantly different compared to equation (4.24); it will impact only if any of the noise sources is high and equal in amplitude, which is unlikely [19] & [31]. So, we will compare our results using the equation (4.22) proposed by Lurton

2000 [22], [24], which stands quite accurate for both CW and frequency modulated pulses.

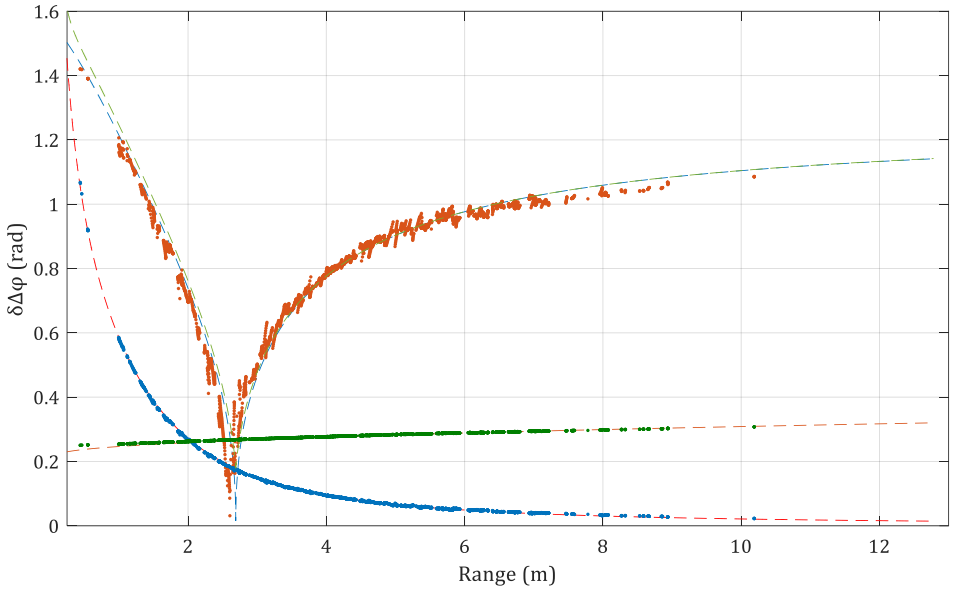

Figure 38 Phase difference standard deviation with different noise sources (e.g. Sliding footprint, Angle Decorrelation, Additive Noise etc.)

Now comparing the estimated total SNR values for different length CW pulses, the results are presented in Figure 39. The solid lines present the mathematical model and the dotted lines are the model redrawn using the measurements taken from the pontoon experiment for a flat seabed; so the field results fit perfectly the mathematical model.

The strongest noise component from the equation 4.21 prevails in Figure 39. We notice here that the overall SNR can be improved by using a longer transmitted pulse.

This is expected in most of the swath range where additive noise is dominating (Figure 37) or the spatial decorrelation is dominating, except the near nadir region, where baseline decorrelation plays a big role. The highest SNR increase due to pulse length can be seen at far range[7] where the additive noise is significant and a longer transmitted pulse has a wider energy envelope, resulting in higher transmitted energy, giving higher SNR at the input. The spatial decorrelation is also directly related to the pulse length (see equation 4.12 & 4.13) and it is also improved with a longer pulse length.

However, the baseline decorrelation dominates in the area before the interferometric axis (where the incidence angle at the transducer is 0°), so an increase in the pulse length introduces more signal decorrelation in this area.

[7] Far range can be considered the range outwards to the interferometer's axis, so it depends on the depth under the transducer

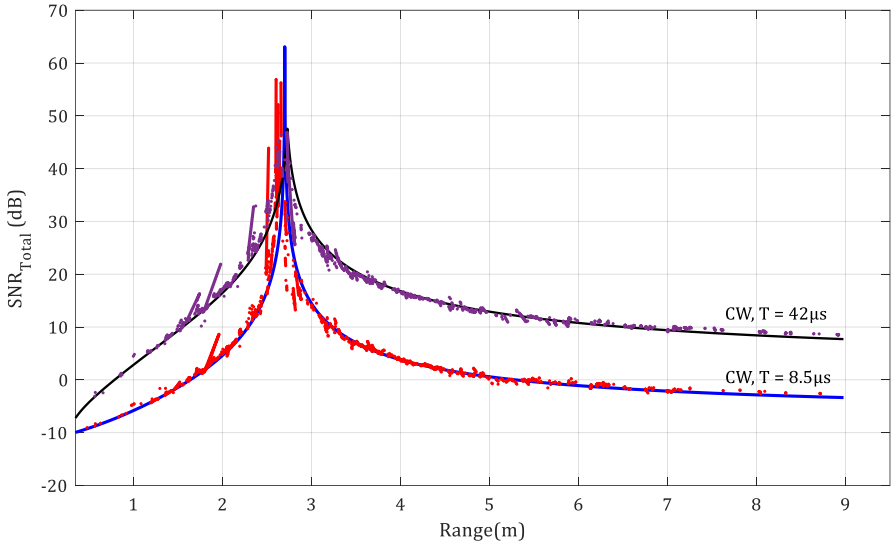

Figure 39 Resulting total SNR for different length CW pulses and LFM pulse

Figure 40 presents the phase difference measurement errors for the resulting SNR computed using the above equation 4.22.

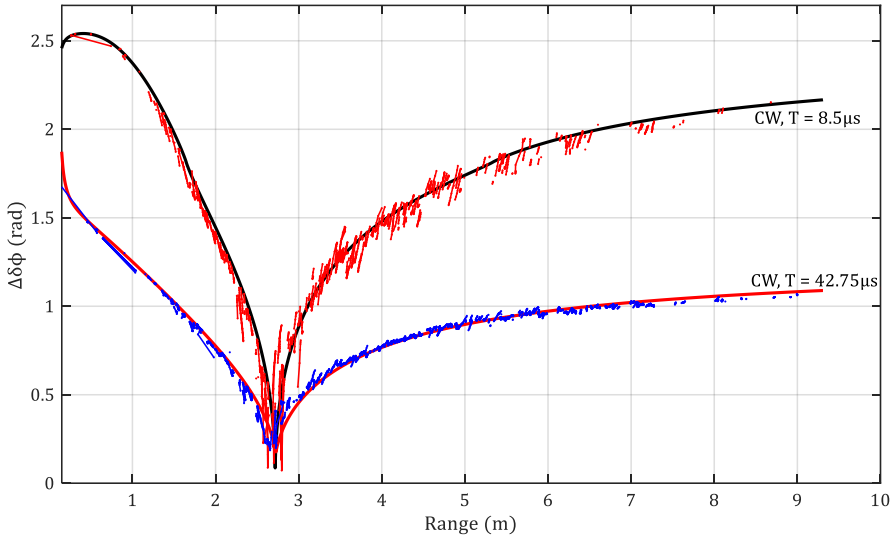

Figure 40 Phase difference measurement errors given using the total SNR calculation.

Figure 41 presents the standard deviation in bathymetry measurements collected from a fixed platform in Annecy lake (pontoon experiment setup 3.3.2) where external noise sources can be neglected. The red dotted line presents the mathematical model given in this chapter and the blue solid line presents the field data averaged over 10 samples. The field data result fits loosely the mathematical model proposed.

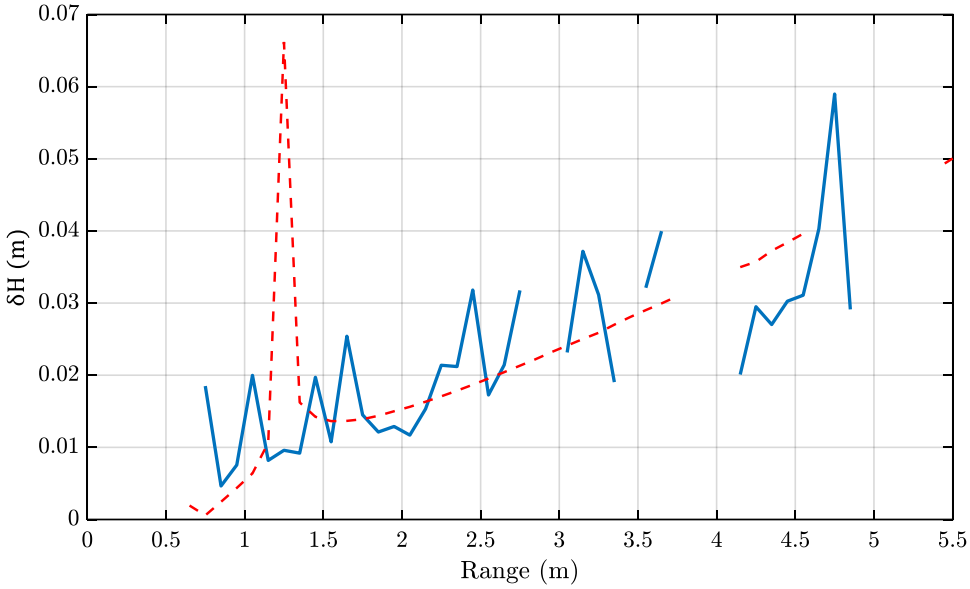

Figure 41 Standard deviation in depth measurement given over the across track range; mathematical model (red) compared with real data (blue)

4.7. Summary of the Chapter

In this chapter, different bathymetry degradation sources are discussed, and a model is proposed for this work. This gives us the better understanding of the performance imitation of an interferometric sonar.

We gave a brief introduction to the external noise sources, but we are considering only the noise sources from the signal processing point of view. The three main noise sources, additive noise, spatial decorrelation and angular decorrelation are considered, and a model is proposed to estimate correctly these noise sources for the Bathyswath interferometric system. We compared the results for two different length transmitted pulses (8.5µs and 42.5µs) to draw a relation between transmitted pulse duration and measurement uncertainty. Each mathematical model is also compared with the data collected from pontoon experiments. Finally, the resulting uncertainty model is verified with the depth measurements collected using a Bathyswath sonar system.

CHAPTER 5 IMPROVEMENTS WITH WIDEBAND SIGNALS

5.1. Improvement in single sensor measurements

5.1.1 Range – Resolution Trade-off

In this section, we address the problem of designing an appropriate waveform for interferometric systems, by optimizing the need for longer pulses and how we can keep a high resolution while doing that.

5.1.1.1 Assessment of Different Signals

5.1.1.1.1 CW Pulses

Continuous frequency pulses, also known as CW (Continuous Wave) or Narrowband, are widely used for both interferometers and beamformers.

A CW pulse can be written as:

$$\boldsymbol{x(t) = a(t)e^{2i\pi f_c t}} \qquad 5.1$$

where, a(t) is the signal's amplitude envelope and f_c is frequency.

It is desirable to have maximum possible backscattered intensity, to have a higher depth and wider swath, so we need to transmit more energy, which depends on the signal envelope. A square amplitude envelope is widely used to give maximum emitted energy.

For a square amplitude envelope, transmitted energy can be given by

$$\boldsymbol{E_e = A^2 T} \qquad 5.2$$

where A is transmitted signal's amplitude and T is the duration of pulse.

The first choice to increase the energy is by increasing the amplitude, but the amplitude of signal is limited by the physical parameters of sonar transducers and power amplifier designs. Generally, the instantaneous power is limited by:

- The maximum applied voltage at the transducer, above which the transducer ceramics becomes "de-polled"
- Cavitation, where the sound pressure level exceeds the vapour pressure of the water, forming bubbles at the transducer surface

So transmitted energy can only be increased by increasing the duration of the transmitted signal. With enough stored energy in the electronics (usually in large capacitors), long pulses can be generated easily.

The range resolution for a square amplitude envelope pulse is given by:

$$\Delta r = \frac{cT}{2} \qquad 5.1$$

Therefore, the range resolution of a narrow band sonar system depends directly on the pulse duration. So, it is in the user's interest to keep a small pulse length to maintain a high resolution. For example, the Bathyswath system is designed to transmit a minimum of 2 cycles, so for a 468kHz system the range resolution is around 3 mm, but the transmitted energy is low, as discussed earlier in this section. With a longer pulse we can have higher input signal to noise (SNR_i) at the receiver. But longer pulses are very sensitive to Doppler effects and this must be taken into account in any bathymetry application [22]. The longer pulses help to accurately determine the Doppler shift, but a side looking sonar such as an interferometer has low velocity in the pointing directions of the transducers.

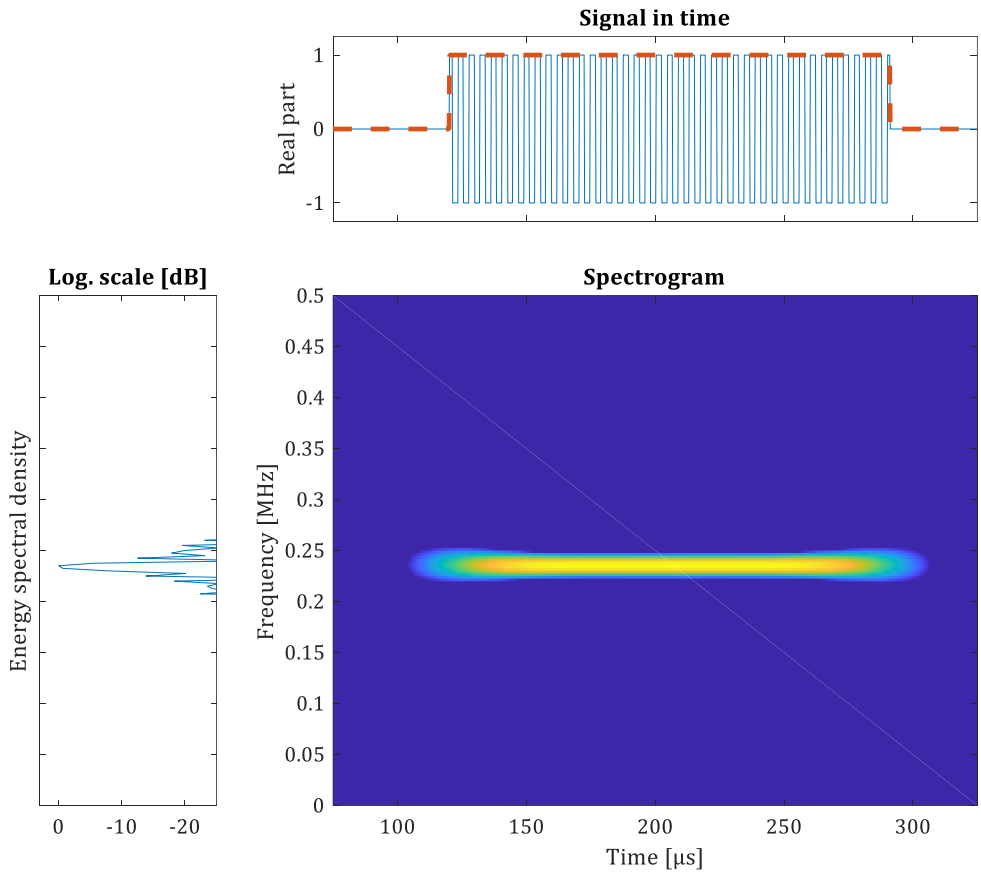

Figure 42 Spectrogram of CW signal with rectangular envelope

For illustrative purposes, Figure 43 shows the results from the water tank experiment, where a ladder shaped target with 2 cm separation between rungs was placed at 0.60-meter distance from transducer. Figure 43(a) shows that with a CW pulse of 468 kHz having a pulse width of 2 cycles, we can easily distinguish both rungs quite

easily, but the backscattered intensity is low (Figure 43**(a))** hence we would get a smaller range. But with increasing transmitted pulse width (Figure 43(b) & Figure 43(C), with pulse width of 10 and 20 cycles respectively) we notice that the rungs merged into a single target, but the overall backscattered energy increases with pulse width (Figure 43(c)).

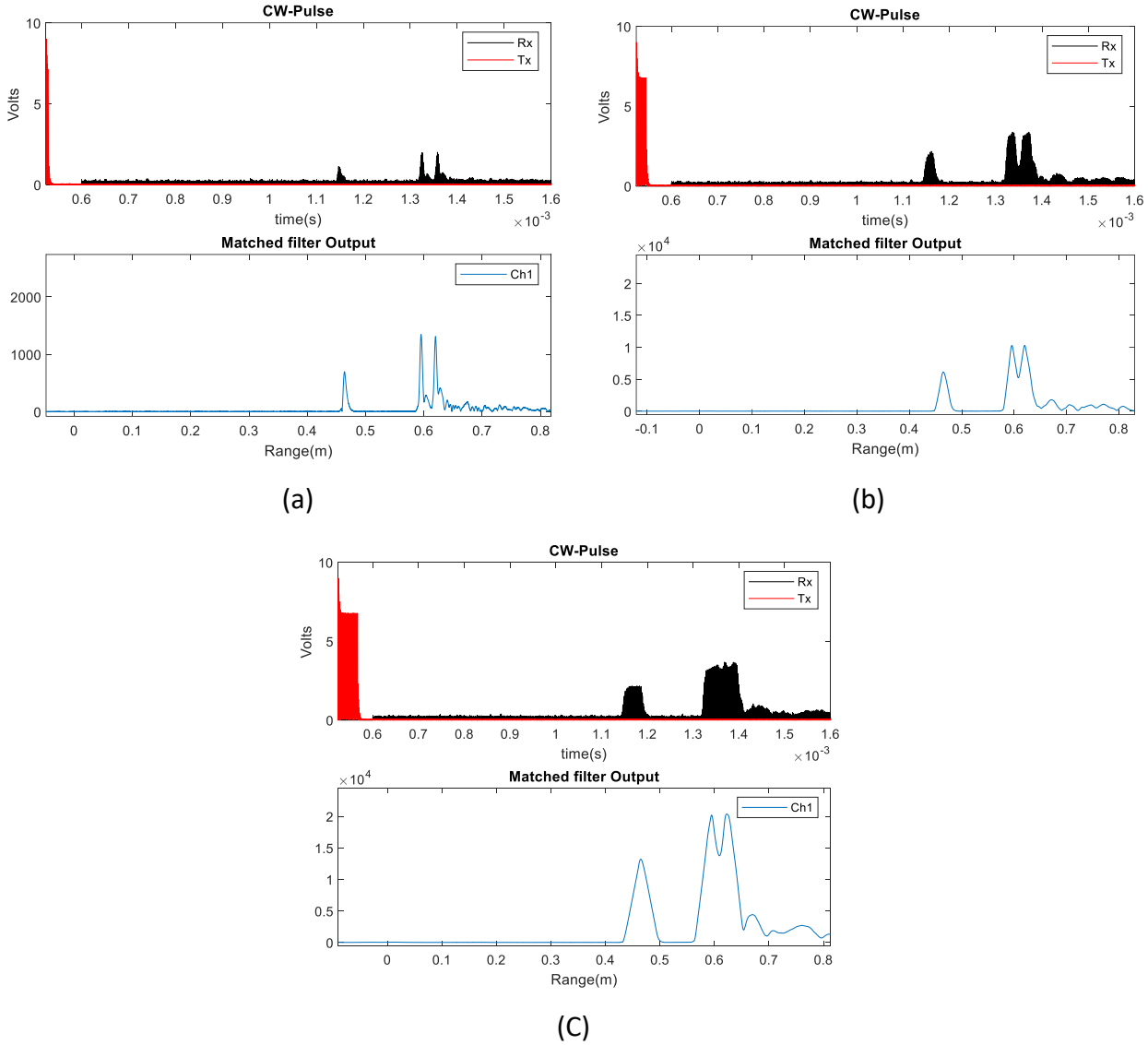

Figure 43 Backscattered echoes with transmitted CW pulse with pulse width of (a) 2 cycles (b) 10 cycles & (C) 20 cycles

Taking an example of real-world survey, we wish to have a high transmitted energy to achieve the widest swath range possible. One of the reasons to use the interferometric technique over other multibeam echosounders is to get a range to depth ratio of 15:1 or more. Also, a higher SNR improves the phase measurement accuracy with respect of additive noise. Hence, we wish to have a longer pulse width for a wider and more accurate bathymetry measurements, but this reduces the spatial resolution of the sonar.

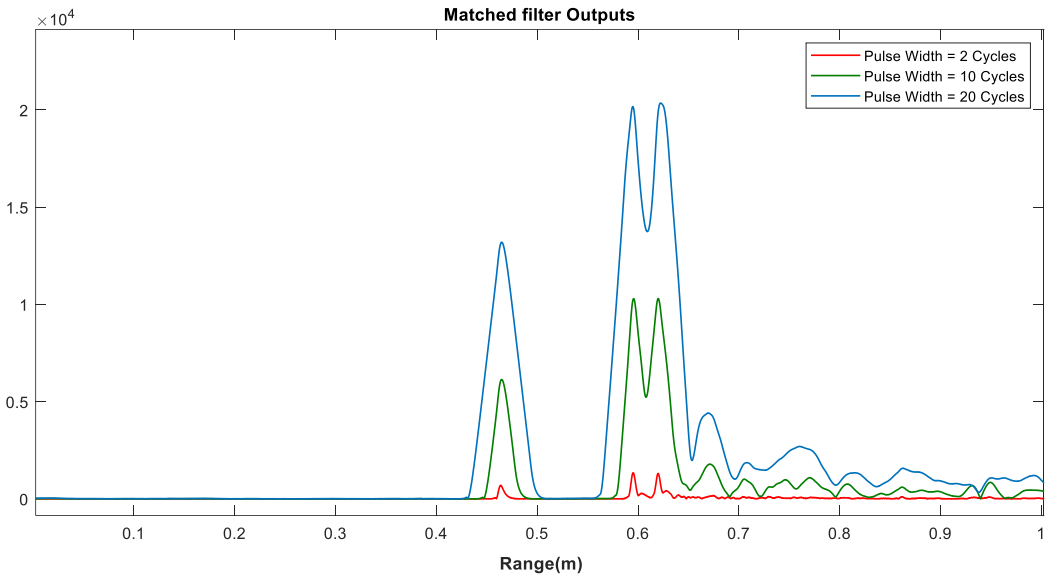

Figure 44 Received signal intensity after Matched filter, for 2-cycles (Red), 10 cycle (Green) and 20 cycles (Blue)

Figure 45 represents data collected using experiment setup -2. It gives a clear image of the range and resolution trade-off. Here the resonant frequency is 234 kHz and sampled at 625 kHz. The cross profiles of Figure a) and b) are measured with the transmit pulse length of 2 cycles (8.5 µs) long and Figure c) and d) are measured with the transmit pulse length of 10 cycles (42 µs) long.

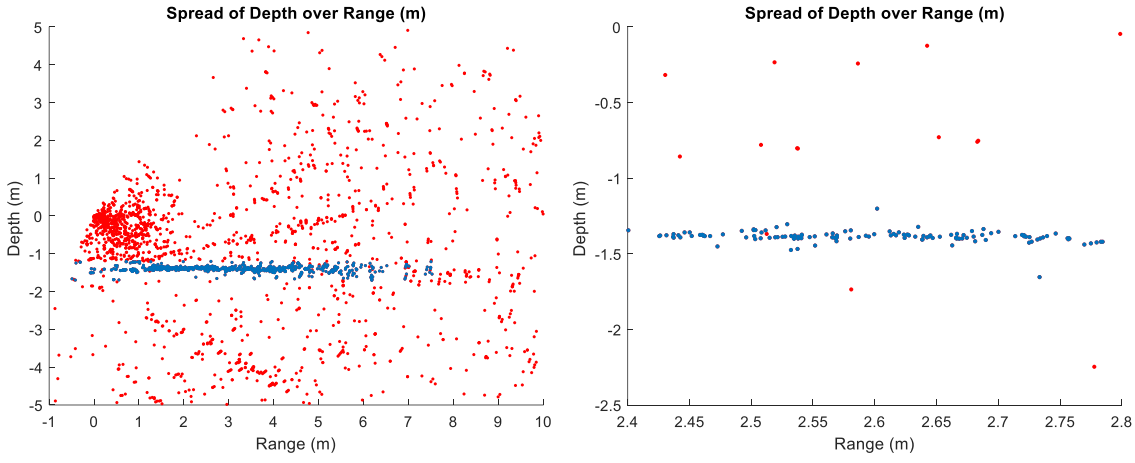

a) b)

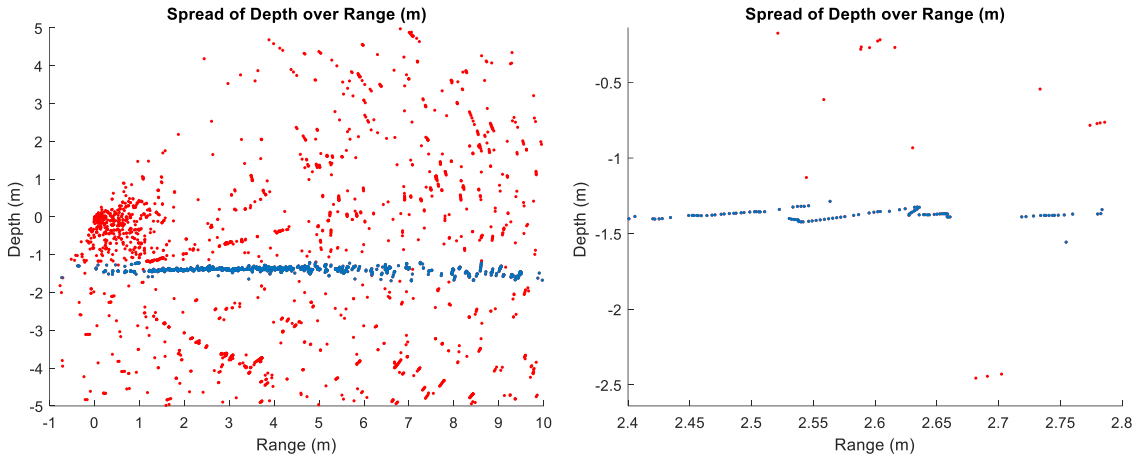

c) d)

Figure 45 Cross profile view of depth while using CW pulse with transmitted pulse length a) & b) 8.5μs and c) & d) 42μs

There are three things we can conclude from these results

- Comparing the figure, a) and c), we can see that the **slant range** of system can be improved significantly by increasing the transmitted pulse length, indeed due to the higher transmitted energy.
- Figure b) and d), show a close-up of view of the spread of depth with 8.5 μs and 42 μs pulses respectively. We can see the higher horizontal resolution with a short pulse compared to the 10-cycle long pulse. Hence, we can see that there is significant trade-off between range and resolution when increasing the transmitted pulse length.
- We also see that the results with longer pulse is less noisy than the short pulse. A higher signal to noise (SNR) helps to reduce the angular measurement uncertainties where the additive noise is dominant.
- We can also draw attention to the "false seabed" at radial angles, which are caused by "phase jumps" in phase to angle process in Figure 45 a) & c) (discussed in 4.3.2).

In some cases where the resolution is not critical, a long range can be achieved by increasing the duration of transmitted pulse. The idea of using interferometry sonar is to save the surveying time and cost, for that we need to have wide swath sonar with high ping rate. And ping rate directly depends on the transmission period which physically limits the ping rate of sonar (or PRF). Mostly sonar systems wait for the last echo from the far range defined in the sonar parameters before they can ping again. This delay is from both the propagation delay and the transmit pulse length. The pulse length is small relative to propagation delay, but putting too much power into the transducers (energy

per pulse x pulse repetition frequency) can overheat and damage the transducers, so the system imposes a limit on this product

5.1.1.2 Wideband Signals and Pulse Compression Technique

As mentioned earlier, one way to improve swath range is by transmitting more energy towards the target, since there is high propagation loss in the water and the backscattered intensity level is low. This can be achieved by using a longer transmitted pulse duration (T). However, the increase in signal envelope duration leads to a loss of spatial resolution of depth measurements, which is given by cT/2 for a transmitted square wave. Resolution also depends on the data sampling rate of the system. But considering only signal theory, the resolution of the system depends on the transmitted signal's envelope width and the frequency used.

To overcome the range – resolution trade-off problem, the pulse compression technique is widely used in radar and sonar. This technique is known to improve the resolution as well as the signal-to-noise ratio (SNR). It is done by using modulated transmitted pulses and then correlating the backscattered echoes to the same transmitted pulse. So, it is a matched filter with wideband modulated signals as the transmitted and reference signals. Theoretically, it allows us to increase the pulse length as much as desired, while keeping the same resolution. There are different modulation techniques available and discussed in this chapter. In the following section we will assess the relative merits of different wideband and narrowband signals to improve the resolution and accuracy of bathymetry measurements.

5.1.1.2.1 LFM Pulses

Linear Frequency Modulated (LFM) pulses (also known as linear chirp) have a frequency component that changes linearly with the time. The frequency component of an LFM pulse is given by:

$$f(t) = f_0 + kt \qquad 5.2$$

Where:

$f_0 = \text{initial frequency}$

$k = \frac{B}{T}$ chirp rate. B is the bandwidth of the pulse swept in duration T

The envelope of the signal is a function of time and denoted by $a(t)$.

Hence, an LFM (Chirp) signal can be written as:

$$\boldsymbol{x(t) = a(t)e^{2i\pi(f_0+kt)t}} \qquad 5.3$$

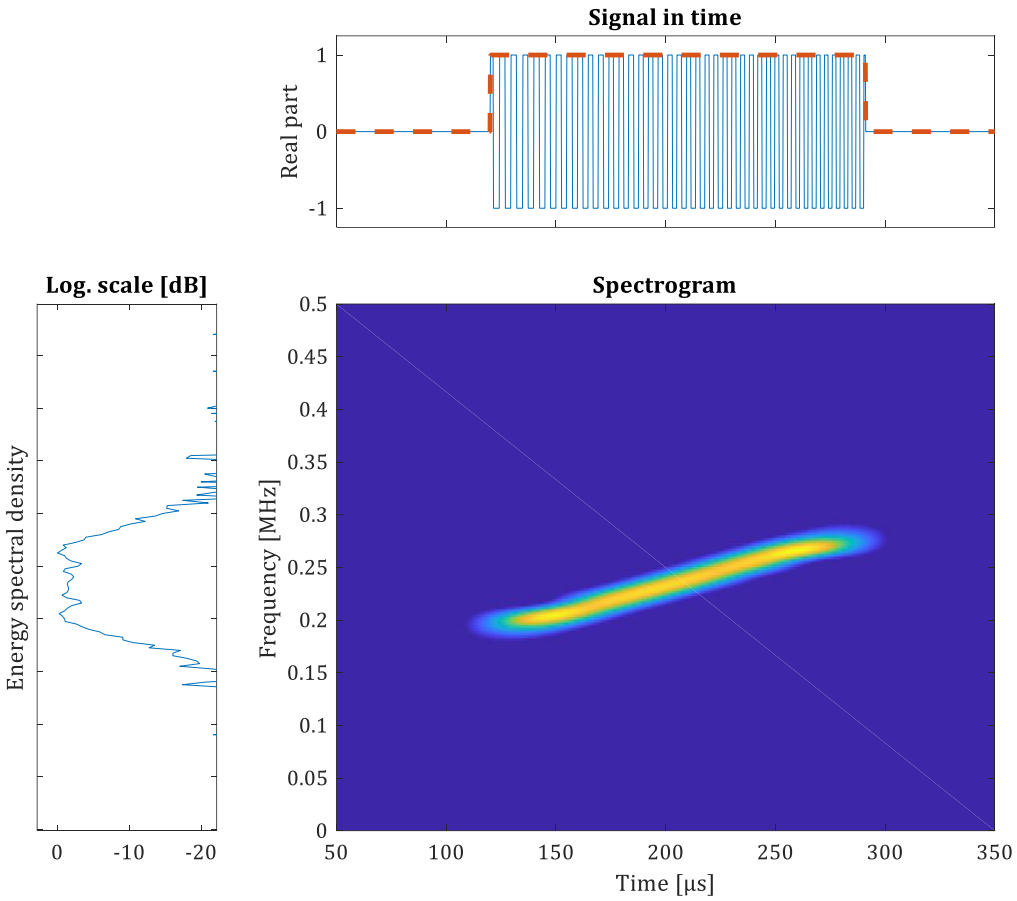

Figure 46 Spectrogram of a Linear Frequency Modulated Pulse (LFM) with rectangular envelope

Figure 47 shows the results of water tank experiment (3.3.1), where the transmitted pulses are LFM of different lengths. In both figures, the top plots show the transmitted pulse (red) and the backscattered echoes (black) and lower plots are the output of the matched filter. From both figures a) and b), we can easily distinguish the both echoes from both target echoes.

As discussed earlier the processing gain of matched filter with modulated signals can be given by the "Time-bandwidth product". It can be seen in Figure 47(b), that the energy of the signal can be increased by increasing the pulse length, but the resolution of system stays the same. The resolution of the sonar is no longer given by the pulse length but by the bandwidth of the modulated signal. Hence, modulated signals are widely preferred where a long range and higher resolution is desired.

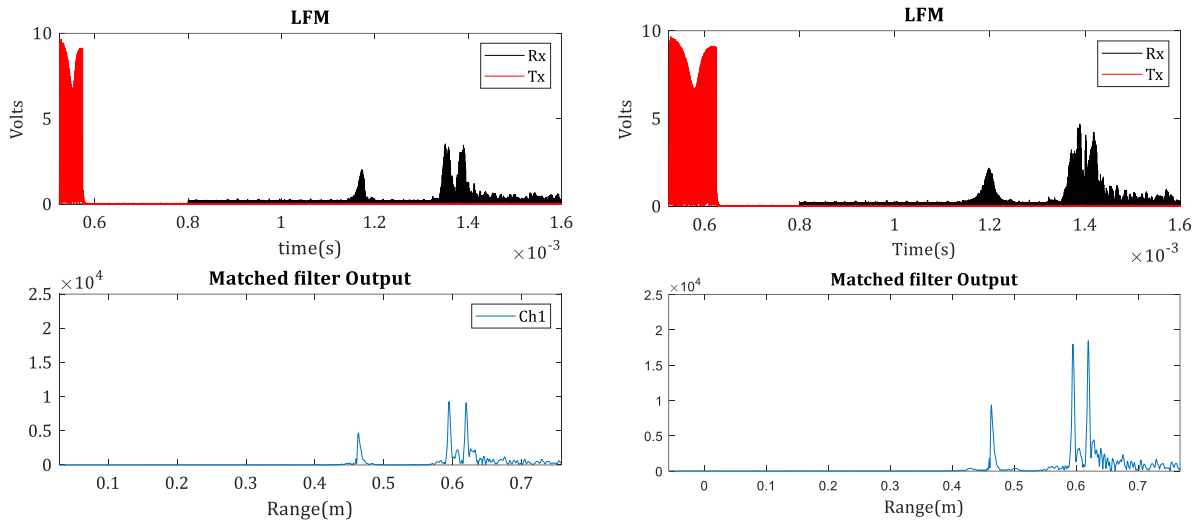

a) b)

Figure 47 Water tank experiment: Backscattered echoes with LFM transmit pulse a) Pulse duration = 0.5ms, b) Pulse Duration = 0.65ms

Now let us consider a real-world environment and compare data with bathymetry measurements. We implemented transmit LFM pulses in Bathyswath-2 hardware and collected raw data in IQ format for post processing. Figure 48 shows the spread of depth across horizontal range calculated using interferometry method. All the red points are the noisy data and the blue points are the filtered depth points [14].

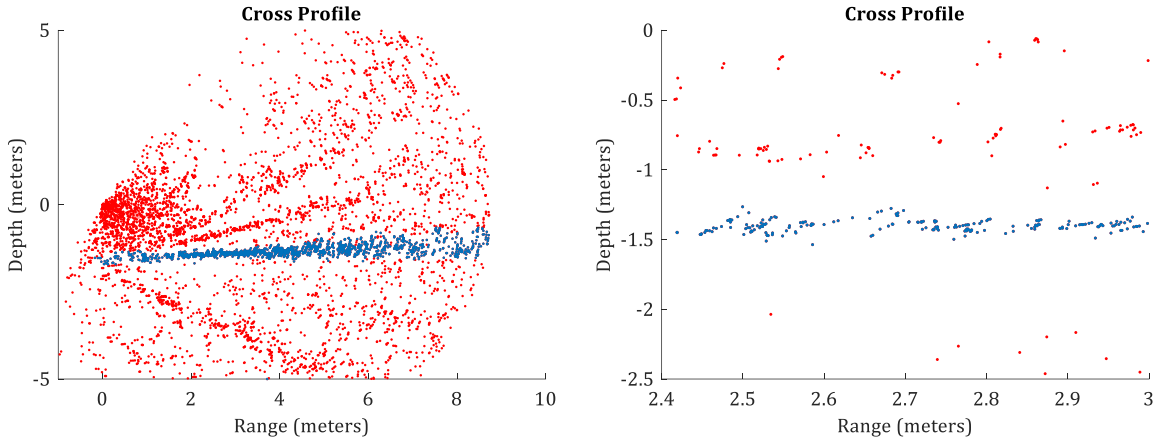

a) b)

Figure 48 Cross profile view of depth while using LFM transmit pulse

Figure 48 confirms the results with the water tank experiment, that the longer slant range can be achieved with the use of frequency modulated (FM) transmit signals rather than conventional narrowband signals, while keeping the high spatial resolution.

The important thing to notice here is the uncertainty of depth measurements while using the LFM pulses. We will be discussing more about the noise modelling in

interferometers in the narrow band and wideband signals, and try to explore some wideband processing techniques to improve the interferometer's measurement accuracy.

5.1.1.2.2 EFM Pulses

As a part of signal assessment, we also considered Exponential Frequency modulated (EFM) signals, also known as exponential chirp.

The instantaneous frequency component of signal varies exponentially as a function of time and given as:

$$f(t) = f_0 k^t \qquad 5.4$$

Where:

$k = \left(\frac{f_1}{f_0}\right)^{1/T}$ chirp rate with total sweep duration of T

f_0 -> initial frequency and f_1 -> final frequency

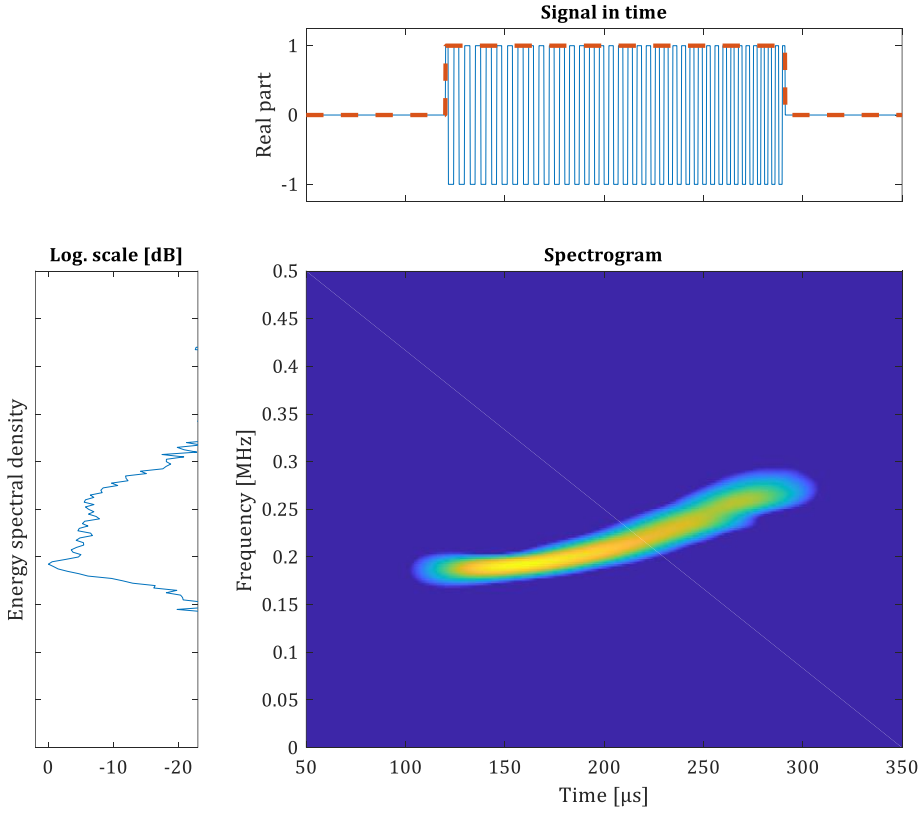

Figure 49 Spectrogram of a Linear Frequency Modulated Pulse (LFM) with rectangular envelope

Hence, the EFM or Exponential Chirp can be written as corresponding time domain function:

$$x(t) = a(t)e^{2i\pi f_0\left(\frac{k^t-1}{ln\,(k)}\right)t} \qquad 5.5$$

Figure 50 shows the results from the water tank experiment (3.3.1), where the EFM transmit pulse is in red and the backscattered echoes in black. The plot in blue is the matched filter output where the reference signal is a replica of transmitted pulse.

The results look similar to the LFM pulses, where the processing gain of matched filter is given by the "Time-Bandwidth product" and the resolution is given as a function of transmit pulse bandwidth rather than the pulse length.

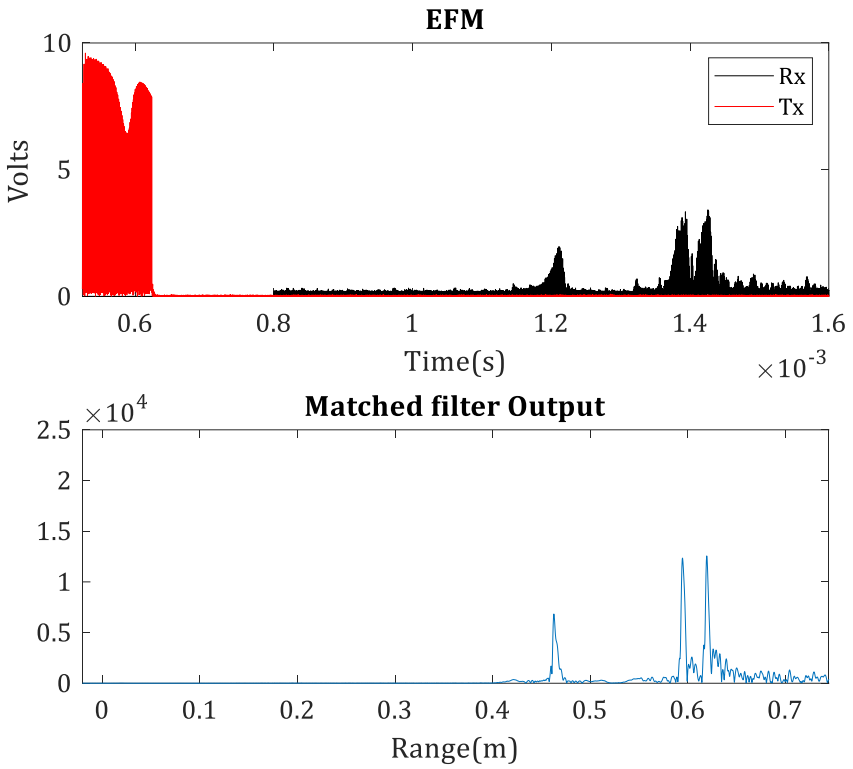

Figure 50 Water tank experiment: Backscattered echoes with EFM as transmit pulse; pulse length: 0.62ms

Exponential modulated signals (Exponential Chirps) are preferred in applications where immunity to Doppler shift is desired.

5.1.2 Summary of the Section

In this chapter we compared the results of narrowband and wideband signals to overcome the range-resolution trade-off. Figure 51 shows matched filter outputs with different transmit pulses, which sums up this chapter. LFM pulses are favoured over EFM pulses, as they give similar results for range-resolution and are slightly less complex to design.

We also noticed the uncertainty in interferometry measurements with the modulated signals, which is probably due to the phase measurement errors. We will be exploring that in following chapters and try to improve the bathymetry measurement uncertainties by improving the wideband signal processing techniques.

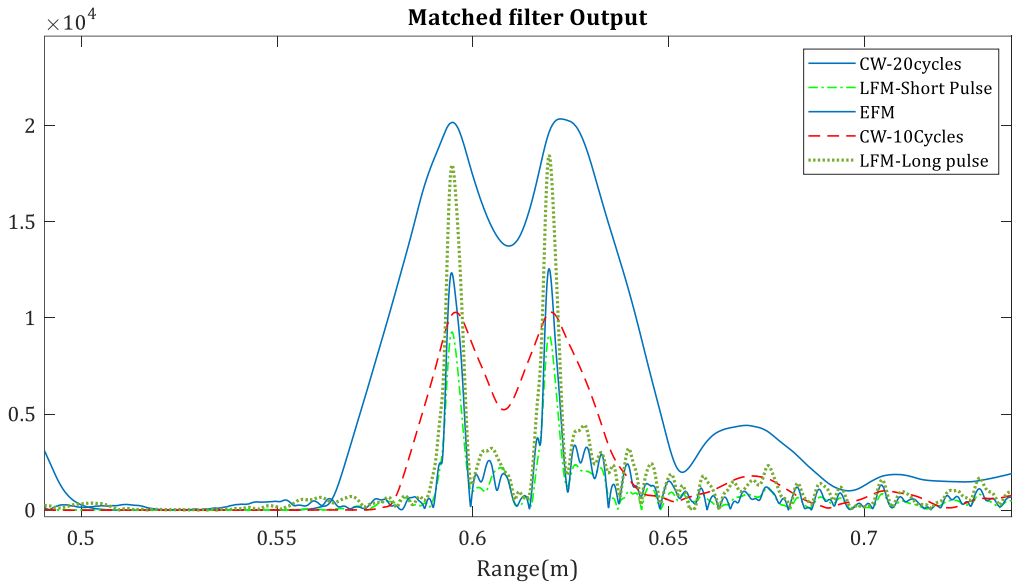

Figure 51 Matched filter outputs with different transmit pulses

5.2. Angle Measurement Improvements

5.2.1 Robustness to Additive Noise

Additive noise estimation plays a vital role in any system design. In 4.4.1, we have discussed the impact of additive noise in interferometry bathymetry calculation. Additive noise dominates and limits data quality in the far range of a swath. A good estimation of additive noise is given by the sonar equation (see section 4.4.1).

Additive noise can easily be reduced, compared with the useful signal, by increasing the overall transmitted energy, resulting in high SNR at receiver. As discussed in 5.1, the transmitted energy can be enhanced by increasing the transmit power and the transmit duration, increasing the width of transmit energy envelope. As from 5.1.2, frequency modulated pulses are preferable over the CW pulses to avoid the range-resolution trade off.

Figure 52 presents the SNR estimation only considering the additive noise for different length CW and LFM pulses. As expected, LFM transmitted pulses with 80 µs duration have higher SNR compares to both CW pulses.

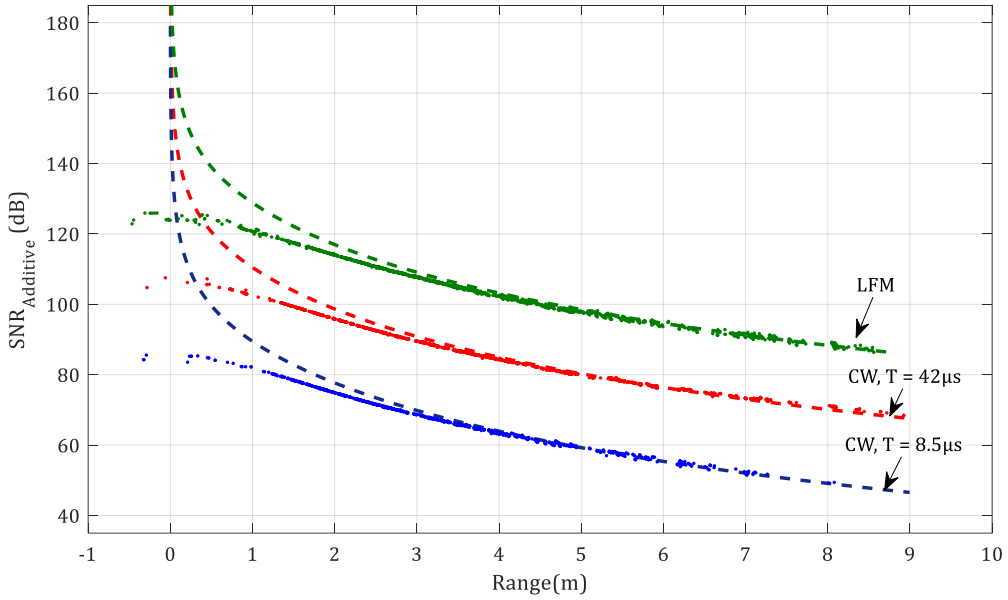

Figure 52 SNR accounting additive noise only, estimated for LFM (80µs), CW (8.5µs) and CW (42.75µs)

From equation 4.8, phase difference standard deviation can be calculated, and is presented in Figure 53.

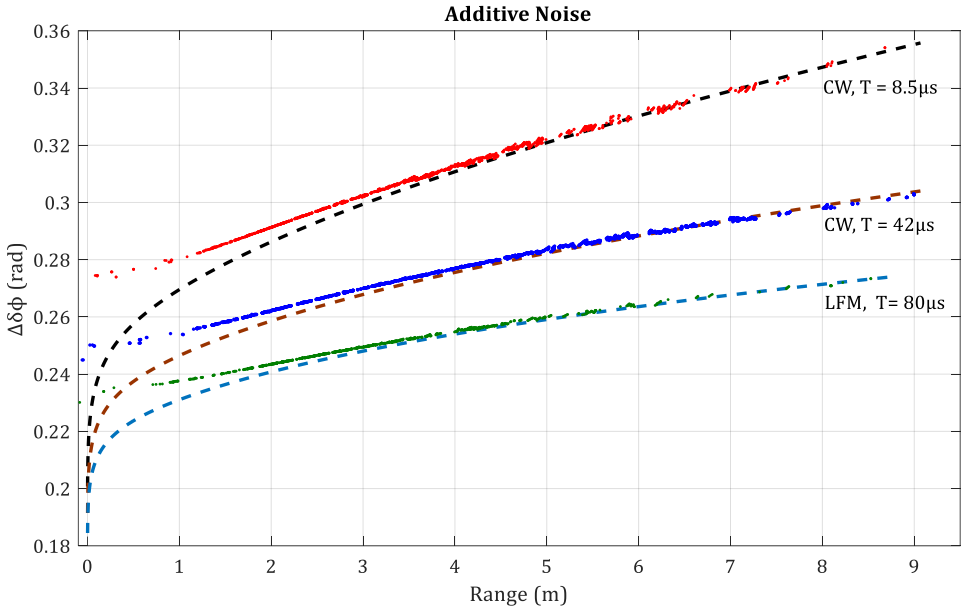

Figure 53 Phase Difference standard deviation only considering the sliding footprint effect, estimated for different length CW pulses and LFM pulses.

So, we can say that the use of LFM pulses improves bathymetry measurement accuracy where additive noise is dominating. From Figure 53, the phase difference standard deviation is improved significantly using the LFM pulses while keeping a high-resolution bathymetry. The improvements are significant at the far range of the swath, thus increasing the operating swath range of an interferometer.

5.2.2 Robustness to Spatial Decorrelation

Now considering the frequency modulated signals, as previously mentioned, the pulse length is given by the bandwidth of the pulse compressed output; the SNR results are compared in the Figure 54. Here we consider the SNR calculated for three different transmitted pulses: CW with T = 8.5 μs (purple), CW with T = 42 μs (red) and an LFM pulse with 80 μs (green), all with a square power envelope.

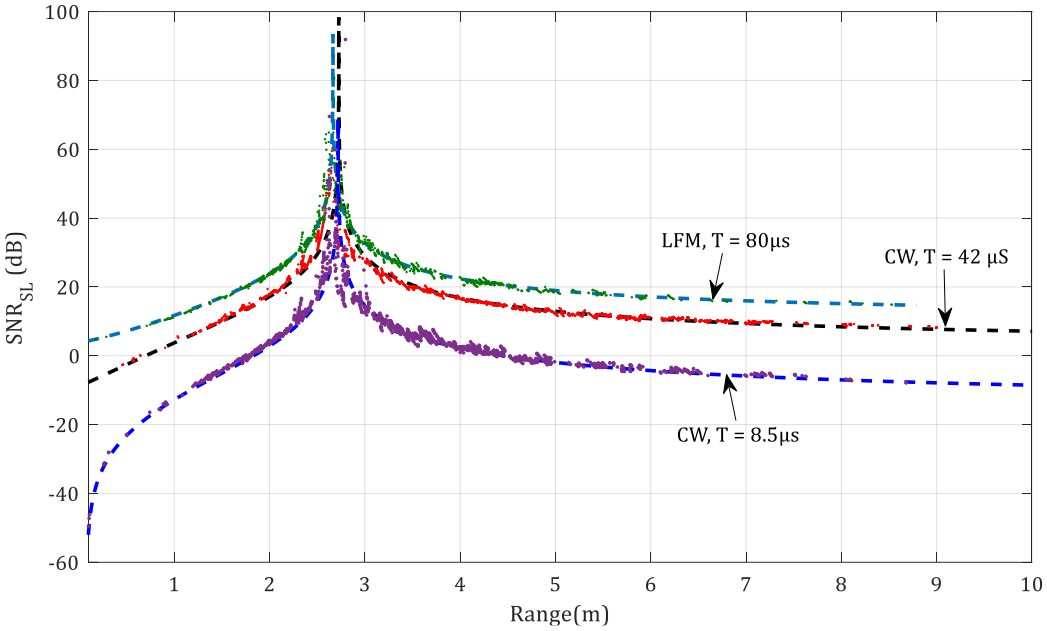

Figure 54 SNR only accounting the sliding footprint effect, estimated for CW pulses with different pulse length and LFM transmitted signals

We see that the SNR_{SL} is increased significantly by just increasing the pulse length of CW pulse. But we must consider that we also lose the spatial resolution with longer CW pulse, as discussed in 5.1.1.1.1

The use of LFM pulse does increase the SNR_{SL} but the improvements are weak comparing the overall transmitted energy of CW pulses and LFM. This is mostly due to the bandwidth for matched filter (B), from where the effective pulse length (T = 1/B) is considered. But on the plus side, we keep the higher spatial resolution of our measurements.

Figure 55 presents similar results for the errors in phase difference measurements. The LFM pulse with transmit length $T_e = 80\ \mu s$ gives the minimum phase error and a short pulse (2 cycles long or T = 8.75µS) gives the maximum errors.

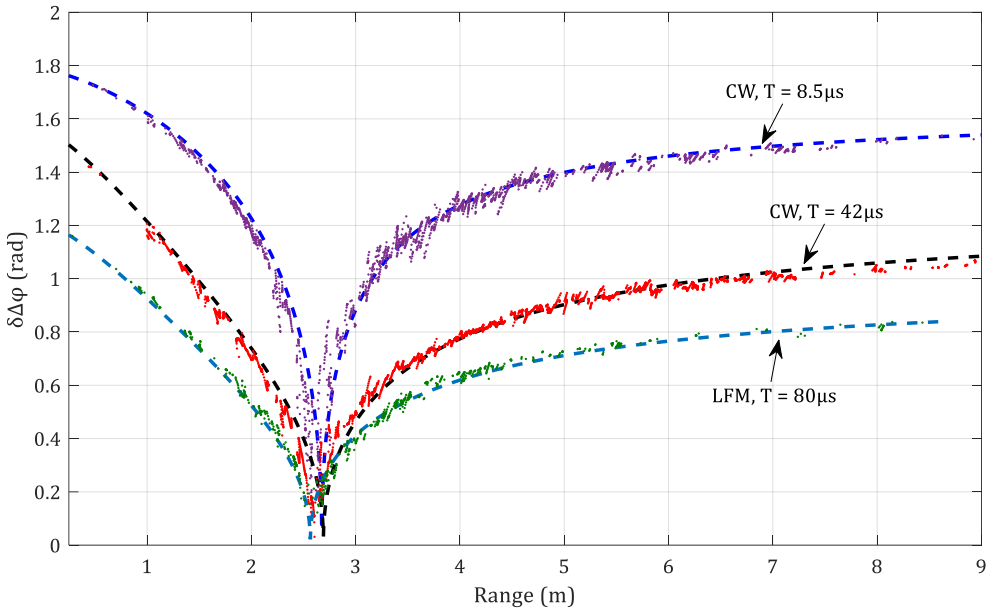

Figure 55 Phase Difference standard deviation only considering the sliding footprint effect, estimated for different length CW pulses and LFM pulses.

The noise model estimator given in equation 5.8 and 5.9 stands correct for our interferometer's configuration. The measurement accuracy comparison between LFM, and different length CW pulses, helps us to conclude that the use of LFM pulses can slightly reduce the overall measurement errors when the sliding footprint is dominating. We can also get similar results with longer CW pulses, but we have to trade-off the resolution. From Figure 54 and Figure 55, we can easily estimate the final bathymetry degradation (δZ) due to sliding footprint (spatial decorrelation).

5.2.3 Robustness to Angular Decorrelation

Now considering the same experiment scenario used throughout this section, we compare the results for different length CW pulse and LFM pulses used with matched filter. We consider a noiseless scenario where the bathymetry degradation is only due to the baseline decorrelation. As in Figure 56, presents the results for CW: T = 8.5 µs (red), T = 42 µs (blue) and LFM: T = 80 µs (green).

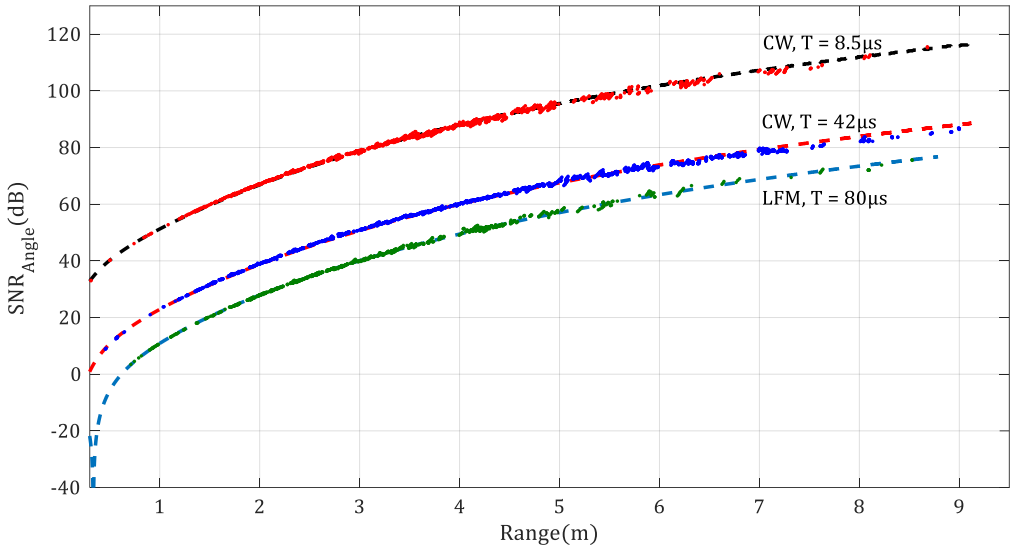

Figure 56 SNR only considering the Baseline decorrelation given over the horizontal range

Figure 57 presents the equivalent phase difference standard deviation for model, using equation 4.8

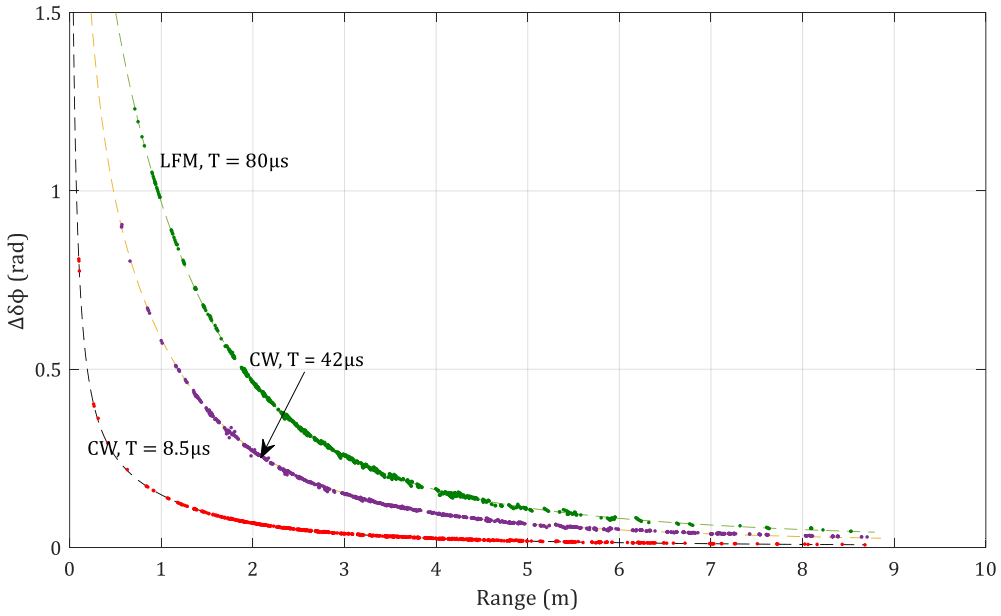

Figure 57 Phase Difference standard deviation only considering the sliding footprint effect, LFM transmit pulse compared with a short and a long CW pulse

Observing the Figure 56 & Figure 57, SNR decreases with the longer CW pulse and with the LFM pulse. This can be directly related to the instantaneous footprint size: a longer pulse length creates a wider footprint, which contributes more in the decorrelation of the received signals of the interferometric term ($S_a S_b^*$). In the case of a frequency modulated signal (LFM in our case), the scenario is slightly different to the CW pulse where the received echoes' pulse-compressed main lobe is smaller and sharper than the

one of continuous wave. The only possible explanation of this measurement uncertainty can be related to the dominant sidelobes in the output of pulse compressed signal. These sidelobes can result in a wider footprint because now the effective footprint considered is wider due to sidelobes. To understand better the problem, we take autocorrelation of CW and LFM transmitted pulses, which can be considered as the matched filter output if neglecting the deformation of pulse. From Figure 58, in the left part, we have autocorrelation of a CW (red) and LFM pulse (blue), with the equivalent resulting main lobe to demonstrate the effect of sidelobes in the pulse compressed output.

This can be reduced by using the shorter LFM pulse, but of course resulting in lower transmitted energy. Again from Figure 58, we can see that the sidelobes get larger for a longer LFM pulse (right).

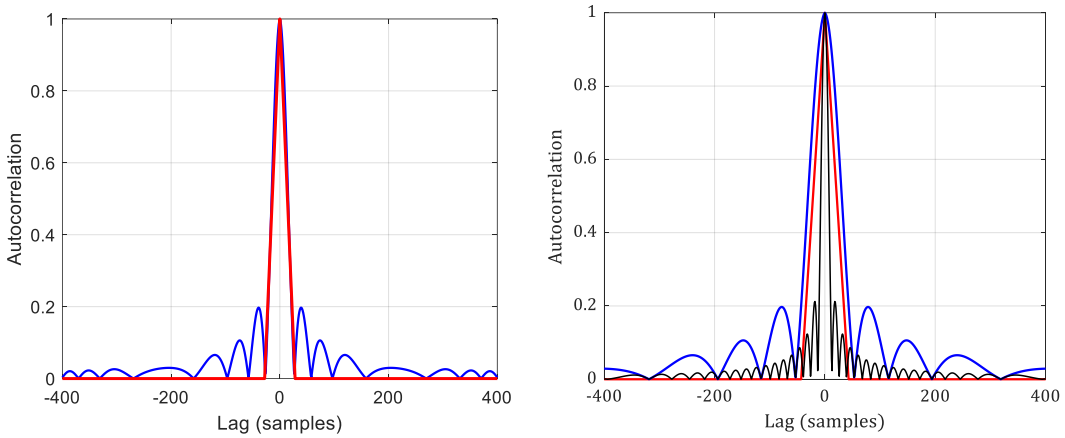

Figure 58 Autocorrelation function of CW pulse and LFM with equivalent bandwidth (left), with different length (right)

5.2.4 Overall SNR Improvements

As discussed previously in 4.6, the resulting signal to noise ratio can be given by adding all the noise sources considering that all noise sources are statistically independent [24]. The resulting SNR can be used to assess the benefits or drawbacks of wideband pulses over the narrowband pulses.

We calculate the overall SNR for CW pulses of different transmit length and an LFM pulse, presented over the across track range in Figure 59.

From Figure 59, we can divide the across track range in three parts 1); Near nadir region (> 1m), boresight region (>1m & < 3m) and far range region (> 3m)[8]. As discussed throughout the chapter and the previous chapter, each noise source is dominating in

[8] These values are taken from the bathymetry of pontoon experiment (3.3.2), where the average depth is 1.5m

different parts of the swath range. The additive noise dominates the far range region, limiting the maximum swath range in noisy environments where the angular decorrelation is more dominating in the area covered before the interferometric axis (nadir region and boresight area). The sliding footprint decorrelation is minimum when the backscatter echoes are coming from the boresight of transducer (interferometric axis) (refer to Figure 37).

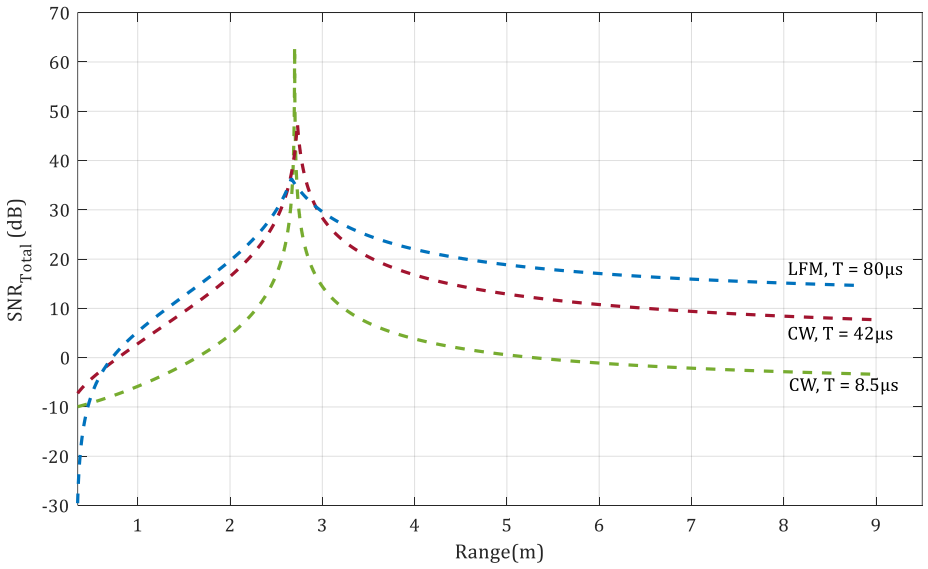

Figure 59 Total SNR model for CW and LFM transmitted pulses

Decoding the Figure 59, the SNR can be improved significantly in far range region (> 3m) while using a frequency modulated (FM) pulse or a long enough CW pulse at the expense of resolution of the system. However, in the near Nadir region or the area before the interferometry axis, the improvement in SNR is limited with the use of LFM pulse. The improvement in SNR with the wider CW pulse is significant in this region, running against the usual situation that the wideband pulse compressed techniques have higher SNR then conventional CW pulses.

Using the relationship of phase difference uncertainty to the SNR of received signals, the phase difference standard deviation over the horizontal range is presented in the Figure 60. Comparing the results for the 8.5 µs long CW pulse[9] and the LFM pulse (expecting a similar across track resolution), the phase difference measurements are significantly better for the LFM pulse. But comparing the 42 µs CW pulse with the LFM results, the phase difference measurements are improved in the far range of swath (> 3m) but in the near nadir region the improvements are negligible.

[9] Frequency of the system is 234kHz

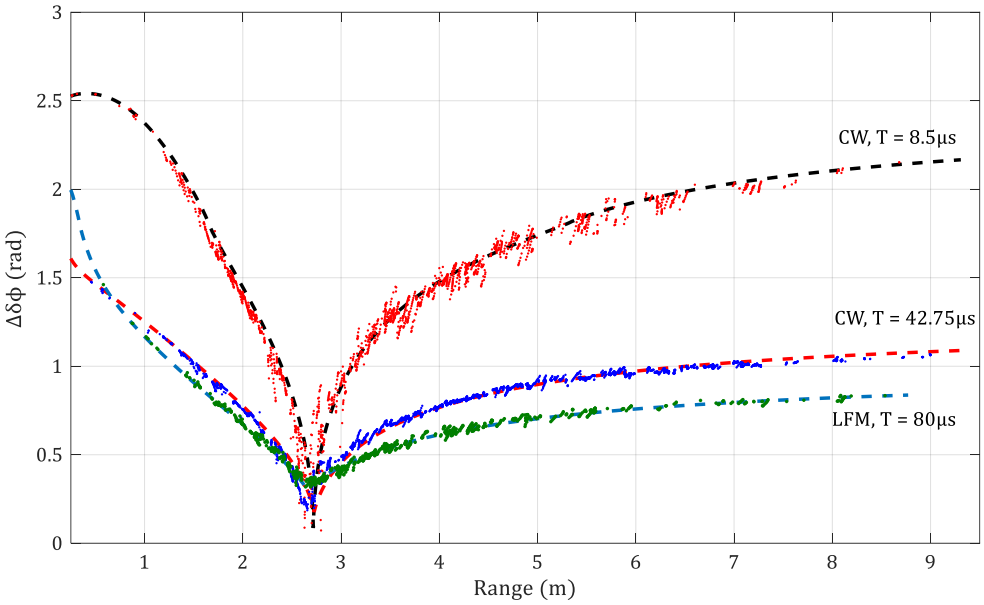

Figure 60 Phase difference standard deviation for total SNR vs Across track range

5.2.5 Considerations on Practical Implementation of Wideband Processing

The Previous chapter concluded that overall bathymetric measurement accuracy can be increased by using frequency modulated signals instead of conventional continuous wave pulses, which suffer from a range – resolution trade off. We can see a significant improvement in depth measurement uncertainty with the use of frequency-modulated transmit pulses, but the improvements are not the same all over the swath. The area before the interferometry axis (closer to nadir) has little or no improvement, and it tends to get worse by increasing the equivalent transmitted pulse length, which might be a necessity for a wider swath. This limits the benefits of using wideband pulses and wideband processing techniques with an interferometer, and as identified earlier this is due to the baseline decorrelation dominance in the near nadir area[10]. In this chapter we propose some methods to reduce the baseline decorrelation effect to get an improved bathymetry measurement accuracy over all the swath with use of wideband signals.

5.3. Pulse Shape design

The current Bathyswath system uses a square energy envelope to keep the maximum transmit energy in the water, but the transducer ceramics can't really replicate the sharp edges of the input transmit pulse, and the output pulse is slightly smoothed at

[10] Not talking about nadir region but the area covered before the interferometry axis

the edges, resulting in the loss of energy mostly in form of heat. So, a controlled smoothing of these edges prior to transmission is desired. Figure 61 presents the transmit pulse input to the transducer (red) and the output pulse of a transducer.

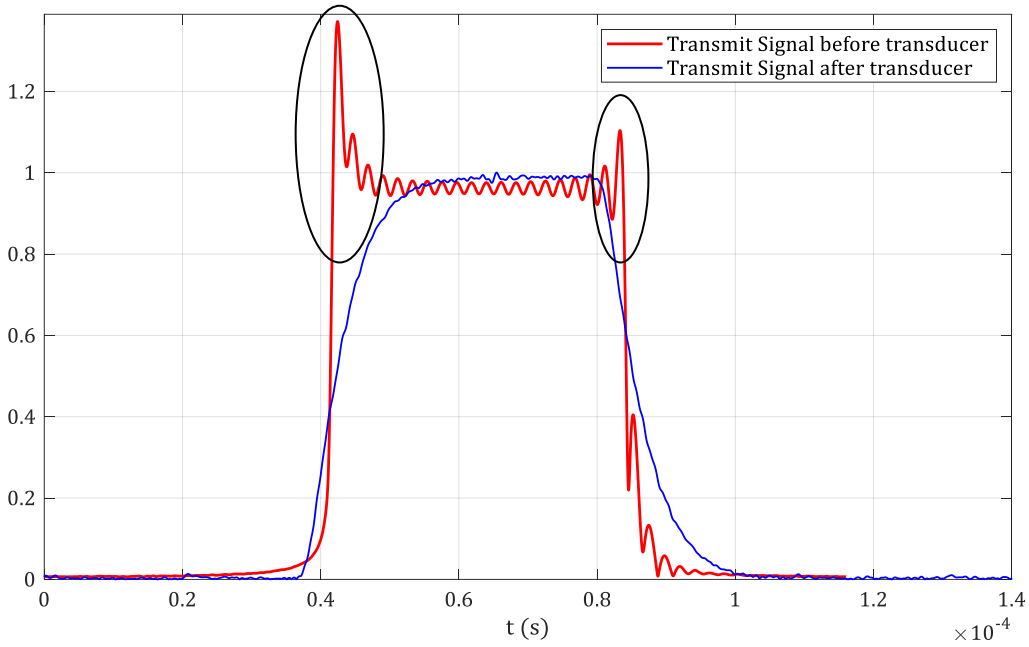

Figure 61 Tranmit pulse as input and output to piezoelectric

There are two simple ways to do that. The first is to taper the amplitude envelope by controlling the amplitude during the transmit duration. The second way is to use windowing the on the transmit signal before applying it to the transducer.

5.3.1 Smoothed Transmit Envelope

Tapering of transmit pulses is mentioned widely in sonar and radar literature to reduce the sidelobe dominance at the receiver; this is also known as array shading in some literature.

If the transmitted signal is given by:

$$S(t) = A\, e^{2\pi i\,(f_c t + k\, t^2)} \qquad 5.1$$

Where A is the amplitude of transmit pulse. The energy of a CW pulse can be given by:

$$E = A^2 T \qquad 5.2$$

The tapering of energy envelope can be done by modifying A as a function of time.

$$S(t) = A(t)\, e^{2\pi i\,(f_c t + k\, t^2)} \qquad 5.3$$

A(t) is amplitude of signal varying over the overall transmit length (T).

The smoothness of the energy variation can be defined as the smoothing factor

$$\alpha = \frac{\tau}{T}$$

Where τ is the duration when the transmit envelope is smoothed. Figure 62 presents envelopes of signals with different smoothing coefficient levels (0, 25, 50 and 100% smoothed).

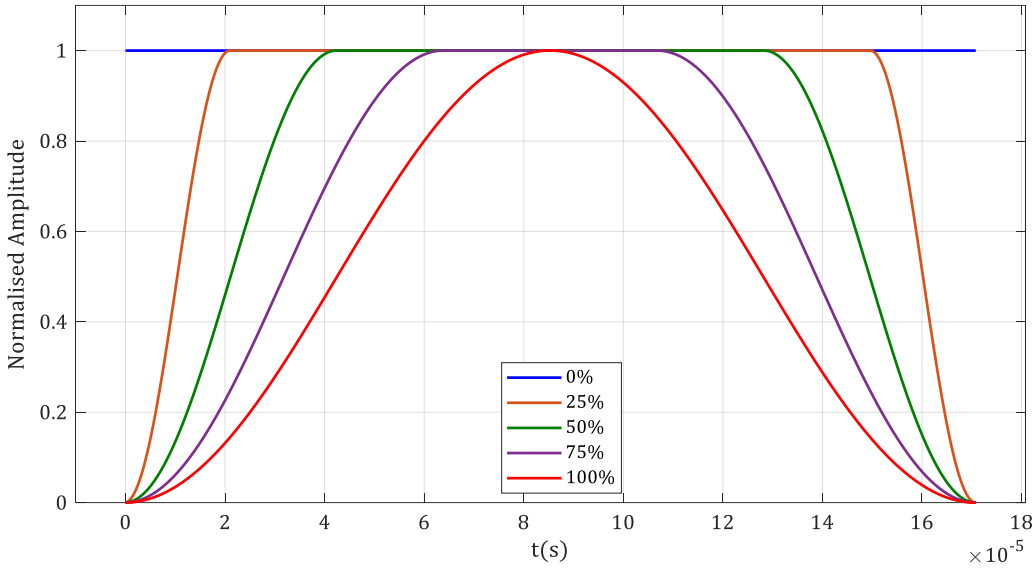

Figure 62 Signal envelopes given for different smoothing level (0% = original square envelope)

Figure 63 shows the auto-correlation output of an LFM pulse with a square amplitude function compared with the output when reducing the edges of envelope. We can see the reduction in the sidelobe of pulse compressed output. The higher the smoothing level, the lower the sidelobes. 100% smoothing removes the sidelobes completely, but at the cost of transmit energy level, since the energy of the signal directly relates to the transmit pulse length. This will benefit the baseline correlation, but the signal gets noisier where additive noise is dominating, resulting in reduced swath range and accuracy.

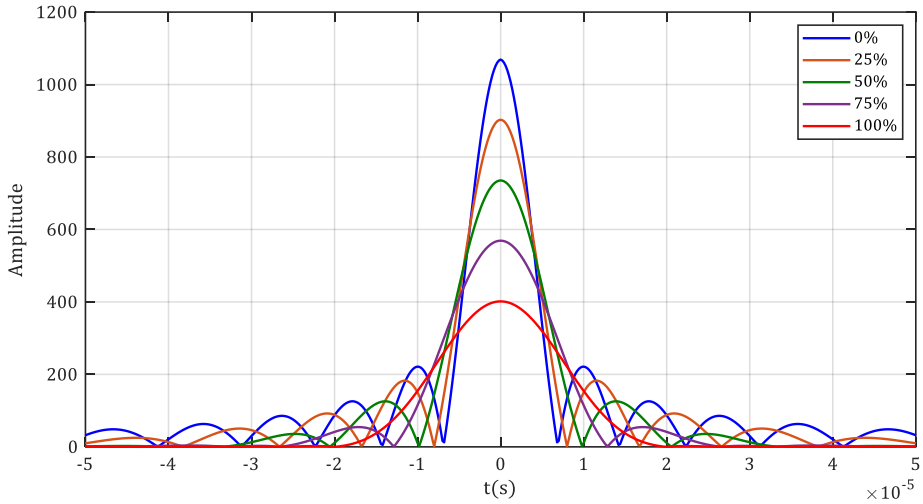

Figure 63 Auto-correlation function of transmitted signals with envelopes mentioned in Figure 63, (0% = original square envelope & 100% is for full cosine envelope)

This loss of transmit energy can be compensated by either increasing the transmit power or transmit duration or both, but that requires additional hardware modification and often it is limited by the hardware design. Another problem with the increase in transmit pulse length is the ping rate. A sonar usually transmits a pulse and waits for the complete reception of backscattered echoes before transmitting again. Thus, a longer pulse will decrease the ping rate reducing the ping density. However, a trade-off between smoothing level and transmit pulse length increase can be set to get the best results while operating with wideband signals and pulse compression

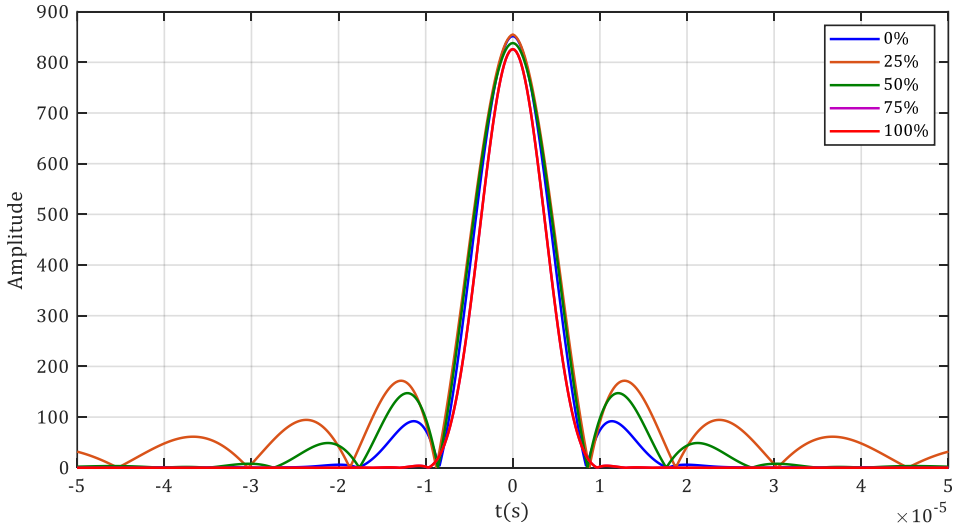

Figure 64 Auto-correlation function of transmitted signals with envelopes mentioned in, Figure 62 but with increased transmit pulse length to compensate the energy loss(0% = original square envelope & 100% is for full cosine envelope)

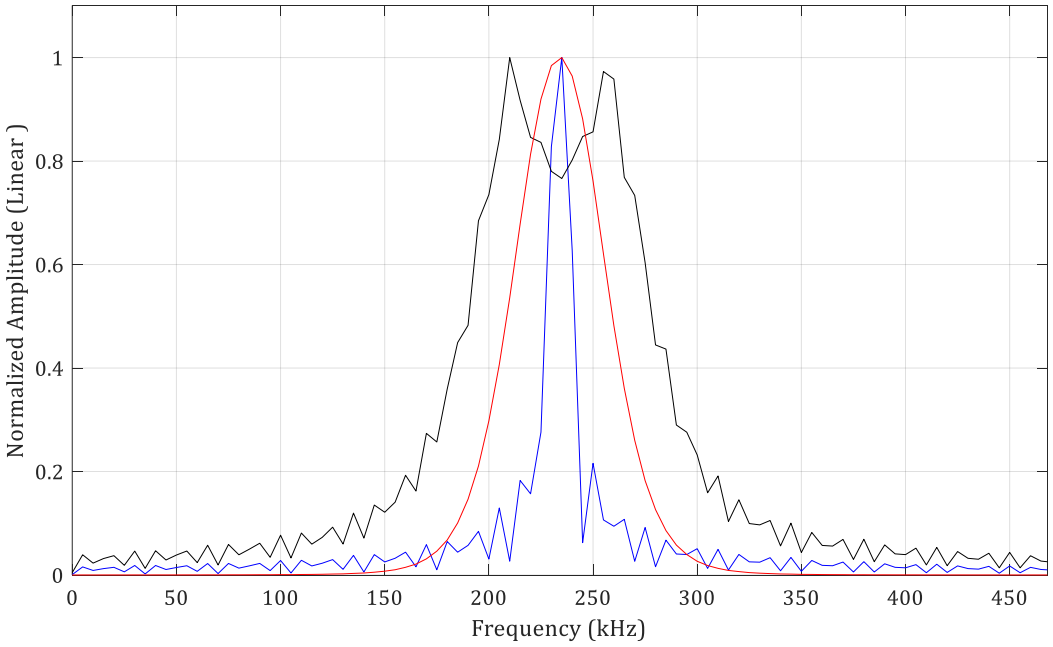

Figure 65 CW (blue), LFM with square envelope (black), LFM with cosine envelope or 100% smoothed envelope (red)

5.4. Filter Design

It is in our interest to keep transmitted energy as high as possible to have maximum range (which is mostly limited by the additive noise). Thus, we prefer to use a rectangular transmit envelope. However, our interest is to reduce the limitation in the bathymetry improvements when using wideband pulses, which is mainly due to baseline decorrelation. We explore some theoretical filtering techniques to reduce the sidelobes in the pulse compressed output **Error! Reference source not found.**.

There are three ways to do that:

- Windowing of transmitted signal before matched filter
- Windowing of matched filter reference signal
- Filtering and smoothing the pulse compressed output in frequency domain

Windowing of the reference signal before the matched filter can be used to reduce the sidelobes in the output signal. This technique is desirable since it does not require any hardware changes. The modified matched filter can be written as

$$h'^{(t)} = a(t) * S_{tx}(-t) \qquad 5.4$$

Where $a(t)$ is windowing function and $S_{tx}(t)$ is transmitted signal

Figure 66 presents the autocorrelation function of the transmitted pulse (unaltered) and transmit pulse after applying different weighting windows. We compare the results for Hamming, Hann, Gaussian and Taylor windows.

It can be noted that windowing the matched filter reduces the sidelobe dominance significantly, but the width of the main lobe is increased, limiting the benefits of sidelobe reduction. A wider main lobe degrades the improvement in the baseline decorrelation. Also, a smaller resulting bandwidth of pulse-compressed output results in reduced processing gain, which is discussed in section 3.2.

From Figure 66, a Taylor weighting window seems to give the best reduction in sidelobes while not increasing the main lobe width significantly.

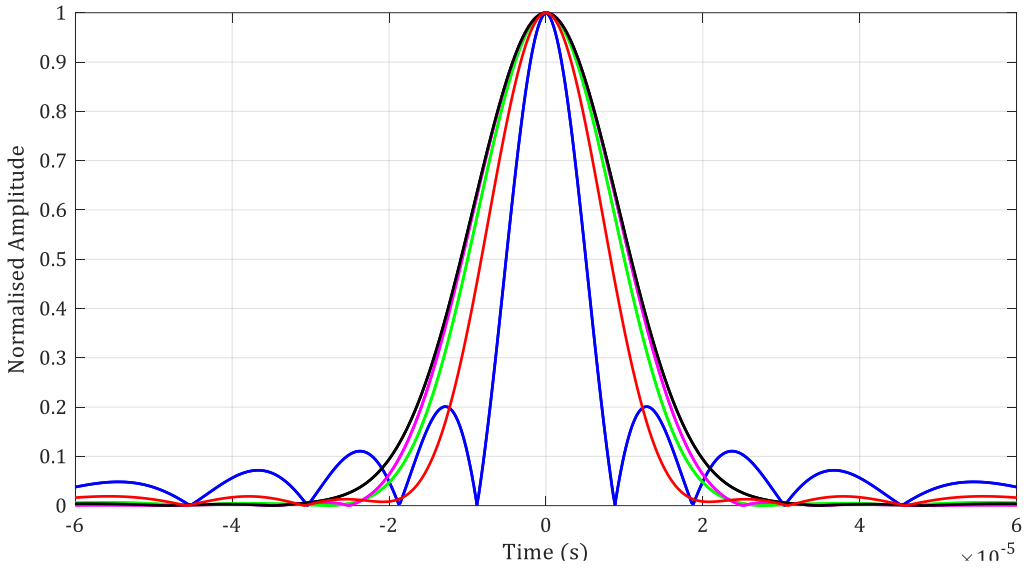

Figure 66 Auto-correlation of transmitted LFM pulse(blue) and widowed transmit pulses with Hamming window (green), Hann (magenta), Gaussian (black) and Taylor (red)

5.5. Conclusion of the Chapter

In this chapter we proposed the use of frequency-modulated pulses to improve the overall bathymetry measurements. We took the noise sources mentioned in Chapter 4, and compared the robustness of FM pulses with each noise source separately.

To conclude, bathymetry measurements can be improved by using wideband pulses over CW pulses with the Bathyswath interferometer. The SNR due to additive noise and spatial decorrelation can be improved significantly with frequency-modulated pulses, but the improvements are limited in the region before the interferometric axis (near-nadir region). This limitation in the bathymetry measurement improvement can be related to the sidelobe dominance in the receiver output of wideband pulses (pulse compressed output) (as discussed in 5.2.3).

A theoretical approach has been discussed here to reduce the sidelobe dominance in the wideband processing output, which is additional contributor in the angular

decorrelation of an interferometer. Several techniques have been discussed with their benefits and drawbacks and limitations.

Figure 67 presents the estimation of uncertainty in depth measurements given using the noise model described in Chapter 4. This estimation is done considering a square transmit envelope and effects of smoothing the edges of the transmit envelope before transmission.

The reduction of sidelobes often comes with a cost of a wider main lobe or reducing the transmitted energy level, so reducing the benefits of higher SNR due to additive noise. Hence, a compromise needs to be done between sidelobe reduction and the width of main lobe.

Altering the pulse compression technique at reception does help to reduce the sidelobes but this leads to reducing the overall processing gain of system, making it more sensitive to additive noise.

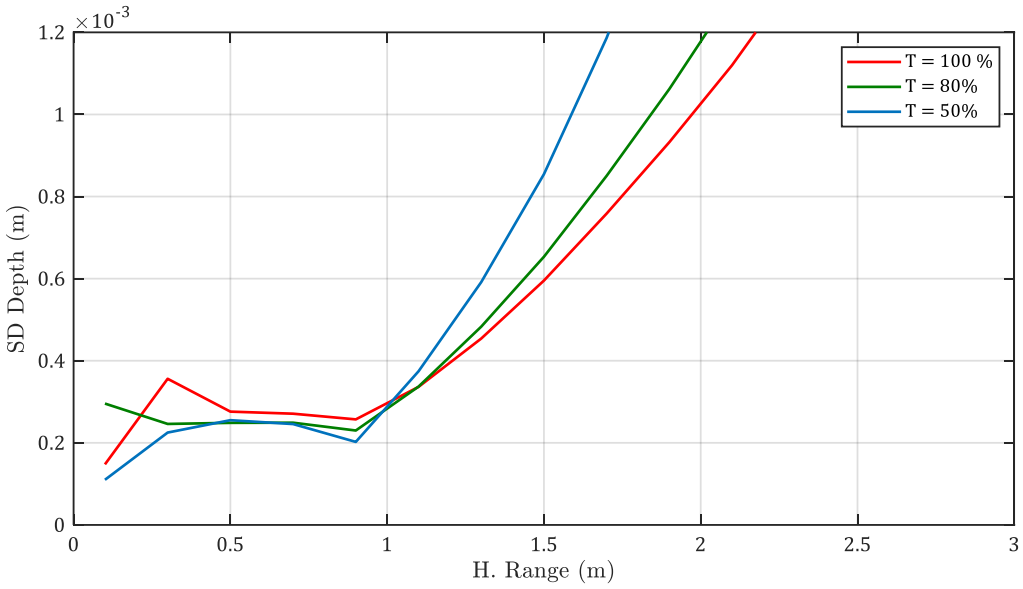

Figure 67 Depth uncertainty estimation with different level of transmit envelope smoothness initial signal 0% (red), 20% (green) and 50%(blue) of the original pulse length

Summarising the results from both techniques, we can say that the sidelobe effect can be reduced significantly, but at the expense of transmit energy and filter bandwidth, which can make it more susceptible to additive noise.

If the transmit pulse length can be increased, then the smoothing of transmit amplitude envelope technique can be useful to have improved bathymetry measurements with an interferometer

Windowing of matched filter does improve the baseline decorrelation but is limited by the increase in the width of main lobe. Also, reduction in processing gain makes it more sensitive to additive noise. Figure 67 presents the estimation of the bathymetry standard deviation, modelled with different smoothing levels. Some slight improvement is seen in the nadir region.

CHAPTER 6 CONCLUSION & PERSPECTIVE

6.1. Work Summery

Interferometry is an important tool for the shallow water exploration. The main objective of this research work is to contribute in the improvement of the interferometry technique of bathymetry from the signal processing point of view. Most of the work in this research is done around the current Bathyswath-2 designs.

Bathyswath-2 is a second-generation sonar system and uses phase differencing techniques for bathymetry measurements. The current design uses narrowband signals as the transmit pulse and is available with three different frequencies:117 kHz, 234 kHz and 468 kHz. For this research we used the 234 kHz and 468 kHz options since the 117 kHz is less favoured due to its bulky size and lower resolution.

Chapter 2 introduces the state of art in the bathymetry measuring tools and the design architecture of interferometers, in particular the Bathyswath system. Two well-known bathymetry measurement methods, multibeam beamformers and interferometers, are introduced and a comparison is done to justify the benefits and need of interferometers in shallow water survey. We discussed the two major problems with the use of narrowband signals: range – resolution trade-off and angular measurement uncertainty.

Chapter 3 describes the methodology used in this research work as well as the experiment setups used to explore the possibilities of improvement with this work. For the reception and recovery of signal we introduced the matched filter.

Chapter 4 we discussed in detail the uncertainty sources for an interferometer. We introduced the noise sources caused by the limitation of ancillary devices e.g. GNSS, motion sensor, sound velocity profiler (SVP), etc. But this chapter is mostly focused on the uncertainties coming from the signals and processing techniques. The main noise sources studied here are: additive noise, sliding footprint decorrelation and angular decorrelation, and their effect on the final bathymetry measurements. We compared the effect of individual noise sources on the phase measurement uncertainty, which can lead to a higher deviation in the final bathymetry measurement. We considered different length transmitted pulses to draw a relation between transmitted pulse length and the uncertainties. We compared the proposed results with real data for the verification of the noise model. This noise model is used in rest of work to validate the improvement proposals.

Chapter 5 proposes the system performance improvement using wideband signals. First, we introduce the use of wideband signals to overcome the range – resolution trade-off problem. We can conclude that the use of wideband processing technique is valuable to overcome the range – resolution trade-off, but we have also to consider how wideband signals perform in angle measurement since it is highly dependent on sensitive phase measurements. We compared the robustness of wideband signals with all three mentioned noise sources (additive noise, sliding footprint and angular decorrelation). The conclusion of these results with wideband signals is as follows:

- Additive noise can be reduced significantly by using a modulated transmitted signal. Matched filtering at the receive end gives a processing gain given by time – bandwidth product (BT). This helps to increase the swath range, since additive noise is more dominant in the far range of swath.
- SNR due to sliding footprint or spatial decorrelation can be improved slightly using LFM pulses but the benefits mostly apply to the seabed beyond the interferometry axis. One way to remove the sliding footprint effect is to estimate the seabed depth and then delay the receive signals to correct the shift of footprint.
- The major problem of using wideband signals is the baseline decorrelation effect. This is mainly due to sidelobe dominance in the matched filter output. The wider the transmitted energy envelope, the more decorrelation between the interferometry signals. A few ideas are given to reduce the baseline decorrelation effect, e.g. tapering the transmitted signal envelope, and improving the matched filter designs. But in both cases, we must trade off some of the energy, as it widens the matched filter's main lobe.
- But looking at the improvement in total SNR we can say that the use of wideband modulated pulses improves the overall bathymetry accuracy, neglecting the near nadir region, and increases the swath range while keeping high-resolution bathymetry.

To end the work of this thesis we proposed the wideband signal processing techniques that can be used to reduce the effect of angular (baseline) decorrelation, which limits the improvement in the bathymetry with wideband signals. However, these techniques give a wider main lobe in the pulse compressed output.

The main objective of this work was to contribute in the improvement of interferometric sonar using wideband signals and processing techniques. We gave a brief introduction to interferometric method of bathymetry measurements and explored different accuracy estimation models based on different noise sources.

The overall performance can be improved using frequency-modulated signals but limited by pulse length. A longer pulse can help in far range, overcoming the additive noise problems, but the near range gets noisier due to the baseline decorrelation effect. In term of measurement accuracy using LFM over a same length CW pulse is mostly limited to higher spatial resolution and wider range.

This research is mainly focused on the study of interferometric techniques and proposed wideband signal processing techniques to improve the overall performance of bathymetry measurement accuracy while having high-resolution bathymetry. This work was progressed in three main parts: first, identification of the problems with the use of Bathyswath-2 system; second, the improvement with the wideband signals and identifying the limitation and some proposals to overcome those limitation. We compare the effectiveness of these techniques with proposed noise model theoretically, since it requires the major modifications the sonar hardware itself. This will be taken in the consideration with the next version of Bathyswath, and the results will be published in future.

6.2. Perspective

We have mostly discussed on the improving bathymetry measurement accuracy from the signal processing point view. All the experiments were done with a limited similarity to the real-world situation. From the application perspective, the further implementation of this research must be considered with an upgraded hardware version of Bathyswath. As discussed in 5.2.5, the more important techniques must be studied further and need to be verified in real-world applications. I present here some direction to be followed for the future development to this research work.

In theoretical context, we should be considering a more accurate quality estimator in the nadir region to investigate the problem further. Nadir region stays one of the main problems with an interferometer. As discussed earlier and also mentioned in the Annex C, the data gap in nadir region is mainly due to measurement geometry, Front-end receiver response and the measurement uncertainty due to footprint response [4].

From the implementation point of view, a possible fix for measurement geometry problem could be to estimate the shape of the seabed from previous pings and then

optimise the data collection rate and down-sampling to increase the number of measurements in the nadir region.

Another work to be considered is the improvement in the front-end amplification of the received signals. When the sound hits the seabed, the size of first returned echo changes very quickly from very low level to high level. This drastic change in response presents a challenge to the amplifier design. An improvement in the hardware design will be considered to cope with this dynamic change is receive signal level and it can improve the data quality in nadir region.

Another work will be the implementation of an improved method to solve the sliding footprint effect. There has been mention of the estimation of shift in footprint to reduce the sliding footprint effect, but it is not yet implemented. The closest estimation of this shift will be done to get more correlated interferometry terms ($S_a S_b^*$), resulting in improved SNR_{shift}. One way to do is by estimating the shift between receivers, and then using signals from different parts of the ping for one of the receivers.

Beamforming implementation with increased number of receive staves to be considered to find the best fit for phase to angle estimation. This supposed to improve the results at nadir and multipath scenarios. This should be considered with the newer generation of Bathyswath.

A new generation of Bathyswath system with the name of Bathyswath-3 is under development and the techniques mentioned in this thesis will be implemented. The core application of this new sonar will be same, bathymetry measurements in shallow water, but some new features are added for some added values e.g. multi-frequency seabed classification and seabed classification. More details will only be disclosed by the ITER-Systems.

APPENDIX

Annex A Propagation of sound in water-column

The speed of sound depends on the temperature, pressure and salinity. So, the speed of sound is not constant throughout the transducer to sea bottom, and the water-column can thus be considered as a stack of layers with different speed of sound. Sound waves are refracted as they move though the ocean. To get accurate bathymetry measurements one needs to trace exactly the sound wave propagation path. Mostly this is done considering the ray propagation of sound in the water-column. So, it is important to know the speed of sound at different levels under water, and it is usually done by lowering a sound velocity profiler, which measures the speed of sound constantly at different levels of sea depth. Ray tracing is the commonest method for modelling sound propagation in the sea.

Thus, to get the quality measurements from any multibeam or interferometer, a mathematical model of the water-column sound velocity profile is needed to correct the propagation path and hence the depth and range.

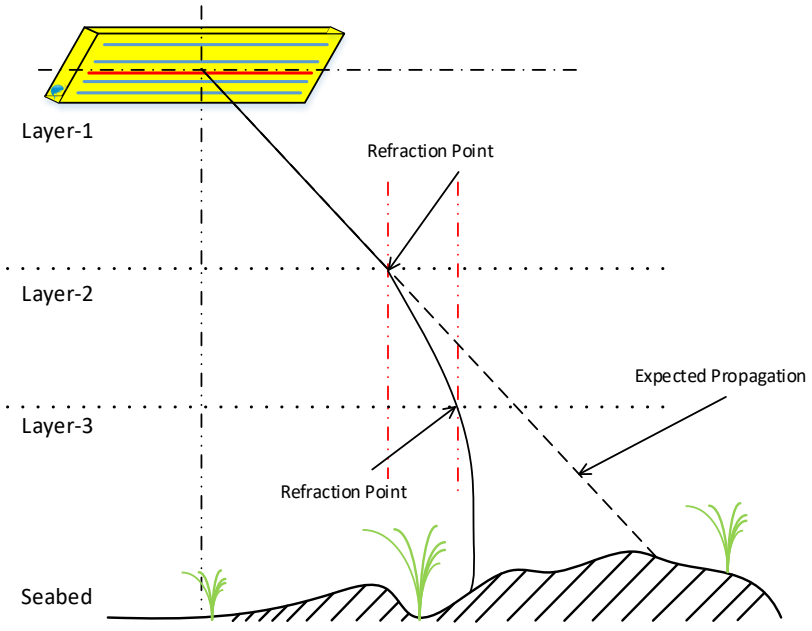

Figure 68 Sound wave propagation due to changing sound velocity

So, it is essential to know the sound velocity profiles at the time of survey to get an accurate bathymetry detection. In practice, multiple sound velocity profiles are taken during the survey at different times and places, because the sound profiles depend on the pressure, temperature and salinity. Any error in the measurement of sound velocity can lead to an incorrect bathymetry measurement. We consider this as an external factor in

the bathymetry degradation and it can be avoided by using a highly accurate and calibrated sound velocity profiler (SVP). All the external bathymetry degradation causes are not studied here.

Annex B Sonar Equation

a. Source Level (SL):

Source level denotes to the transmitted energy level in *dB re 1µPa @1m (acoustic pressure (RMS value) in micropascals at 1 metre from the transmit element)*. The transmitted energy level is specific to the sonar system used. In most of the cases the transmitted energy level is specified by the manufacturer. Also, the energy level depends on the sonar parameters used during the survey of interest. For example, for a fixed central frequency system the transmitted energy level is specified according to the water depth. Shallower water requires less transmitted energy level, where higher transmitted energy level can achieve higher range, and that depends on the type of pulse, duration of transmitted envelope and amplitude of the envelope.

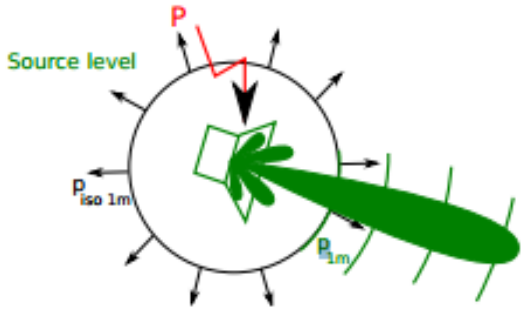

The source level is defined as the proportion of the measured pressure at 1-metre distance from the projector and a reference pressure.

$$SL = 10\,log\left(\frac{Pressure\ at\ 1-meter\ distance\ from\ source}{Reference\ pressure}\right) \quad 1$$

$$SL = 20\,log_{10}\left(\frac{P_{vrms}}{P_{ref}}\right) \quad 2$$

Where, P_{ref} is reference pressure measured at 1-metre distance from transmit element while inputting 1V of signal. And the P_v is output pressures measured at 1-metre distance with an applied voltage v_{rms}.

$$SL(\theta_e) = S_v + 20\,log_{10}(V_{rms}) \quad 3$$

where S_v is the transmit channel (projector)'s sensitivity and usually provided by the transducer manufacturer.

b. Transmission loss (TL):

When sound transmitted from a point source propagates in outward direction in an underwater medium the loss of energy includes the **geometric spreading** loss, loss of energy due to **absorption** in the medium and loss due to reflection and refraction. Transmission loss is the reduction in sound intensity between source and receiver. There are two main reasons for that:

- **Propagation loss** or geometrical divergence loss of a spherical wave

  Let's consider the transmitted energy is from a point source, and spherical propagation in a homogeneous medium. The transmitted energy from the source is constant, and it propagates through the surface of a sphere that grows with the radius of the sphere. That surface is given by:

$$S = 4\pi R^2 \qquad 4$$

  So, the spread of energy over the sphere is: $E = 4\pi R^2 I(R)$

  Thus, the ratio of the intensity at 1m distance from source and at a distance of R is:

$$\frac{I_{1m}}{I_R} = (R)^2 \qquad 5$$

  Thus, propagation loss in dB is given by

$$PL = 10\, log_{10}\left[\frac{I_{1m}}{I_R}\right] \qquad 6$$

  Thus,

$$PL \approx 20\, log_{10}\, R \qquad 7$$

- **Absorption loss** in the medium

  Absorption loss in any medium can be given by the attenuation coefficient. The coefficient value not only depends on the physical stress in propagation but also on the time derivatives. For example, higher-frequency waveforms have higher absorption while propagating through water medium, which results in energy loss as in heat. Many models are deployed to estimate the attenuation coefficient, such as the François Garrison equation [7]:

$$AL = \alpha R \qquad 8$$

  where α is the absorption coefficient (logarithmic) given in dB/km. It depends on the sea water properties and frequency of the transmitted sound wave.

  For a frequency range between 100 kHz and 1 MHz, the simplified formula given by Ainslie and McColm 1998 [18] gives values of α with reasonable accuracy.

Thus, total **transmission loss** for one-way propagation is the sum of divergence loss and the absorption loss.

$$TL \approx 20\, log_{10} R + \alpha R \qquad 9$$

For active sonar, we need to consider the transmission loss for two-way propagation, which explains the factor 2 in the sonar equation.

Suspended sediments and bubbles also have a major effect in the rivers and coastal areas that interferometric sonars are usually used in, but neglected here since it requires a complex model to estimate.

c. Target Strength (TS):

When a transmitted sound pulse hits the target seabed, a small portion of energy is reflected back towards the sonar receivers. The proportion of reflected energy is known as target strength. It is given by the ratio of the reflected intensity or radiated intensity from the target at 1m distance, to incident intensity.

$$TS = 10\ log_{10} \frac{I_r}{I_i}\ dB \qquad 10$$

Where:

I_r is reflected intensity from the target at 1m distance

I_i is incident intensity and can be calculated by sound pressure level (SPL) at the target (SL -TL).

Simplifying the equation 0.10

$$TS = BS + 10\, log\, A \qquad 11$$

Where A is ensonified footprint area and ***BS*** is backscatter strength

Backscatter strength depends on the reflectivity of bottom types and incident angle and a simple model can be given by the Lambert's law:

$$BS = BS_0 + 20\, log(cos(\theta)) \qquad 12$$

Reflected intensity depends on target properties and on the transmitted pulse type, length of pulse and also on the incidence angle. Correct estimation of target strength is a complex process, and can be used for seabed classification applications.

d. Processing Gain (PG):

The improvement in signal to noise ratio of received signals at the receiver's front end is usually known as processing gain of the sonar system. The matched filter (MF)

usually improves the SNR and this improvement in SNR is called processing gain here. If the signal to noise ratio before the filter is:

$$\boldsymbol{SNR_0 = \frac{max|s|^2}{N_0/T_{eq}}} \quad 13$$

And signal to noise ratio after the MF is given by:

$$SNR_A = \frac{\int |s|^2 dt}{N_0} = \frac{E}{N_0} \quad 14$$

Thus, processing gain is given by the level of improvement:

$$PG = 10\ log\left(\frac{\int |s|^2 dt}{max|s|^2 T_{eq}}\right) \quad 15$$

For pulse compression techniques, the processing gain is given by the product of system bandwidth and emission duration.

$$PG\ = 10\ log_{10} BT \quad 16$$

e. Directivity Index (DI):

Directivity index is measure of the fraction of sound energy that is emitted in the desired direction.

$$DI_e = 20\ log_{10}\left(\frac{P_{1m}(\theta,\psi)}{P_{iso1m}}\right) \quad 17$$

Where: $P_{1m}(\theta,\psi)$ pressure measured towards target direction and P_{iso1m} is sound pressure at 1m as if isotropic.

The transducer manufacturer provides us the beam width for transducer in both azimuth and elevation angle. It can be used to calculate the emission antenna efficiency characteristics (Ref.: ITER-Systems internal documents):

Here are some parameters provided by the Bathyswath-2 manufacturer:

	Sonar Frequency		
	117 kHz	**234 kHz**	**468 kHz**
Sonar Level, db re 1µPa@1m	224	220	222
Transmit Pulse Length	60µs to 1ms	34µs to 500µs	17µs to 250µs
Maximum Swath Width	800 metres	400 metres	200 metres

Maximum water depth	350 metres	150 metres	75 metres
Beam Width, Elevation 3dB	50°	50°	50°
Beam Width, Elevation 10dB	100°	100°	100°
Beam Width, Elevation 20dB	120°	120°	120°
Beam Width, Elevation 25dB	140°	140°	140°
Beam Width, Azimuth	1.7°	1.1°	1.1°

Table 1 Bathyswath Transducer Manufacturer's Specifications

f. Noise Level

In ideal case we are expecting to receive and measure only the backscattered echoes, but that's not the case in real environment. The received signal is combination of desired signal and different noisy interferences, that could be ambient noise (e.g. mixture of ship traffic noise, marine animals, bubbles, environmental waterborne sounds etc.), reverberation (e.g. backscattered echoes due to floating bodies in water-column, in which we are not interested) or self-noise[11] of sonar hardware and measurement platforms.

We can assume that the backscattered echo's intensity level is high enough that we can easily define the threshold level to neglect the noise component. The effect of additive noise can be reduced significantly by the directivity index of receive transducer arrays.

Ambient noise can be given the Wenz curve [19]:

$$NL = NL_0 + 10\,log_{10}(B) \qquad 18$$

[11] The aim of any good sonar electronics design is to keep this below the sea noise

Annex C Nadir Region

One of the well-known disadvantages of phase differencing sonar is the low data density directly under the boat, known as nadir region or nadir gap [20]. In this section we will discuss some reasons for this.

Figure 69 and Figure 70 are some examples of the data gap in nadir region problem. You can notice easily low density of depth measurements directly under the transducers (port and starboard). The main reason behind the gap in nadir region is the geometrical relation of interferometer's transducers with the seabed, and the way that samples are collected during a survey.

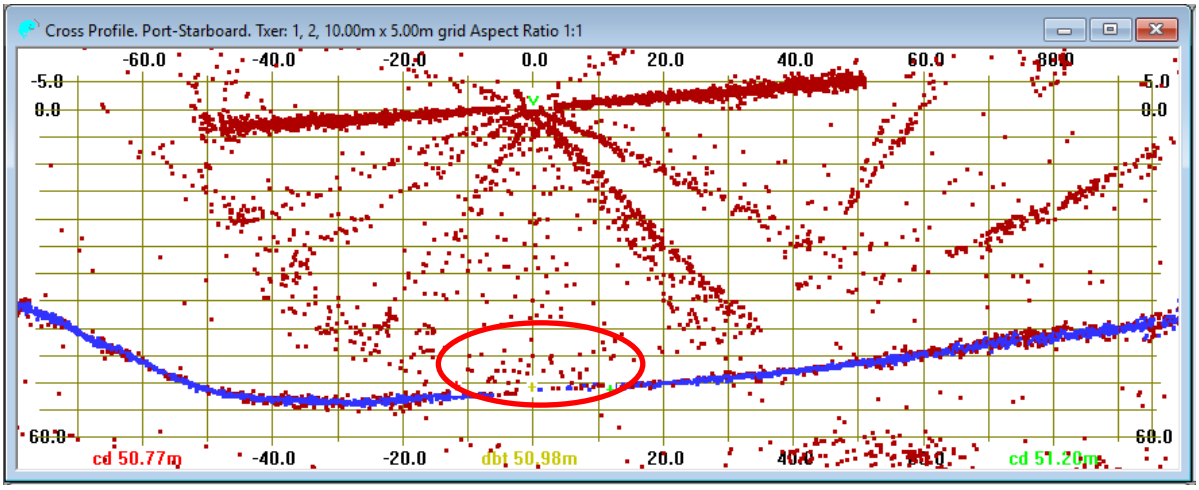

Figure 69. Cross profile (Nadir Depth = 51m)

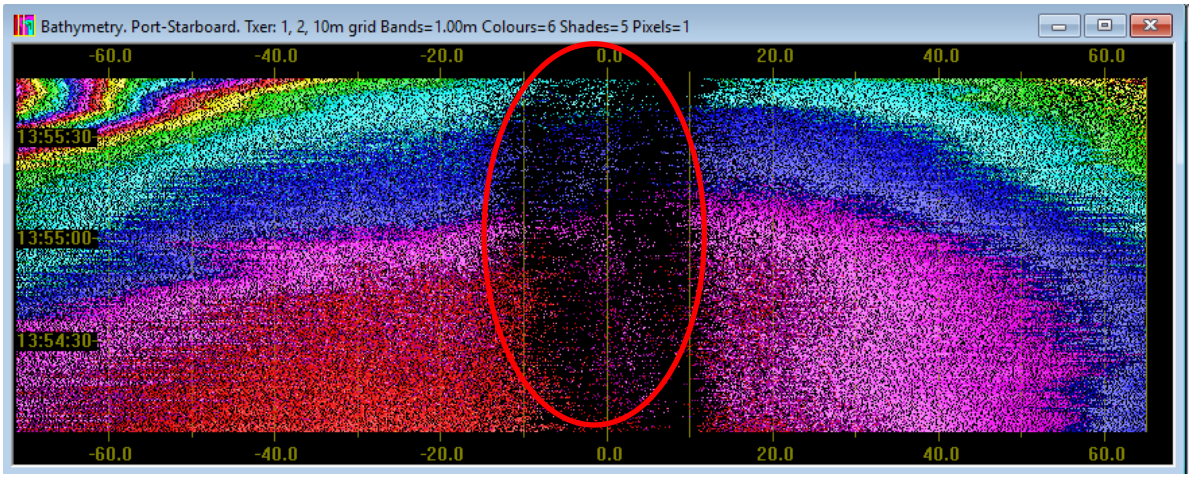

Figure 70. 2-D waterfall view of seabed while boat passes over seabed

- **Measurement Geometry**

For an interferometer, we sample the angle to a seabed at fixed sampling period. The angle and time of each sample is used to calculate the depth and horizontal range. Range (slant range) is calculated using 2-way time of travel and speed of sound, so regular

time steps give regular range steps. However, a regular slant range does not produce a regular horizontal range (distance along the seabed starting from directly underneath the transducer).

For example, taking a regular slant range size of $\delta \mathrm{R}$ produces a horizontal range step in the nadir region of δH_1. By simple trigonometry, the horizontal range step δH_1 is much larger than the slant range step δR. Now take the sample from further out along the swath profile. Here the horizontal range δH_2 is produced by the same size slant range step δR. And here the δH_2 step size is much closer to the slant range step $\delta \mathrm{R}$. So, the horizontal range measurements under the transducer (nadir region) are much more spread out compared to the other parts of swath profile.

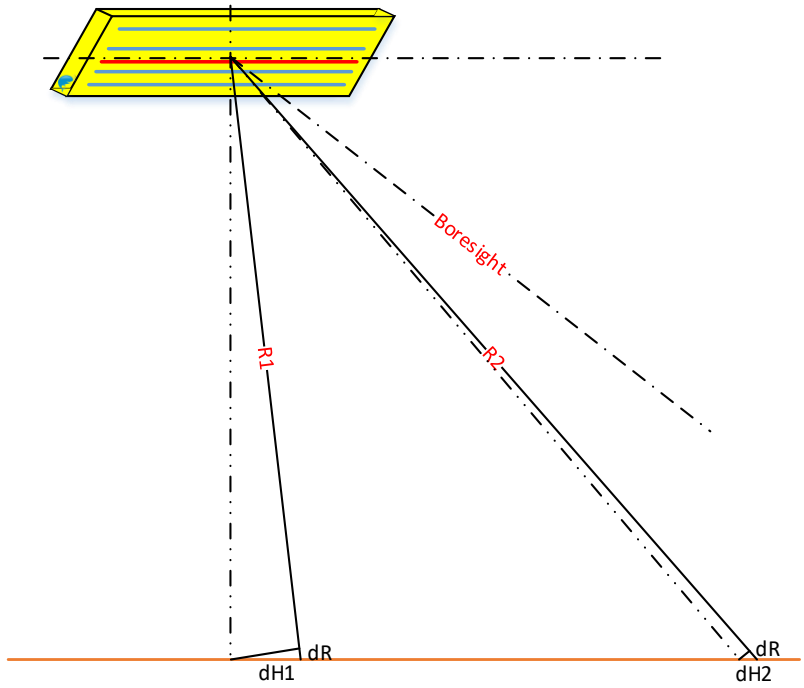

Figure 71. Measurement geometry in nadir region

This effect occurs where a normal to the seabed meets the transducer, so it is directly below the transducer for flat seabed, but moves up-slope on a sloping seabed.

A possible fix for this problem could be to estimate the shape of the seabed from previous pings and then optimise the data collection rate and down-sampling to increase the number of measurements in the nadir region.

- **Transmit Beam Footprint**

As discussed earlier in the section [4.5.2] we have noticed a low SNR at close range due to a wider footprint size.

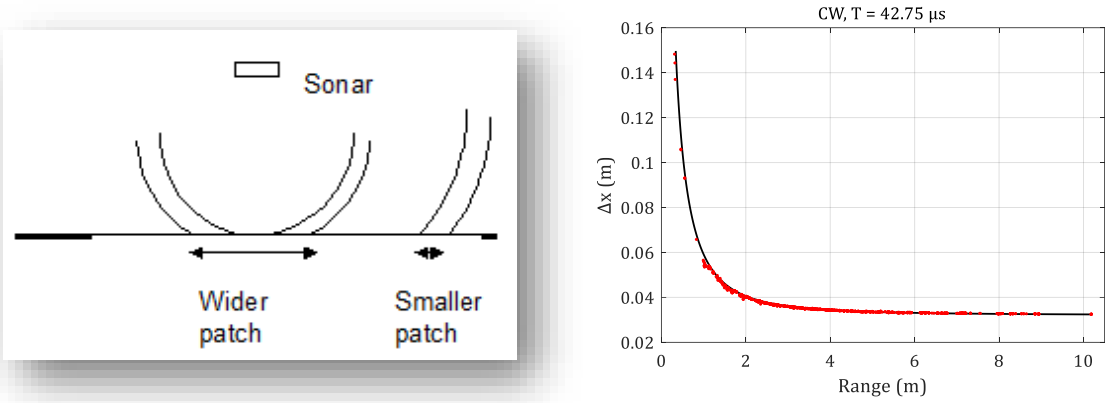

Figure 72 Footprint patch in nadir region and far range (left), footprint length given over horizontal range

- **Amplifier response**

In a ping, when the transmitted sound pulse travel through the water column and hits the seabed for first time, the intensity of the returned echo at receiver changes very quickly from very low level to a very high level. This drastic change in received signal level creates a challenge for front end amplifier designer Most of the current systems use either square amplification law or logarithmic amplifier [35], but these designs can be further improved.

This page is left blank intentionally

PUBLICATIONS

External

[1]. J. S. Sewada, C. Ioana, M. Geen and J. Mars, "Interferometric Measurements with Wideband Signal Processing Techniques," OCEANS 2019 - Marseille, Marseille, France, 2019, pp. 1-7, doi: 10.1109/OCEANSE.2019.8867232.

[2]. J. S. Sewada, C. Ioana, M. Geen and J. Mars, "Wideband signal processing techniques for Interferometric Sonars," OCEANS 2018 MTS/IEEE Charleston, Charleston, SC, 2018, pp. 1-4, doi: 10.1109/OCEANS.2018.8604641.

[3]. J. S. Sewada, C. Ioana, M. Geen and J. Mars, "Wideband Signals for Phase Differencing Sonar Systems," 2018 OCEANS - MTS/IEEE Kobe Techno-Oceans (OTO), Kobe, 2018, pp. 1-5, doi: 10.1109/OCEANSKOBE.2018.8559146.

[4]. Jitendra S. Sewada, Cornel Ioana, Matt Geen and Jêrome Mars, “Wideband signals for Interferometric Sonar systems”, Gretsi, Jean-les-Pins, France, September 2017

[5]. Jitendra S. Sewada, Cornel Ioana, Matt Geen, David Maillotte, “**Poster:** Interferometric Sonar & its future with Wideband signal processing techniques”, SERENADE, SeaTech Event, Brest 2016

Internal

[1]. Jitendra Singh SEWADA, Matt GEEN, “ITD_1023_Bathyswath-3 Design Specification”, Internal Technical Document 2019, ITER-Systems [Classified]

[2]. Jitendra Singh SEWADA, Matt GEEN, “ITD_1028_Bathyswath-3 TEM Design Specification”, Internal Technical Document 2019, ITER-Systems [Classified]

This page is left blank intentionally

BIBLIOGRAPHY

[1]. IHO Standards for Hydrographic Surveys, 5th Edition, Special Publication N° 44, International Hydrographic Bureau, February 2008

[2]. “Echo Sounding / Early Sound Methods”, National Oceanic & Atmospheric Administration (NOAA), NOAA Central Library

[3]. A.D. Waite, “Sonar for Practicing Engineers”, Wiley, Third Edition, 2002

[4]. ITER Systems Product Documents, “Bathyswath -2 Technical Information”, Sep. 2016

[5]. R. Fezzani, B. Zerr, A. Mansour, M. Legris and C. Vrignaud, "Fusion of Swath Bathymetric Data: Application to AUV Rapid Environment Assessment," in IEEE Journal of Oceanic Engineering, vol. 44, no. 1, pp. 111-120, Jan. 2019, doi: 10.1109/JOE.2017.2773139.

[6]. Maury, Matthew Fontaine, “Explanations and sailing directions to accompany the Wind and current charts”, approved by Commodore Charles Morris, chief of the Bureau of Ordnance and Hydrography 1853

[7]. X. Lurton, G. Lamarche, Craig Brown, V. Lucieer, G. Rice, Alexandre Schimel, Tom Weber, “Backscatter measurements by seafloor-mapping sonars: Guidelines and Recommendations”, Geohab, May 2015

[8]. Ainslie M. A., McColm J. G., "A simplified formula for viscous and chemical absorption in sea water", Journal of the Acoustical Society of America, 103(3), 1671-1672, 1998.

[9]. M.J.P. Heaton and W.G. Haslett, “Interpretation of Lloyd mirror in sidescan sonar”, Proc. Soc. Underwater Tech, vol. 1, no. 1, pp. 24- 38, 1971.

[10]. A.R. Stubbs and Dr B.S. McCartney, ““Telesounding” – Multiple Depth Measurement with a Side-Scan Sonar”, Journal of the Acoustical Society of America, Vol. 54, Iss. 2, 1973. pp. 554

[11]. P. N. Denbigh, "Swath bathymetry: principles of operation and an analysis of errors," in IEEE Journal of Oceanic Engineering, vol. 14, no. 4, pp. 289-298, Oct. 1989, doi: 10.1109/48.35979

[12]. P.N. Denbigh, “A bathymetry sidescan sonar”, In proc. Ultrasonic Int.’79 Conf., 1979

[13]. ITER Systems internal documents, ‘’Interferometric Processing in Bathyswath”, Ver. 1.04, March 2019

[14]. ITER Systems User Manuals, “Bathyswath Software Online Help/ How to Filter bathymetric Data”, Software version 3.16 onwards

[15]. R.L Cloet, S.L. Hurst, C.R. Edwards, P.S. Phillips, A.J. Duncan, “A Sideways-looking Towed Depth-measuring System”, Journal Royal Institute of Navigation, Vol. 35, Iss 3, Sep 1982, pp. 411 - 420

[16]. P. Byham, “Filling the Gap – Addressing the Nadir issue in Interferometric Sonar”, PhD Thesis, Faculty of Science and Technology, Plymouth University, March 2013

[17]. X. Lurton, An introduction to Underwater Acoustics, Springer, 2003

[18]. Ainslie M. A., McColm J. G., "A simplified formula for viscous and chemical absorption in sea water", Journal of the Acoustical Society of America, 103(3), 1671-1672, 1998.

[19]. Gordon M. Wenz, “Acoustic Ambient Noise in the Ocean: Spectra and Sources”, The Journal of the Acoustical Society of America, Vol. 34, Iss. 12, Dec 1962

[20]. R. Fezzani, B. Zerr, M. Legris, A. Mansour and Y. Dupas, "Swath bathymetric data fusion application to autonomous underwater vehicles," OCEANS 2015 - Genova, Genoa, 2015, pp. 1-5, doi: 10.1109/OCEANS-Genova.2015.7271464.

[21]. C. Sintes and B. Solaiman, "Strategies for unwrapping multisensors interferometric side scan sonar phase," OCEANS 2000 MTS/IEEE Conference and Exhibition. Conference Proceedings (Cat. No.00CH37158), Providence, RI, USA, 2000, pp. 2059-2065 vol.3, doi: 10.1109/OCEANS.2000.882242.

[22]. P. Vincent, Ch. Sintes, X. Lurton, R. Garello, “Influence of the Doppler Effect on Multibeam Echo Sounder Bathymetry”, OCOSS Proc. (Brest, France), June 2010

[23]. X. Lurton, "Swath bathymetry using phase difference: theoretical analysis of acoustical measurement precision," in IEEE Journal of Oceanic Engineering, vol. 25, no. 3, pp. 351-363, July 2000, doi: 10.1109/48.855385.

[24]. X. Lurton, “Theoretical Modelling of Acoustical Measurement Accuracy for Swath Bathymetric Sonars”, International Hydrographic Review, vol. 4 No. 2 ,2003

[25]. J. S. Bird and G. K. Mullins, "Analysis of swath bathymetry sonar accuracy," in IEEE Journal of Oceanic Engineering, vol. 30, no. 2, pp. 372-390, April 2005, doi: 10.1109/JOE.2005.850869.

[26]. Guoliang Jin and Dajun Tang, "Uncertainties of differential phase estimation associated with interferometric sonars," in IEEE Journal of Oceanic Engineering, vol. 21, no. 1, pp. 53-63, Jan. 1996, doi: 10.1109/48.485201.

[27]. G. Llort-Pujol, C. Sintes and D. Gueriot, "Analysis of Vernier interferometers for sonar bathymetry," OCEANS 2008, Quebec City, QC, 2008, pp. 1-5, doi: 10.1109/OCEANS.2008.5151958.

[28]. C. Sintes, G. Llort-Pujol and J. Le Caillec, "Vernier interferometer performance analysis," OCEANS'11 MTS/IEEE KONA, Waikoloa, HI, 2011, pp. 1-6, doi: 10.23919/OCEANS.2011.6107048.

[29]. P. Vincent, F. Maussang, X. Lurton, C. Sintès, R. Garello, “Impact of FM pulse compression sidelobes on Multibeam Bathymetry Measurements”, Proc. ECUA 2012, July 2012, Edinburgh, UK

[30]. P. Vincent, F. Maussang, X. Lurton, C. Sintès and R. Garello, "Bathymetry degradation causes for frequency modulated multibeam echo sounders," 2012 Oceans, Hampton Roads, VA, 2012, pp. 1-5, doi: 10.1109/OCEANS.2012.6404799.

[31]. P.Vincent, “Modulated Signal impact on Multibeam Echosounder Bathymtery ”, PhD Thesis, Université Rennes, 2013

[32]. M. J. Alam, E. H. Huntington and M. R. Frater, "Relationship between length of the chirp and depth of the ocean in active sonar processing," 2013 IEEE International Conference on Signal Processing, Communication and Computing (ICSPCC 2013), KunMing, 2013, pp. 1-6, doi: 10.1109/ICSPCC.2013.6664099.

[33]. G. LLort Pujol, Amélioration de la résolution spatiale des sondeurs multifaisceaux, PhD Thesis, Université Rennes 1, 2007

[34]. L. R. Varshney and D. Thomas, "Sidelobe reduction for matched filter range processing," Proceedings of the 2003 IEEE Radar Conference (Cat. No. 03CH37474), Huntsville, AL, USA, 2003, pp. 446-451, doi: 10.1109/NRC.2003.1203439.

[35]. Le Chevalier, Fraçois, “Principle of radar and sonar signal processing”, 2002

Résumé - Avec l'augmentation des activités côtières, il existe un besoin croissant de bathymétrie haute résolution et d'imagerie latérale. De nombreux types d'équipements de mesure acoustique sont disponibles pour étudier les fonds marins. Notre intérêt principale est étudier des techniques de mesure interférométriques. La large bande fournie par un interféromètre est un outil souhaitable dans les environnements en eaux peu profondes, où le temps et le coût de la surveillance jouent un rôle important. Dans ce travail de recherche, nous cherchons à étudier les principaux problèmes de dégradation de la qualité du point de vue du traitement du signal, et nous proposons quelques moyens d'améliorer les techniques actuelles. L'utilisation de signaux acoustiques à bande étroite (monofréquence) nécessite un compromis entre plage et résolution. Une impulsion transmise pour une période plus longue contient une énergie plus élevée ; par conséquent, l'intensité des échos rétrodiffusés dans le champ lointain est également supérieure et se distingue par le bruit ambiant. Cependant, une impulsion plus longue crée également une plus grande empreinte (zone insonifiée) sur le fond de la mer et dégrade la résolution : la possibilité de mesurer les deux cibles très proches (dispersion sur le fond de la mer). L'autre problème réside dans la capacité à mesurer les profondeurs avec précision dans un environnement bruyant. La mesure de profondeur par technique interférométrique est effectuée en mesurant l'angle d'incidence, qui est calculé à partir de mesures de différence de phase au niveau du réseau de réception. Ainsi, toutes les erreurs dans les mesures de phase entraîne une bathymétrie inexacte. Cela le rend très sensible à toutes les sources de bruit liées à la phase. Nous donnons un modèle d'incertitude du point de vue du traitement du signal. Nous nous intéressons ici à différentes sources de bruit dans la dégradation globale de la bathymétrie. Nous proposons l'utilisation de signaux à large bande pour résoudre les problèmes présentés dans ce travail. Nous commençons par résoudre le compromis de résolution en distance en évaluant différents signaux, par exemple. Signaux à bande étroite et ainsi que large. Ensuite, dans la deuxième partie, nous proposons des signaux à large bande pour surmonter les sources de dégradation bathymétriques introduites précédemment. Nous explorons chaque source de bruit séparément et comparons les améliorations apportées aux composantes de bruit individuelles par les impulsions à large bande. Nous concluons en évaluant l'amélioration globale de l'utilisation des signaux à large bande, tout en présentant les limites et les problèmes de cette approche.

Mots-clés - Sonar bathymétrique, sonar de bathymétrie à phase différentielle, PDBS, interféromètre, signaux à large bande, filtres adaptés, compression d'impulsion, estimation du fond, bathymétrie en bande, résolution du sonar

Abstract - With the increase in the coastal activities, there is an increasing need for high-resolution bathymetry and sidescan imagery. Many types of acoustic measurement equipment are available to investigate the sea bottoms. Our main interest is in the study of interferometry techniques of measurement. The wide swath given by an interferometer makes it a desirable tool in shallow water environments, where time and cost of survey plays an important role. In this research work we aim to investigate the major quality degradation issues from the signal processing point of view, and we propose some ways to improve the current techniques. Using narrowband (single-frequency) acoustic signals requires a trade-off between range and resolution. A longer transmitted pulse contains higher energy; hence the intensity of far range backscattered echoes is also higher and distinguishable in ambient noise. However, a longer pulse also makes a bigger footprint (insonified area) on the sea bottom, and degrades resolution: the ability to measure the two closely placed targets (scatters on sea floor). The other problem lies with the ability to measure the depths accurately in a noisy environment. Depth measurement with interferometric technique is done by measuring the incident angle, which is calculated from phase difference measurements at receive array. So, any error in phase measurements results in inaccurate bathymetry. That makes it highly sensitive to all phase related noise sources. We give an uncertainty model from the signal processing point of view. Here we focus on different noise sources in the overall bathymetry degradation. We propose the use of wideband signals to overcome the problems introduced in this work. We start with solving the range-resolution trade off by doing an assessment of different signals, e.g. narrowband and wideband signals. Then in the second section, we propose wideband signals to overcome the previously introduced bathymetry degradation sources. We explore each noise source separately and compare the improvements in individual noise components given by wideband pulses. We conclude by assessing the overall improvement from using wideband signals, while introducing the limitations and issues with this approach.

Keywords - Bathymetric Sonar, Phase Differential Bathymetry Sonar, PDBS, Interferometer, Wideband signals, Pulse compression, Bottom estimation, Swath Bathymetry, Sonar resolution